MECHANISTIC AND STRUCTURAL STUDIES OF PANNEXIN CHANNELS

A Dissertation

Presented to the Faculty of the Graduate School

of Cornell University

in Partial Fulfillment of the Requirements for the Degree of

Doctor of Philosophy

by

Kevin Ronald Michalski

August 2018

MECHANISTIC AND STRUCTURAL STUDIES OF PANNEXIN CHANNELS

Kevin Ronald Michalski, Ph.D

Cornell University 2018

Pannexin channels are a family of recently discovered membrane proteins found in nearly every tissue of the human body. These channels have been classified as large 'pore forming' proteins which, when activated, create a passageway through the cell membrane through which ions and molecules transit. Current literature suggests that the actual pannexin channel is formed from a hexameric arrangement of individual monomeric pannexin subunits, resulting in a central permeation pathway for conducting ions. Opening of pannexin channels can be accomplished through several mechanisms. During apoptosis, for example, cleavage of the pannexin C-terminal domain results in a constitutively open channel through which ATP is released. However, curiously, pannexins have also been known to be activated by a variety of other stimuli such as cellular depolarization, exposure to signaling ions like Ca^{2+} and K^{+}, and interacting with various other membrane receptors like members of the ATP-sensing P2X and P2Y family. How can pannexin channels sense and respond to such a diverse array of stimuli, and what is the fundamental 'gating process' that defines channel opening?

Here, we use electrophysiology to study the activation of pannexin-1 (Panx1). We used a protein chimera approach to identify that the first extracellular domain of Panx1 is critical for inhibitor action. Mutagenesis of this region identified that bulky

hydrophobic amino acids in this region confer sensitivity of the channel to various drug compounds. We also identified that the very N-terminus of Panx1 is important for voltage sensing, and that subtle modifications of the N-terminus results in channels with altered channel gating when exposed to voltage stimulation. Finally, we made attempts to solve the structure of a Panx1 channel. Iterative rounds of optimization yielded crystals that diffract x-rays just beyond 5 Å.

BIOGRAPHICAL SKETCH

Kevin grew up in New England and spent his childhood in Massachusetts and Vermont. He acquired his BS in Biochemistry from Siena College where he developed an interest in biological research. He matriculated into the BMCB graduate program at Cornell in 2012 and, for the past 5 years, he has worked under the supervision of Toshi Kawate.

ACKNOWLEDGEMENTS

I would like acknowledge the current members of the Kawate lab for being a pleasure to work with. I would also like to thank past and present members of the Department of Molecular Medicine who are always funny to talk to.

TABLE OF CONTENT

INTRODUCTION

Adenosine triphosphate (ATP) is classically recognized as the 'energy currency' of the cell. The high energy stored within ATP's γ-phosphate can be expended to fuel a multitude of biological reactions which cause a broad repertoire of downstream biochemical and biophysical effects. For example, energy released by the hydrolysis of ATP can be harnessed to transport molecules across a cell membrane resulting in nutrient movement within tissues, or to stroke myosin along an actin filament resulting in muscle contraction (1, 2). Furthermore, transfer of the γ-phosphate to protein substrates is one of the most widespread mechanisms used to toggle proteins between different conformational states (3). Thus, ATP and its hydrolysis are essential for life. However, not only can the energy stored in ATP be used for diverse cellular processes, but ATP itself can also act as a signaling molecule (4, 5). Adenosine, along with other purine and pyrimidine nucleotides, can be released into the extracellular space where they act as agonists for several types of receptor families, giving rise to the field of extracellular purinergic signaling.

Three broad protein families which bind to and are activated by nucleosides are the P1, P2X, and P2Y families. P1 and P2Y receptors are canonical G-protein couple receptors (GPCRs) which contain 7 transmembrane domains and an extracellular ligand binding pocket. Activation of P1 receptors by adenosine or P2Y receptors by ATP and other nucleosides results in a corresponding activation of G-protein signaling, either through $G_{q/11}$ or G_i. Downstream signaling mediated by these receptors can have broad physiological impacts such as modulation of neurotransmission, cardiac rhythm regulation, and immune cell communication (4). One important physiological example

of purinergic signaling is the essential role of P2Y12 in platelet function (6, 7). ADP found in high concentrations at the site of blood vessel injury will bind to P2Y12 receptors found on the surface of circulating platelets (7). Binding of ADP to this receptor stimulates platelet activation by raising the cytoplasmic Ca^{2+} concentration as a function of decreased adenylate cyclase activity (7). Ultimately, this triggers aggregation of platelets around the site of injury to promote blood clotting and wound healing. The importance of P2Y12 is demonstrated by patients with congenitally decreased or mutated forms of this receptor who suffer from prolonged bleeding due to impaired ability to form blood clots (8). As regulators of such important biological processes, receptors involved in purinergic signaling are promising targets for the treatment of various pathologies like Alzheimer's, asthma, and cardiovascular diseases. A variety of pharmaceuticals have been developed to specifically target these receptors in attempt to counteract the symptoms of these conditions (8, 9, 10).

A nucleotide-based signaling event is quenched by the rapid degradation of nucleotides into their purine or pyrimidine bases. This reaction is catalyzed by a family of ectonucleotides, which are membrane-embedded enzymes with an extracellular enzymatic domain (11, 12). Rapid degradation of ATP and other phospho-nucleotides results in only transient exposure of tissues to purine-based ligands outside of cells.

As implied by the name of this field, extracellular purinergic signaling depends on nucleotides found in the extracellular space. How are nucleotides released from cells and how is their release regulated?

One mechanism of nucleotide release is through regulated exocytosis of ATP-rich vesicles which commonly occurs at sites of neurotransmission (13, 14, 15). Similar to other neurotransmitters, ATP is transported into the lumen of vesicles which are poised to fuse with the cell membrane (14). When triggered by some cellular mechanism, vesicles fuse to the cell membrane and ATP is released into the synaptic space where it can interact with receptors in an autocrine or paracrine fashion (15).

A second mechanism of nucleotide release occurs during membrane breakdown during cell death (16). Cells which have initiated apoptosis or are experiencing pathological stress eventually lose membrane integrity. As cellular contents leak into the surrounding tissue, ATP acts as a 'find-me' signal to attract circulating macrophages. The macrophage travels to the site of high ATP concentration and consumes the apoptotic cell for nutrient salvage and recycling (17).

A third mechanism of ATP release is through large conductance ion channels. For years, the genetic identity of the ATP release channel remained elusive. Recently however, several ion channels have been proposed to release ATP including connexins, CALHM, TTYH, voltage-dependent anion channel-1, and pannexins (18, 19, 20, 21). These proteins putatively form pores or channels in the cell membrane that are spacious enough to accommodate the passage of large organic molecules. In particular, pannexins have emerged as *bona fide* ATP release channels with clear cellular and physiological phenotypes.

An overview of pannexin biology

The pannexin family was first reported in 2000 by Yuri Panchin *et al.*, who were searching for gap junction proteins common between vertebrates and invertebrates (22). Previously, the connexin family had been characterized as a gap junction channel present only in vertebrates while the innexin family had been discovered as the gap junction family in invertebrates. It's important to note that there is no genetic evidence suggesting that innexins and connexins are homologous – the primary sequences of these two protein families are different despite similar functional roles in different phyla. However, given that innexins are not present in vertebrates, one might expect to find that this family of proteins diverged significantly in evolutionary history. Thus, using PCR with degenerate primers on mollusc and flatworm cDNA libraries, Panchin *et al.* sought to identify innexin homologues in higher eukaryotes. They were successful in cloning sequences that, when entered into a BLAST homology search, matched with two human proteins of unknown function (one of which had the tentative name, "MRS1"). Further computational work predicted these two proteins each contained 4 transmembrane helices and two cysteine residues found in their extracellular loops – both features being hallmarks of the innexin and connexin primary sequences. Under the assumption that these two unknown proteins shared homology with innexins, they were dubbed "pannexins", meaning 'universal innexins' (22). It is now generally accepted that pannexins have weak homology with innexins and none with connexins.

Pannexin expression has since been confirmed in mammalian organisms. The distribution patterns of pannexin-1 (Panx1) and pannexin-2 (Panx2) are surprisingly ubiquitous with both proteins found in almost every human tissue (23, 24, 25, 26, 27). In particular, Panx2 is highly expressed in the skin (27). Pannexin-3 (Panx3)

expression is more conservative and has only been identified in skin, cartilage, heart, and osteoblast cells (28, 29). The fairly broad distribution of the pannexin proteins within human tissues may suggest this protein family performs a general functional role in biology that is common between all cell types, rather than a cell-specific or tissue-specific function. However, because Panx1 and Panx2 expression has been confirmed in the central nervous system researchers have been tempted to speculate on a potential role for these proteins in neurotransmission, considering their putative channel-forming properties. Though this vision is seductive to physiologists, the function and channel activity of Panx2 have yet to be firmly established and characterized. Panx3 is similarly enigmatic and currently no evidence suggests this protein forms an ion channel. This could imply that these putative channels may only open under a specific set of conditions (binding partners, post-translational modifications, lipid interactions, etc.) which may be governed by cell type, and this may be challenging to mimic in experimental setups. Overall, the expression pattern of pannexins is broad but it is unclear how this necessarily correlates to activity of these proteins.

Initial characterizations of pannexin channel properties were tumultuous. In 2003, Bruzzone *et al.* were first to report channel activity of Panx1 (25). Their reports suggest that Panx1 is capable of forming a voltage-gated channel which activates at voltages greater than +20 mV. Panx2 and Panx3, in contrast, presented no channel activity. Furthermore, their data concluded that Panx1 is capable of forming gap junctions in paired *Xenopus* oocytes, suggesting pannexins might be a new family of vertebral gap junction proteins.

This study initiated a significant debate regarding whether pannexins are capable of forming gap junctions. Over several years, after enough experimental evidence emerged, arguments were proposed which rationalized that pannexins are incapable of and do not form gap junctions (30). These arguments were based on glycosylation, localization, and channel activity in certain cell types. First, pannexins are unlikely to form gap junctions due to post-translational glycosylation found on the extracellular loops of all members of the pannexin family, since a chain of branched carbohydrates extending from the extracellular protein surface would prevent two pannexin units from docking face-to-face (31, 32). Second, localization studies revealed big differences in the expression pattern of pannexins compared to true gap junction forming proteins. Pannexins preferentially partition to the apical membrane of polarized cells, are diffusely found in intracellular compartments, or are found distributed evenly across the plasma membrane (30, 33). In contrast, true gap junction forming connexins (such as connexins-43) concentrate as dense puncta connecting the basolateral membranes of two neighboring cells (31, 34). Finally, pannexin channel activity has been found in cell types which do not typically form gap junctions such as erythroctyes, T cells, and macrophages (16, 26, 31). Combined, this evidence suggests pannexins do not form gap junctions but instead function as individual channels.

As a newly discovered ion channel with speculative ATP releasing activity, physiologists were curious about the consequences and phenotype of Panx1 knockout mice. $Panx1^{-/-}$, $Panx2^{-/-}$, and double knockout $Panx1^{-/-}$ $Panx2^{-/-}$ mice were generated and found to be completely viable, suggesting a non-essential role in physiology for Panx1 and Panx2 (35). Interestingly, data garnered from $Panx1^{-/-}$, $Panx2^{-/-}$, or double

knockout mice did not recapitulate many cellular based phenomena previously discovered to be dependent on pannexin channels (for example, IL-1β release and ATP release from astrocytes) (35). Instead, these mice were found to have a protective phenotype in murine models of stroke. Pannexin knockout mice displayed increased resistance to damage caused by ischemia as measured by behavioral assays, infarction size, and retinal ganglion cell death, suggesting a damaging role for pannexins during stroke (35). The mechanism surrounding this protective phenotype is still unclear, but hypotheses suggest ischemia is unable to cause as much cellular damage due to slower apoptosis progression in the absence of pannexins. Because ATP release through pannexins is a symptom of apoptosis, removing these channels from the system may prevent or slow this process from occurring. Based off these data Panx1 inhibitors are predicted to be beneficial for stroke victims.

A second line of pannexin knockout mice was generated at the University of Virginia. As previously reported, $Panx1^{-/-}$ mice were viable and displayed no differences from wild-type littermates (36). Here, pannexins were investigated for a role in neuropathic pain sensitivity and blood pressure regulation. Using sciatic nerve injury models, Panx1 was found to provide protection from mechanical pain hypersensitivity. In other words, $Panx1^{-/-}$ mice experienced reduced neuropathic pain after having their leg nerves cut, and this phenotype was persistent over 28 days compared to non-injured mice. This suggests a mechanism where Panx1 is directly related to pain sensitivity, but by what means? Interestingly, Panx1 expression in the nervous system was not required for pain sensing, however, expression in immune cells and hematopoietic cells was necessary for neuropathic pain transmission (36). Additional

work linked Panx1 expression in smooth muscle cells to blood pressure regulation. Previous experiments had established that activation of the α_1-adrenergic receptor results in downstream opening of Panx1 channels, but it was unclear what the physiological significance of this was. Mice treated with tamoxifen to induce the Panx1 deletion were found to have reduced arterial blood pressure compared to littermates lacking a floxed Panx1 gene. Interestingly, this phenotype was observed only during the night when rodents are most active, suggesting that epinephrine signaling through the α_1-adrenergic receptor is linked to Panx1 activity (56). As such, Panx1 may be a viable target for hypertension treatment.

Arguably, the physiological significance of pannexin activity has only been lightly probed. By and large, pannexin knockout mice do not experience any wildly unusual physiological or developmental defects (35, 36, 56). This could suggest that pannexins share overlapping functional roles with other ion channels or that pannexins play only a minor inconsequential role in greater biological systems. Finally, as discussed below, pannexin knockout mice may be a poor representation of pannexin biology. Mouse Panx1 has emerged to be vastly different in channel behavior compared to human Panx1. Due to this, it is unclear if pannexin knockout mice have any meaningful relevance to human biology.

The biophysical channel properties of Panx1 have been explored by various groups. Interestingly, a theme which has emerged suggests that the channel properties of Panx1 change depending on the expression system used. For example, when expressed in *Xenopus* oocytes, single channel conductance of Panx1 is generally reported to be ~500 pS (37, 38). A conductance this high is indicative of a remarkably

large pore. In mammalian cells, such as HEK293 cells, single channel conductance of Panx1 is reported to be between 70-100 pS, which is roughly 5-times smaller than the conductance displayed in oocytes (39, 40). Not only is single channel conductance confounding between expression systems, but mechanisms of activation are also different. In *Xenopus* oocytes, a repertoire of activation mechanisms have been reported including high concentrations of extracellular K^+, high concentrations of intracellular Ca^{2+}, and membrane stretching (mechanical activation) (37, 38, 41). In contrast, when expressed in mammalian cells pannexins can be activated by a different subset of stimuli like phosphorylation, cleavage of its C-terminal tail, and by voltage gating (16, 42, 43). Unfortunately, there is very little information exploring why discrepancies exist between these expression systems. There is at least some evidence that the activation mechanisms found in oocytes are not recapitulated in mammalian cells and that they may be exclusive only to that system (43). For example, Panx1 expressed in HEK293 cells exposed to elevated extracellular potassium or intracellular calcium displayed no evidence of channel activation, whereas these stimuli readily activate Panx1 in oocytes (43). It is likely that perhaps cellular components or lipid compositions might influence channel activity in either expression system, which may account for these differences in activity. For brevity and relevance, I will only summarize mechanisms of activation of Panx1 expressed in mammalian cells.

The P2X7-Panx1 interaction

The first characterization of Panx1 in mammalian cells linked Panx1 activation with activation of the ATP-gated P2X7 receptor. Previous studies had noted the unusual characteristic of P2X7 to initiate cell death upon prolonged activation, which

resulted in opening of an unusual large pore. Pelegrin and Surprenant initially attributed this unusual channel to Panx1 (44). They found that applying Panx1 inhibitors while also stimulating P2X7 with ATP caused a reduced amount of cell blebbing, dye updake, and IL-1β release. These were characteristics of the large 'unknown pore' and thus, were attributed to activity of Panx1. These data suggest that Panx1 opens in a P2X7-dependent mechanism, and was confirmed in HEK293T cells as well as human macrophage cell lines in addition to using siRNA against Panx1 (44). Unfortunately, the authors were using indirect means to measure Panx1 activity, such as dye uptake and cytokine release, without establishing whether the Panx1 ionic currents were changing. A more thorough investigation published by the same group at a later time refuted their previous results (45, 46). By measuring actual ionic currents of cells expressing both Panx1 and P2X7, no link between these two proteins was identified. Interestingly, they found that ATP (used to activate P2X7 in their previous experiments) is an inhibitor of Panx1, again confounding their previous studies.

Nonetheless, the P2X7-Panx1 complex still garners attention, perhaps suggesting this mechanism of Panx1 activation might be physiologically relevant. For example, P2X7 receptors found on intestinal enteric neurons of patients suffering from irritable bowel syndrome are capable of opening downstream Panx1, as measured by activation of nearby glial cells which respond to ATP released from the neurons (86). There are additional reports suggesting that activation of Panx1 in response to P2X7 activation is splice-variant sensitive. As reported by Xu *et al.,* only the P2X7aL451 variant displays evidence of Panx1 dye uptake as a function of P2X7 activation,

suggesting P2X7-Panx1 complex formation may not be a widespread phenomenon but can be observed only under certain genetic backgrounds (47).

Overall, characterization of Panx1 activation in response to P2X7 receptor activation is challenging to interrogate due to overlapping pharmacologies and pore properties. Both channels have been speculated to permeate large (300-900 Da) molecules but it was unclear if these molecules were directly permeating P2X7, Panx1, both channels, or if perhaps they were transiting the cell membrane by other means (connexins, exocytosis). It has since been established that P2X7 itself is capable of dye permeation, but it is still unclear if purified Panx1 can as well (48). Nonetheless, these studies were the first to establish that Panx1 currents could be measured in mammalian cells, which incited further interest in Panx1 physiology and biophysics.

Caspase cleavage of the Panx1 C-terminal domain

Caspase cleavage of the Panx1 C-terminal domain provides a curious link between channel regulation and cell biology. The motif “DVVD” located within the C-terminal domain of human Panx1 was identified as a cleavage site of caspases 3 and 7, which become active enzymes during apoptosis (16). Cleavage of this C-terminal site during apoptosis results in constitutive channel opening and prolonged ATP leakage. This mechanism recruits leukocytes and macrophages, which can sense the released ATP, to the site of apoptosis for clearance of the deceased cell and nutrient scavenge (16). Based off these data one would imagine that the C-terminus of Panx1 is tightly involved in regulating channel activity.

Indeed, further biochemical studies elucidated the mechanism of C-terminal pore blockage. One of the first experiments exploring this used a cysteine-cross linking strategy to decipher if the C-terminus was truly in the pore (49). In this experiment a putative pore lining residue was mutated to cysteine which would be able to form a disulfide bond to the very carboxy-terminal amino acid of Panx1, cysteine 426, only if it was sticking up into the pore. Under native conditions this mutant channel presented virtually no conductance. Treatment with a protease to cleave the C-terminus had little effect on channel activity, but, treating with both protease and TCEP fully opens the channel. Because protease alone did not open the channel, the C-terminus was still linked by the non-native disulfide bond, preventing ion conductance (49). This experiment suggests that distal C-terminal region likely acts as an auto inhibitor by sterically blocking the permeation pathway.

Details surrounding this mechanism were more thoroughly investigated in a follow-up study which sought to answer the question, how many C-terminal domains need to be removed from the pannexin oligomer for full channel opening? Concatameric channels – where 6 Panx1 subunits were fused in tandem – were generated where the C-terminal domain of some (or all) subunits contained a TEV protease recognition sequence. By comparing overall current density and ATP release from each variation of the TEV-cleaved concatameric channels, it was found that channel opening occurred stepwise as each individual C-terminal domain was removed from the overall pannexin oligomer (43). In other words, a channel where the C-terminal domain of one subunit was cleaved (leaving 5 intact C-terminal domains) had approximately $1/6^{th}$ the channel activity compared to a channel with all 6 C-terminal

domains removed (43). This discovery has interesting implications for Panx1 regulation. For example, in cells, is it possible for Panx1 to be regulated by how many C-terminal domains are removed? Perhaps there are scenarios where only several are processed to open low-conductance channels instead of having all cleaved to form the high-conductance ATP release channel. However, even the partially opened low-conductance channel would remain constitutively open unless additional regulation methods are identified.

Concerns might be raised when synthesizing literature about Panx1 from the past with newer information regarding this C-terminal cleavage mechanism of channel activation. For example, with all 6 C-terminal domains intact, recent studies propose that Panx1 is putatively non-conductive (activation by phosphorylation appears to mildly override this) (43). However, over a decade of previous electrophysiological experiments have been reported in which channlel activity could be observed from in-tact (not cleaved) Panx1 channels (25, 40, 44, 45). Some of these experiments were performed in oocytes, which already introduces a number of inconsistencies compared to mammalian cells, but many experiments were also performed in mammalian cells using full-length channels. The reasons for this discrepancy is unknown but it is tempting to hypothesize the possibility that pannexins may be regulated by additional factors not controlled for. As discussed below, post-translational modifications like phosphorylation have been shown to influence channel activation, which may not have been accounted for in previously published reports.

Phosphorylation control of Panx1

Post translational modifications of Panx1 have been the subject of several studies. In addition to glycosylation sites found on the extracellular portions of the channel, Panx1 can be subject to S-nitrosylation *in vitro*, which inhibits channel activity (50). Although two cysteines can be chemically modified with nitrosylation reagents, whether this can occur in native tissues is still in question.

In addition, phosphorylation has long been hypothesized to regulate Panx1 activity. As a general channel gating mechanism, phosphorylation is known to activate several types of ion channels including voltage gated K^+, L-type Ca^{2+} channels, GABAA receptors, NMDA receptors, and nicotinic acetylcholine receptors (51, 52). Prediction software has identified several tyrosine residues which may be subject to phosphorylation on Panx1, but *bona fide* evidence of this occurring had not been reported until recently. Two groups have each independently identified separate tyrosine phosphorylation sites which, when phosphorylated, promote channel opening.

The first evidence of phosphorylation control of Panx1 was identified as a downstream effect of NMDA receptor activation in the central nervous system. Over-activation of NMDA receptors on the postsynapse of cultured hypocampal neurons under ischemic conditions results in Panx1 activation as measured by cell blebbing and the appearance of secondary currents which appear even when NMDA receptors are blocked (53). These secondary currents are sensitive to Panx1 inhibitors. Interestingly, this mechanism of Panx1 activation is independent of ion influx through the NMDA receptor, as occupancy of both NMDA receptor ligand binding sites results in Panx1 activation even in the presence of NMDA receptor pore blockers. Src, a member of the

SFK family, was found to activate under these conditions and to phosphorylate Panx1 at tyrosine 308, located in the C-terminus, to promote channel opening (53, 54).

As part of a longstanding study on mechanisms of Panx1 activation as a result of α_1-adrenergic receptor (α_1AR) activation, a second phosphorylation site was identified as tyrosine 198, located on the Panx1 intracellular loop (42, 55, 56) . In vascular smooth muscle cells, activation of α_1AR by phenylephrine results in Panx1 activation. This mode of activation depends upon a specific sequence of amino acids found in the intracellular loop of Panx1, which curiously contains a highly conserved tyrosine residue (56). Further work in endothelial cells identified a second signaling mechanism, where activation of the TNF-α receptor by TNF-α also leads to Panx1 activation (42). Here, Src kinase was also found to act downsteam of TNF-α receptor activation to phosphorylate Panx1 at tyrosine 198 to induce channel opening.

Curiously, phosphorylation at either tyrosine position (308 or 198) appears to act completely independent from each other. Phosphorylation of either site by Src will induce channel opening, but details surrounding this mechanism are obscure. For example, it is currently unclear whether channel opening occurs only if one site is phosphorylated or if both are required. If phosphorylation at only one site is needed, what mechanism controls where Src phosphorylates? An interesting hypothesis could be that Panx1 is subject to alternative forms of phosphorylation depending on tissue expression. For example, Panx1 in the central nervous system might only be phosphorylated on Tyr308 while Panx1 in endothelial or smooth muscle cells might be phosphorylated only on Tyr198.

Voltage-gated channel activation

Ma *et al.* was first to report evidence of voltage-gated Panx1 currents in mammalian HEK293 cells (45). These currents are “outwardly rectifying”, meaning that stronger currents are found when a cell experiences positive membrane potentials compared to negative potentials. Panx1 channels appear to activate at +10 mV or greater and were sensitive to the small molecule compounds, carbenoxolone (CBX), DIDS, and probenecid, all of which had been previously characterized as Panx1 inhibitors in oocytes. Because this method of channel opening is ideal for patch-clamp electrophysiology experiments, it has been used to gather insights into the biophysical properties of the pannexin pore. The permeability properties of the voltage-gated Panx1 currents were explored by substituting the extracellular NaCl-based solution with solutions containing various anions. Currents were found to be anion selective with a permeability preference of $NO^{3-} > I^- > Br^- > Cl^- > F^-$ (39). While there is clear evidence that Panx1 has a preference for anions, this experiment does not necessarily exclude the possibility that sodium or other cations are able to transit the channel. Substitution of chloride with a larger anion like gluconate or aspartate caused a substantial decrease in current amplitude, but, a persistent and noticeable residual current remained apparent across a broad voltage range, perhaps suggesting the presence of weak sodium currents or weak permeation of these large anions. Considering Panx1 is characterized as a ‘large conductance ATP release’ protein, it is challenging to envisage it harboring an exquisite selectivity filter that only permeates anions. In any case, the physiological significance of Panx1 forming an anion selective channel have yet to be investigated.

Properties of the voltage gated Panx1 channel have only been marginally explored but it remains a controversial subject. The voltage gated Panx1 currents are significantly different from canonical voltage gated channels which may explain why this mechanism of channel activation is met with skepticism in regards to physiological relevance. Traditional voltage-gated channels are basally inactive until they experience a membrane depolarization. In the case of voltage-gated sodium channels, channel opening occurs with a $V_{1/2}$ of approximately -40 mV (57). These channels rapidly activate upon cellular depolarization and immediately begin to inactivate afterwards. In contrast, recombinant Panx1 channels experience channel opening across all voltages. This means, for example, Panx1 opening is observed even at physiological membrane potentials (-60 mV). However, the open probability of Panx1 channels is reported to change based on voltage. Single channel recordings from Panx1 transfected HEK293 cells have suggested that open probability of Panx1 changes from ~25% at physiological potentials to ~60% at positive potentials, revealing that Panx1 possesses a voltage-sensing channel gate (40). This study is further supported by additional experiments which clearly show voltage dependence of channel open probability.

In contrast, using caspase-cleaved or artificially truncated Panx1 channels, *Chiu et al*. report that channel open probability (~40%) does not change across a voltage range between -80 mV to +80 mV (43). This suggests that the ability of Panx1 to sense voltage does not necessarily influence the channel gate, as open probability is constant. This data would effectively rule out the idea that Panx1 activates by a change in membrane potential. However, this experiment is performed in context of the caspase cleaved channel which would naturally result in a constitutively open pore. One might

suggest that channels where the C-terminal domains of each subunit are truncated may exhibit properties different than the wild-type channel, but, as argued, the current-voltage relationship does not change as each C-terminal domain is progressively removed from the channel. This suggests that individual each C-terminal domain does not influence Panx1 voltage gated activity (43).

As a final note, there is currently no evidence suggesting that Panx1 voltage-gated currents are linked with ATP release through the channel (38). While pannexin activity can be clearly observed upon membrane depolarization, these currents only measure movement of sodium and chloride ions (typically). The subject of measuring ATP release while simultaneously performing electrophysiology has been addressed only in oocytes. Here, holding an Panx1-expressing oocyte at a membrane potential of +40 mV over the course of 20 minutes did not result in significant ATP release (38). In context of mammalian cells, the mechanism of ATP release is more obscure and does not always correlate with observed voltage gated currents. As described below, this trend is shown for mouse Panx1, which is reported to be constitutively active via electrophysiology but is incapable of releasing ATP (58).

To summarize, activation of Panx1 remains a subject of interest due to the complexity of mechanisms which affect channel gating. A brooding topic which needs to be addressed is how Panx1 is capable of sensing and integrating a number of diverse stimuli to regulate the release of ATP. Given the broad tissue distribution of pannexins, it is likely that cell-specific mechanisms may be in control of the channel, and understanding the details of this would be the key to determining physiological impacts of Panx1 activity. One final topic which is only marginally explored is that

electrophysiological evidence of Panx1 activity from native tissues has never been solidly reported. To study traditional voltage gated channels, one can extract tissue from mice and perform electrophysiological recordings from channels to understand their function in a native environment. This is particularly helpful for ion channels which utilize accessory proteins to modulate channel activation *in vivo*. For pannexin channels, direct electrophysiological evidence supporting that ion movement is occurring through pannexins in tissues has not been established. Indirect measurements of channel activity are used instead, including ATP release and dye uptake. In controlled systems these indirect measurements are helpful and robust for measuring Panx1 activity, but a host unknown factors may be present in native tissues which may obfuscate what is typically reported as pannexin channel opening.

The pannexin field is still relatively young, yet inconsistencies have emerged which confuse the field. In particular, comparing experimental data between research groups showcases obvious conflicting reports of channel activity. For example, some groups claim wild-type Panx1 is 'not functional' in the absence of additional stimuli, and that voltage does not activate the channel. Older studies, which established the activity of Panx1, suggest the opposite. These report that wild type Panx1 channels readily open upon membrane depolarization. An example of this is seen when comparing data from Ma *et al* or Romanov *et al* with data from Chiu *et al*, in which all groups report using the "wild-type" Panx1 in the same expression system (HEK cells), yet contrasting results are obtained (43, 45). Further confusion emerges when comparing different pannexin orthologs. Some groups have performed their experiments using mouse Panx1 and others have used human Panx1. While human Panx1 has accumulated

conflicting reports of activity (or that it only opens after its C-terminus is truncated), mouse Panx1 is purported to be constitutively active without any additional stimuli (60). Mouse and human Panx1 share 87% sequence identity, suggesting very subtle differences in channel primary sequence could result in substantially different channel activities. There is also an interesting difference when comparing ATP release from human and mouse Panx1. Counterintuitive to what one would expect, mouse Panx1 does not release ATP even though it is reported to be constitutively active, and human Panx1 is naturally inactive but will release ATP only when activated. An interesting experiment could be to gather various orthologs of Panx1 and rigorously characterize each for electrophysiology and ATP release to understand if human Panx1 is the norm or the exception in regards to pore properties. Nonetheless, it is unclear why various groups report vastly different channel activities, but we suspect some subtle differences in expression, cell quality, or technique may be at play.

One overarching question which has not been addressed is in regards to the molecular gating machinery which governs channel opening and closing. We know that pannexins can be activated by a variety of stimuli, but how do all these result in a conformational change that leads to channel opening? To answer this question, we pursued three avenues: Where do inhibitors interact and bind? Where and how does the voltage sensor work? And what is the structure of a pannexin channel?

There are several compounds discovered to inhibit Panx1 channels. These include the glycyrrhetinic acid derivative carbenoxolone (CBX), the gout remedy probenecid, the antidiabetic drug glybenclamide, the Cl^- transport inhibitor DIDS, and ATP. These compounds share virtually no structural similarities with each other and

have different affinities for Panx1, with CBX being the most potent with an IC50 of ~5 μM (45). The mechanism of action of these compounds is currently unknown. For a molecule to inhibit an ion channel, it must either block the permeation pathway or bind to a location that disrupts the conformational changes necessary to promote channel opening. We therefore hypothesize that by identifying binding site residues for Panx1 inhibitors we will locate general domains involved in regulating Panx1 channel activity. Additionally, identifying these positions would be important for understanding the chemistry behind how these compounds interact with Panx1.

Second, given that Panx1 can open in response to membrane depolarization, we hypothesized that this channel harbors a voltage sensor, as previously reported (40). This putative voltage sensor must be unusual since pannexins lack a traditional voltage sensing domain, as determined by analyzing their primary amino acid sequences. Understanding this mechanism of channel opening would try to establish the details of this gating mechanism and may characterize a novel voltage sensing mechanism. To go along with this, we also sought to explore differences between human and mouse Panx1 which have different basal activities.

Finally, we were interested in solving the first structure of a pannexin channel using x-ray crystallography. Doing so would answer many additional questions regarding pannexin function. For example, many general features of this protein are still uncertain. A structure would define the ion permeation pathway and channel gate, which would create more complete biophysical picture of this channel. Combined with the above functional work, crystallographic studies would define the structure of the drug binding pocket which would be beneficial for designing high affinity channel

antagonists. Furthermore, the overall architecture of the complex would be revealed to define the number of subunits that form the overall channel and display interfaces between them. Combined, the work presented here would have an impact on the field by clarifying mechanistic details surrounding pannexin activation and regulation.

CHAPTER I – Carbenoxolone inhibits Pannexin1 channels through interactions in the first extracellular loop [1]

Introduction

Pannexin1 (Panx1) constitutes an ATP release channel that plays important roles throughout the body (59, 60). In the immune system, for example, Panx1 mediates release of intracellular ATP as a “find-me” signal from apoptotic cells, facilitating the recruitment of macrophages for efficient cell clearance (16). In the nervous system, Panx1 controls synaptic excitability and plasticity (52, 61) and mediates propagation of astrocytic calcium waves (52; 62). Furthermore, recent studies using Panx1 knockout animals revealed that Panx1 contributes to noradrenergic vasoconstriction, which is important for blood pressure regulation (56). Although the list of physiological and pathological roles of Panx1 has been rapidly extending, the mechanism of Panx1 channel opening remains poorly understood (63).

Interestingly, Panx1 can be activated by a remarkably wide range of stimuli. Panx1 channels open in response to activation of different membrane receptors (26, 44, 52; 56), a high concentration of extracellular K^+ (37, 38) or intracellular Ca^{2+} (26), hypoxemia (64), caspase activation (16, 49), and voltage stimulation (25). How does Panx1 respond to such diverse stimuli? Functional Panx1 channels are most likely a hexamer (65), where each subunit harbors four predicted transmembrane helices and intracellular N and C termini. One proposed Panx1 activation mechanism involves the C terminus, which has been shown to plug the transmembrane pore,

[1] Content from Michalski K and Kawate T. Carbenoxolone inhibits Pannexin1 channels through interactions in the first extracellular loop. 2016. *J Gen Physiol*. 147(2):165-74.

rendering a resting Panx1 channel closed (49). Cleavage of this plug by caspase, in turn, opens the transmembrane pore. Although multiple studies support this mechanism (66, 67), other gating mechanisms likely exist, as Panx1 channels truncated by ~70 residues at the C terminus still remain closed at resting membrane potential (−60 mV) and open at a positive membrane potential (>+20 mV; 68).

Regardless of the kind of activation stimulus, most previous studies, including those supporting the C-terminal plugging mechanism, demonstrate that Panx1 channel activity can be attenuated by application of a commonly used gap-junction blocker, carbenoxolone (CBX; 52; 16; 64; 49; 38). We therefore rationalized that understanding how CBX inhibits Panx1 would be instrumental for dissecting the mechanism of how Panx1 channels open. This approach has been successfully used for dissecting the gating mechanisms of other ion channels, such as the *Shaker* K^+ channel (69) the *drk1* K^+ channel (70, 71), and the TRPV1 channel (72). Here, we describe how CBX inhibits Panx1 opening using electrophysiology and mutagenesis of human Panx1 (hPanx1) expressed in HEK293 cells. We chose to use voltage as the Panx1 opening stimulus because it is a robust and commonly used stimulus for probing Panx1 channel function.

Materials and Methods

Reagents

All chemicals were purchased from Sigma-Aldrich unless described otherwise.

Molecular biology

The full-length human Panx1 (Panx1; NCBI Protein GI: 39995064) and human Panx3 (Panx3; NCBI Protein GI: 16418453) genes were synthesized based on their protein sequences (GenScript) and cloned into the BamHI and XhoI sites of the pIE2 vector (modified from the pIRES-EGFP RK6 vector provided by M. Mayer, National Institutes of Health, Bethesda, MD) or a modified pIE2 vector containing an N-terminal flag tag. Point mutations were introduced into constructs via QuikChange site-directed mutagenesis (Agilent Technologies) or by PCR. The loop1 chimera construct was generated by PCR and contains residues 56–107 of Panx3. Chimera A contains residues 89–105 of Panx3, and chimera B contains residues 58–88 of Panx3. All chimeras and point mutations were generated based on the full-length Panx1 construct.

Electrophysiology

HEK293 cells were maintained in a humidified CO_2 incubator at 37°C in DMEM (Gibco) supplemented with 10% FBS (Atlanta Biologicals) and 10 µg/ml gentamicin (Gibco). 2 d before recording, cells were plated at a density of 10^5 cells/well onto 12-mm glass coverslips in wells of a 6-well plate (Corning). Cells were transfected with 300–800 ng plasmid DNA using FuGENE 6 (Promega) as per the manufacturer's instructions and used for electrophysiological recordings after 16–24 h. For recordings using Chinese hamster ovary (CHO) cells (CHO-K1; ATCC), cells were cultured in F-12K nutrient mix media (Gibco) supplemented with 10% FBS and 10 µg/ml gentamicin. Cells were plated to confluency on 35-mm dishes and transfected with 2 µg DNA using FuGENE 6 as

directed by the manufacturer. Cells were trypsinized 24 h later, plated onto glass coverslips in wells of a 6-well plate, and used for electrophysiological recordings 2–6 h after plating. Borosilicate micropipettes (Harvard Apparatus) were pulled and heat polished to a final resistance of 1–6 MΩ and backfilled with pipette buffer containing (mM) 147 NaCl, 10 HEPES, and 10 EGTA, which was adjusted to pH 7.0 with NaOH. Whole cell patches were obtained in external buffer containing (mM) 147 NaCl, 2 KCl, 2 $CaCl_2$, 1 $MgCl_2$, 13 glucose, and 10 HEPES (adjusted to pH 7.3 with NaOH). Whole cell patches were perfused with external buffers with or without inhibitors using a rapid solution exchange system (RSC-200; Bio-Logic). Currents were recorded using an Axopatch 200B patch clamp amplifier (Axon Instruments), filtered at 2 kHz (Frequency Devices), digitized using Digidata 1440A (Axon Instruments) with a sampling frequency of 10 kHz, and analyzed using pCLAMP 10 software (Axon Instruments). To record pannexin channel activity, three similar voltage step protocols were used. In the first protocol, cells were held at −60 mV, stepped to a potential between −100 and 100 mV for 1 s (20 mV per step), and returned to −60 mV for 10 s to allow channels to close before the next step. In the second, which was used for current quantification (bar graphs and dose responses), cells were held at −50 mV, stepped to a potential between −100 and 100 mV for 0.5 s (50 mV per step), and returned to −50 mV for 2 s before the next step. In the third, used for conductance-voltage (G-V) plots, cells were held at −60 mV, stepped to a potential between −100 and 180 mV for 0.1 s (20 mV per step), and returned to −60 mV for 2 s. Because Panx1-expressing HEK293 cells sometimes exhibit leak currents that are relatively CBX insensitive even at negative potentials, we used the cells if the maximum current amplitude at 100 mV was at least 10-times greater than

the current amplitude at −100 mV. Inhibitors of Panx1 were prepared fresh daily and used on the same day. Stock solutions of CBX (30 mM), ATP (1 M), and 4,4′-diisothiocyano-2,2′-stilbenedisulfonic acid (DIDS; 30 mM) were prepared in water and stock solutions of probenecid (300 mM) and glybenclamide (50 mM) were prepared in DMSO. All external solutions containing Panx1 inhibitors were adjusted to pH 7.3 with NaOH before application to cells.

Cell surface biotinylation

HEK293 cells were cultured as described in the previous section, plated in wells of a 6-well plate, and transfected at ~80% confluency with 2 µg plasmid DNA (N-terminal flag tagged pannexins) using polyethylenimine (Polysciences). After 2-d incubation, cells were washed twice with PBS, transferred to a microcentrifuge tube, resuspended in 2 ml of 0.5 mg/ml sulfo-NHS-SS-biotin (Thermo Fisher Scientific), and rotated at 4°C for 40 min. Labeling was quenched by resuspending cells twice in PBS with 50 mM NH_4Cl for 5 min at 4°C, followed by two more washes with PBS. Cells were lysed by rotating for 30 min in RIPA buffer containing 150 mM NaCl, 3 mM $MgCl_2$, 1% NP-40, 0.5% deoxycholate (Anatrace), 0.1% SDS (Bio-Rad Laboratories), and 20 mM HEPES (adjusted to pH 7.4 with NaOH) and supplemented with protease inhibitor cocktail (Thermo Fisher Scientific). Lysates were cleared by centrifugation (22,000 *g*, 15 min), and equal amounts of protein were incubated with 35 µl streptavidin-Sepharose slurry (GE Healthcare; 50%; pre-equilibrated in RIPA buffer) for 2.5 h with inverting. Resin was washed six times with 700 µl RIPA buffer and eluted with SDS-PAGE sample buffer with 75 mM DTT (Thermo Fisher Scientific) for 30 min at 55°C with intermittent

vortexing. Protein content was resolved using standard blotting techniques. In brief, protein was separated on 8% SDS-PAGE gels, blotted onto a PVDF membrane (Bio-Rad Laboratories), probed with monoclonal flag-M2 antibody (1:1,000) or monoclonal actin antibody (1:1,000; line AC-40), labeled with an anti–mouse AP-conjugate secondary antibody (1:1,000; Bio-Rad Laboratories), and developed using colorimetric AP substrate (Bio-Rad Laboratories).

Results

A chimera between Panx1 and Panx3 reveals that the first extracellular loop plays a crucial role in CBX-mediated inhibition

The objective of this study was to dissect the action mechanism of CBX, a widely used small molecule for inhibiting Panx1 channel function. Because CBX can inhibit Panx1 channels activated by a variety of stimuli, understanding the action mechanism of CBX would help investigate the mechanism underlying Panx1 channel gating. To probe Panx1 channel activity, we performed whole cell voltage-clamp experiments using HEK293 cells transfected with Panx1. As reported previously (25, 44, 45), voltage stimuli gave rise to outwardly rectifying currents that were suppressed by extracellular CBX (Figure 1.1A). Notably, the extent of Panx1 current suppression by CBX was greater for strongly rectifying channels (~90% suppression at 100 mV) than those weakly rectifying (~50% suppression at 100 mV; Figure 1.1B), which was confirmed by a linear regression analysis ($R = -0.75$; Figure 1.1C). We therefore decided to use Panx1-expressing cells whose maximum current amplitude at 100 mV was at least 10-times greater than the current amplitude at −100 mV. We confirmed that the recorded

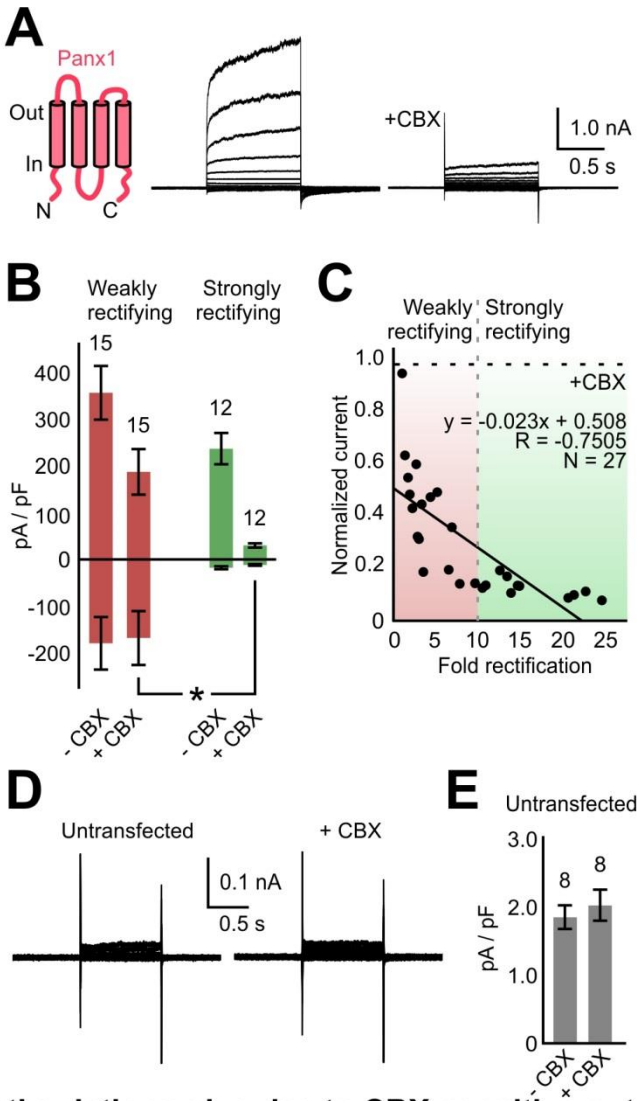

Figure 1.1. Voltage stimulations give rise to CBX-sensitive outward currents mediated by human Panx1 expressed in HEK293 cells. (A) Whole cell recordings of Panx1 in the absence (left) or presence (right) of 100 μM CBX. Voltages were stepped (−100 to 100 mV, 20-mV increments) from a holding potential of −60 mV. (B) Comparison of CBX sensitivity between Panx1-expressing HEK293 cells displaying weakly rectifying currents (red) and those displaying strongly rectifying currents (green). Bars represent mean current density at 100 and at −100 mV in the presence or absence of 100 μM CBX. Numbers above the graphs indicate the number of cells used for this experiment, and error bars represent SEM. Asterisks denote significance with $P < 0.05$ determined by Student's t test. (C) Linear regression analysis comparing current rectification with normalized current in the presence of 100 μM CBX. Each point represents a single cell used in B. (D) Whole cell recordings from an untransfected HEK293 cell in the absence (left) or presence (right) of 100 μM CBX. Cells were held at −60 mV and stepped between −100 and 100 mV (20-mV intervals). (E) Mean current density of untransfected HEK293 cells when stepped from a holding potential of −50 to 100 mV with or without 100 μM CBX. Bars represent mean current density of the indicated number of cells, and error bars represent SEM.

channel activity was mediated by transfected Panx1, as untransfected cells exhibited little channel activity with or without CBX (Figure 1.1D and E).

To localize the important regions of Panx1 for CBX action, we took advantage of Panx3, a closely related Panx1 homologue that likely adopts a similar architecture to Panx1 (shares ~45% sequence identity). Unlike Panx1, however, Panx3 does not give rise to current by voltage stimulation (Figure 1.2A, top) even though the surface expression in HEK293 cells was verified (Figure 1.2B, lanes "3"). Although the effect of CBX on Panx3 is unknown, it is possible that a Panx1/3 chimera, in which a domain of Panx1 important for CBX action is replaced with an equivalent domain of Panx3, may become insensitive to CBX. We generated a series of Panx1/3 chimeras and systematically analyzed the voltage-gated channel activity and the effect of CBX on each chimera. To our surprise, the voltage-gated channel activity of one of the chimeras, whose first extracellular loop of Panx1 was replaced with the equivalent loop of Panx3 (loop1 chimera), was actually enhanced by an application of CBX (Figure 1.2A, bottom). This result indicates that the action of CBX is likely mediated by the first extracellular loop. Although the mean current density of the loop1 chimera in the absence of CBX was about four times smaller than that of Panx1 (Figure 1.2C), this was not caused by a lower number of channels as this chimera expressed well on the cell surface (Figure 1.2B, lanes "C"). Also, the enhanced channel activity of the loop1 chimera by CBX was unlikely caused by unknown channels expressed in HEK293 cells, as we observed similar current enhancement from CHO cells transfected with the loop1 chimera (Figure 1.3). Current enhancement of the loop1 chimera was dose dependent, and the enhanced voltage-gated channel activity obtained with a saturating

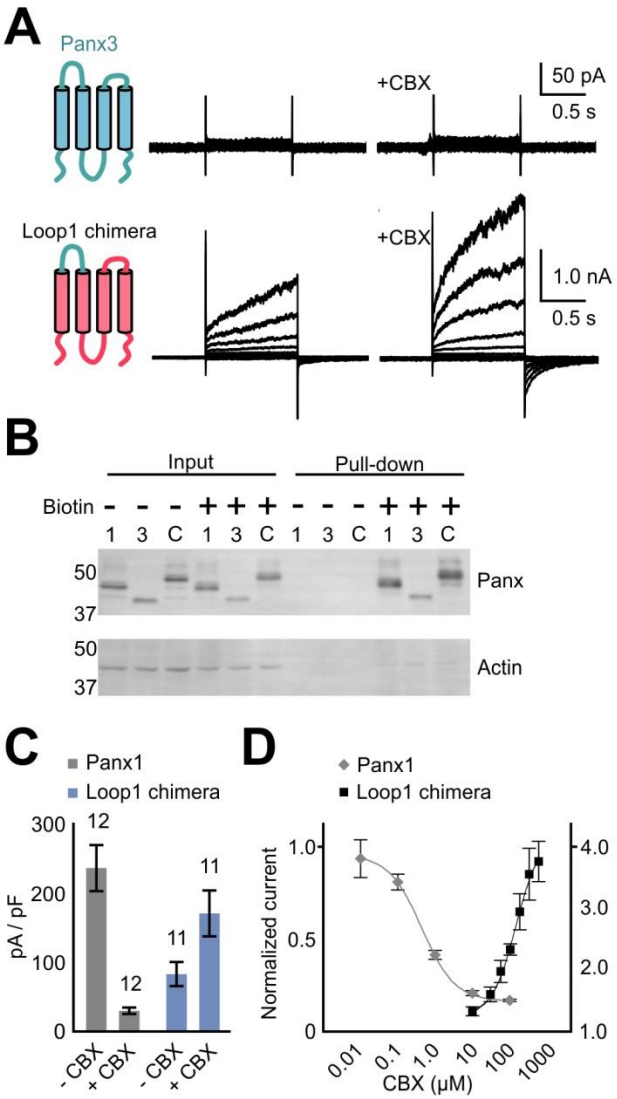

Figure 1.2. Inhibitory effect of CBX on voltage-activated Panx1 currents is reversed by swapping the first extracellular loop with Panx3. (A) Whole cell recordings of Panx3 (top) and the Panx1/3 loop1 chimera (bottom) in the absence (left) or presence (right) of 100 μM CBX. Voltages were stepped (−100 to 100 mV, 20-mV increments) from a holding potential of −60 mV. Loop1 chimera contains amino acids from the first extracellular loop of Panx3 (Q56 to L107). (B) Validation of cell surface–expressed Panx1, Panx3, and the loop1 chimera (1, 3, C, respectively). Each pannexin was tagged with an N-terminal flag peptide, and surface-expressed protein was labeled with sulfo-NHS-SS biotin. Labeled protein was enriched and analyzed by Western blots using anti-flag antibody (top). For loading and pull-down controls, Western blots using anti-actin antibody are also shown (bottom). Units are in kilodaltons. (C) Mean current densities of Panx1 (gray) and the loop1 chimera (blue). Voltages were stepped from −50 to 100 mV in the presence or absence of 100 μM CBX. Numbers above the bars indicate the number of cells used for this study, and error bars represent SEM. (D) CBX dose response of Panx1 (gray) and the loop1 chimera (black) activated by voltage stimuli (stepped from −50 to 100 mV). CBX-modified currents were normalized to the currents without CBX (left axis: Panx1; right axis: loop1 chimera). Each point represents the mean value of 5–12 cells, and error bars represent SEM.

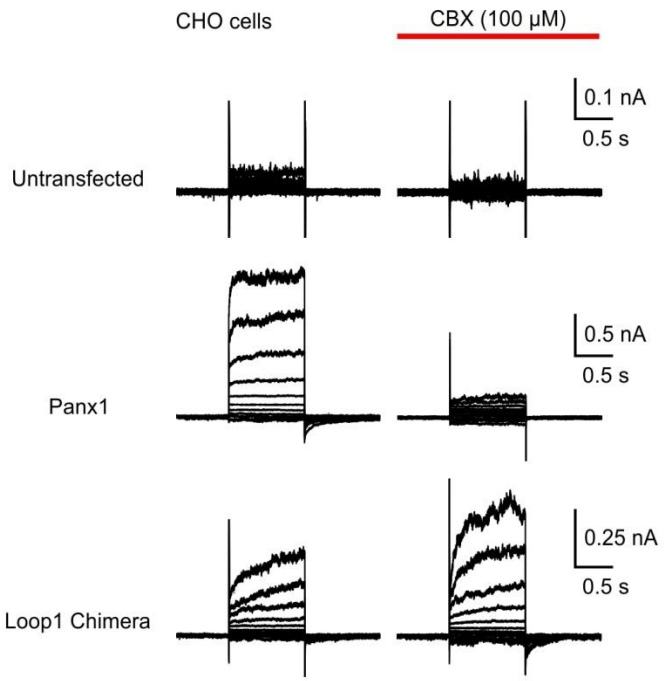

Figure 1.3. CBX potentiates the voltage-gated channel activity of loop1 chimera expressed in CHO cells. (A) Representative whole cell recordings of untransfected CHO cells (top), CHO cells transfected with Panx1 (middle), or the loop1 chimera (bottom) in the absence (left) or presence (right) of 100 μM CBX. Voltages were stepped (100 to 100 mV, 20-mV increments) from a holding potential of -60 mV.

concentration of CBX (562 μM) was almost fourfold greater than that without CBX (Figure 1.2D). These findings suggest that CBX is probably not a pore blocker, but likely a gating modulator that acts through the first extracellular loop of Panx1.

W74 plays central roles in CBX-mediated inhibition of Panx1

Among the 52 residues in the first extracellular loop, 26 residues are different between Panx1 and Panx3. Interestingly, the majority of different residues (15 out of 26) are clustered in the last 20 residues in this loop (Figure 1.4). We wondered whether this variable region mediates CBX-dependent inhibition of Panx1 and whether substitution of this region with Panx3 confers the opposite effect of CBX on the loop1 chimera. To test this idea, we generated two variants of the loop1 chimera. The first chimera (chimera A)

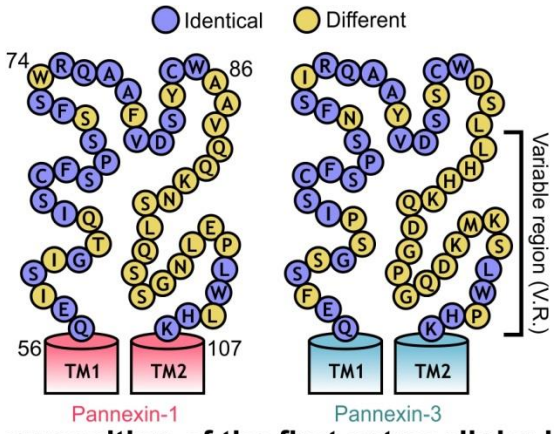

Figure 1.4. Sequence composition of the first extracellular loops of Panx1 and Panx3. Amino acids constituting the first extracellular loops of Panx1 (left; Q56 to K107) and Panx3 (right; Q56 to K108). Identical residues are colored in purple, and different residues are colored in yellow. The variable region (V.R.) is marked with a bracket.

harbors the variable region of Panx3 but is otherwise Panx1 in this loop. The second chimera (chimera B) harbors the variable region of Panx1 but is otherwise Panx3 in this loop. Both chimeras responded well to voltage stimulation; however, chimera A was effectively inhibited by CBX (Figure 1.5A), which was against our idea that the variable region harbors important residues for CBX-mediated inhibition of Panx1. On the contrary, the voltage-gated channel activity of chimera B was enhanced by CBX, similar to what we observed with the parent loop1 chimera (Figure 1.5B). These results suggest that the relatively conserved region in the first extracellular loop harbors important residues for mediating CBX-dependent inhibition of Panx1.

To identify the residues important for CBX dependent inhibition of Panx1, we generated 11 single point mutants of Panx1, each of which contains a different Panx3 residue within the first ~30 residues of the first extracellular loop. Among those, nine mutants were effectively inhibited by CBX, to an extent which WT Panx1 was inhibited (Figure 1.5C). In contrast, voltage-activated currents of the W74I mutant were unchanged (or slightly enhanced), and that of the A86D mutant were inhibited only to 50% of its maximum (Figure 1.5C). Notably, CBX enhanced the voltage-activated

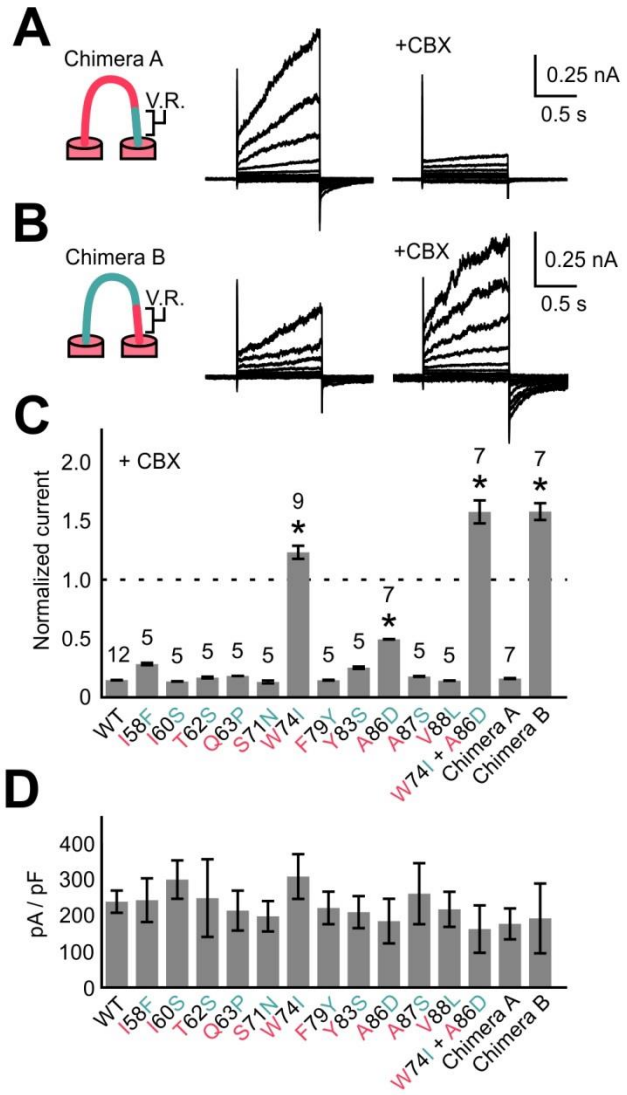

Figure 1.5. W74 in the first extracellular loop plays a central role in determining the polarity of CBX action. (A and B) Whole cell recordings of chimeras A and B in the absence (left) or presence (right) of 100 μM CBX. Voltages were stepped (−100 to 100 mV in 20-mV increments) from a holding potential of −60 mV. Chimera A harbors the variable region of Panx3, and chimera B harbors the other part of Panx3 in the first extracellular loop. (C) Panx1 point mutants were generated based on their Panx3 counterparts and tested for CBX-mediated current modification using the whole cell patch clamp method. Bars represent mean currents at 100 mV in the presence of 100 μM CBX normalized to the currents obtained in the absence of CBX. Error bars represent SEM of the indicated number of patches. Asterisks indicate significance of $P < 0.05$ determined by one-way ANOVA followed by Dunnett's test comparing WT with each mutant. Numbers above the bars indicate the number of cells used for this study. (D) Current densities of Panx1 mutants. Each bar represents mean current density at 100 mV, and error bars represent SEM.

current of W74I/A86D double mutant to a similar extent as this drug enhances the

chimera B channel activity. Current densities of these mutants in the absence of CBX

were comparable (Figure 1.5D). These data suggest that W74 and A86 in the first extracellular loop play important roles in CBX-mediated Panx1 inhibition. In particular, W74 seems to play a crucial role in determining the polarity of CBX action.

If W74 plays a key role in allowing CBX to function as an inhibitor, a single I74W mutation would convert loop1 chimera into a channel that is inhibited by CBX. Indeed, the voltage-activated current from the I74W loop1 chimera mutant was inhibited by 100 μM CBX (Figure 1.6A), a concentration that would enhance the voltage-activated current of the loop1 chimera by ~2.3-fold (Figure 1.2D). This result strongly supports the idea that residue 74 in the first extracellular loop determines the polarity of CBX action and that tryptophan at this position enables CBX to function as an inhibitor. To further explore what kind of amino acid at position 74 possesses the ability to determine the polarity of CBX action, we created a series of single mutants at this position and compared the effect of CBX on voltage-gated channel activities. When W74 was mutated to alanine, we observed strong enhancement of the voltage-activated current (Figure 1.6C, W74A). When W74 was substituted with charged residues (i.e., Lys or Asp), CBX either weakly enhanced or only slightly inhibited the voltage-activated currents (Figure 1.6C, W74K and W74D). Likewise, when W74 was substituted with cysteine, CBX only slightly inhibited the voltage-activated current (Figure 1.6C, W74C). In contrast, when W74 was substituted with phenylalanine, CBX strongly inhibited the voltage-activated current (Figure 1.6C, W74F). The effect of CBX was unrelated to the current density of each mutant (Figure 1.6D and E). These results suggest that an aromatic amino acid at position 74 in the first extracellular loop mediates the inhibitory action of CBX, whereas other amino acids compromise or reverse this action.

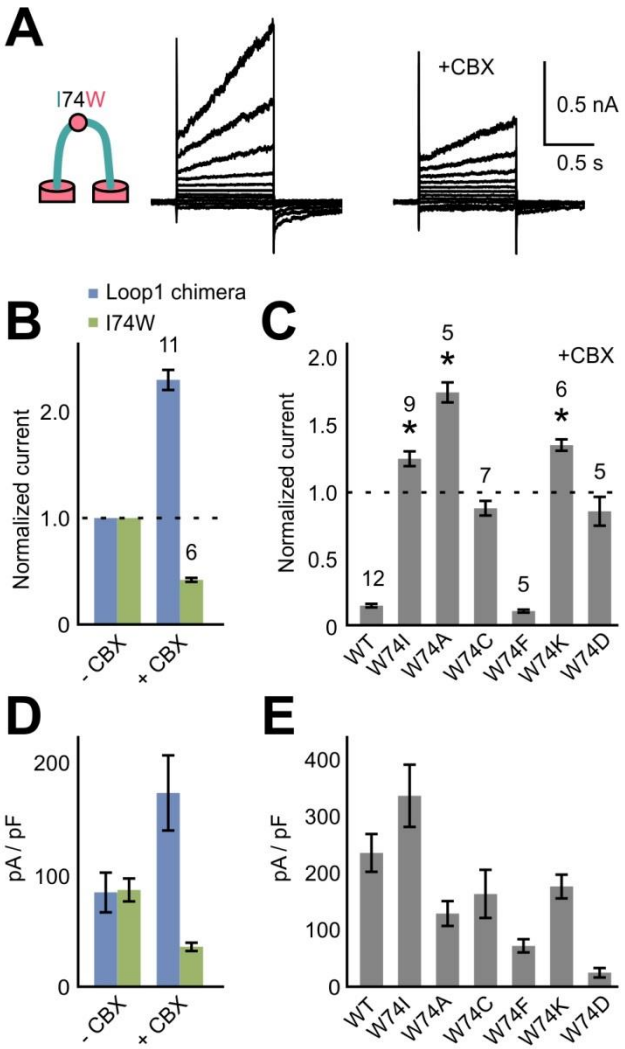

Figure 1.6. Amino acid at position 74 heavily influences the polarity of CBX action on voltage-activated Panx1 currents. (A) Whole cell patch clamp recordings presenting that the I74W mutation restores the inhibitory action of CBX on the loop1 chimera. Voltages were stepped (−100 to 100 mV with 20-mV increments) from the holding potential of −60 mV. (B) Normalized voltage-activated currents (100 mV) of the loop1 chimera (blue) and I74W mutant of the loop1 chimera (green). (C) Normalized CBX-modified currents of Panx1 mutants at position 74. Asterisks denote significant potentiation with $P < 0.05$ determined by one-sample Student's t test comparing each mutant with a value of 1.0. (D) Current densities of the loop1 chimera (blue) and the I74W mutant (green) at 100 mV in the absence (left) or presence(right) of 100 μM CBX. (E) Current densities of Panx1 mutants. Numbers above the bars indicate the number of cells used for these experiments. Each bar represents mean current density at 100 mV, and error bars represent SEM.

Several conserved residues between Panx1 and Panx3 also play important roles in

CBX-dependent inhibition of Panx1

Thus far, we have focused on the different residues between Panx1 and Panx3 in the first extracellular loop, as these residues confer the enhancing activity of CBX on the loop1 chimera channel function. Given that CBX positively functions on the loop1 chimera, however, it is likely that the conserved residues between Panx1 and Panx3 also play roles in CBX action. For example, some of the conserved residues may mediate CBX binding. To systematically investigate the residues that contribute to CBX-dependent Panx1 inhibition, we generated cysteine mutants for all residues in this loop (residues 56–107) in Panx1 and examined the inhibitory action of CBX. To avoid potential disulfide formation between the introduced cysteine and naturally existing ones, we generated these cysteine mutants in “less cysteine” background, where five internal cysteines were mutated to serine (WT-5S: C136S, C170S, C216S, C347S, and C426S). Although a previous study suggests that the C426S mutation results in a constitutively open channel (73), in our hands using HEK293 cells, WT-5S behaved similar to WT Panx1 (Figure 1.7). We left C40 because a mutation at this position renders Panx1 channel constitutively open (74). We also left C66 and C84 for their potential roles in forming a native disulfide bridge. Except for D81C, all cysteine mutants gave rise to voltage-dependent currents. When 100 μM CBX was included in the extracellular solution, currents from most mutants diminished to ~10–20% of their maximum currents in a manner similar to WT-5S (Figure 1.8A). In contrast, currents from W74C, F67C, Q76C, and F79C remained mostly unchanged or only slightly reduced to ~80% of their maximum currents. These results suggest that, besides the Panx1-specific W74, the conserved residues F67, Q76, and F79 also play important roles in CBX-mediated inhibition of Panx1. In this region (i.e., residues 67–86), the other

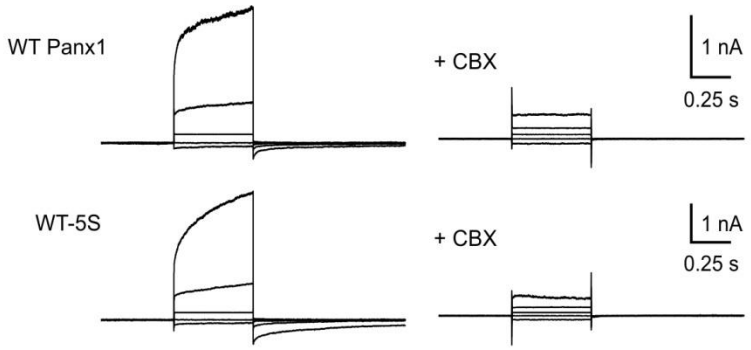

Figure 1.7. The WT-5S construct behaves similarly to Panx1. Whole cell currents from WT-5S and Panx1-transfected HEK293 cells. Voltage steps (-100 to 100 mV, 50-mV increments) from a holding potential of -50 mV were applied before (left) or during (right) an application of 100 μM CBX.

mutants, except S68C, S71C, and A77C, presented mild but statistically significant resistance to CBX (currents reduced to ~30–40%), suggesting that this region in the first extracellular loop plays central roles in the inhibitory action of CBX. Notably, A86C was inhibited by CBX to ~25% of its maximum, suggesting that cysteine at this position mimics the role of alanine rather than aspartate. Altogether, these results suggest that conserved residues between Panx1 and Panx3 located between residues 67 and 86 in the first extracellular loop play crucial roles—mediating CBX binding, for example—in CBX-mediated inhibition of Panx1 channel activity.

We found no obvious correlation between the current density and CBX-normalized currents from these Cys mutants (Figure 1.8B). To analyze the relationship between the current density and CBX-normalized current in general, we plotted these values for all the cells that were treated with CBX (n = 396), divided into two groups (inhibited vs. potentiated by CBX), and performed a linear regression analysis for each group (Figure 1.8C). We found only a minor correlation for the cells that are inhibited by CBX ($R = -0.31$), where 100 pA/pF difference would change the effect of CBX only by ~3%. This result disputes the idea that a moderate effect on inhibition could simply be caused by larger starting currents. Although we did observe a mild correlation between

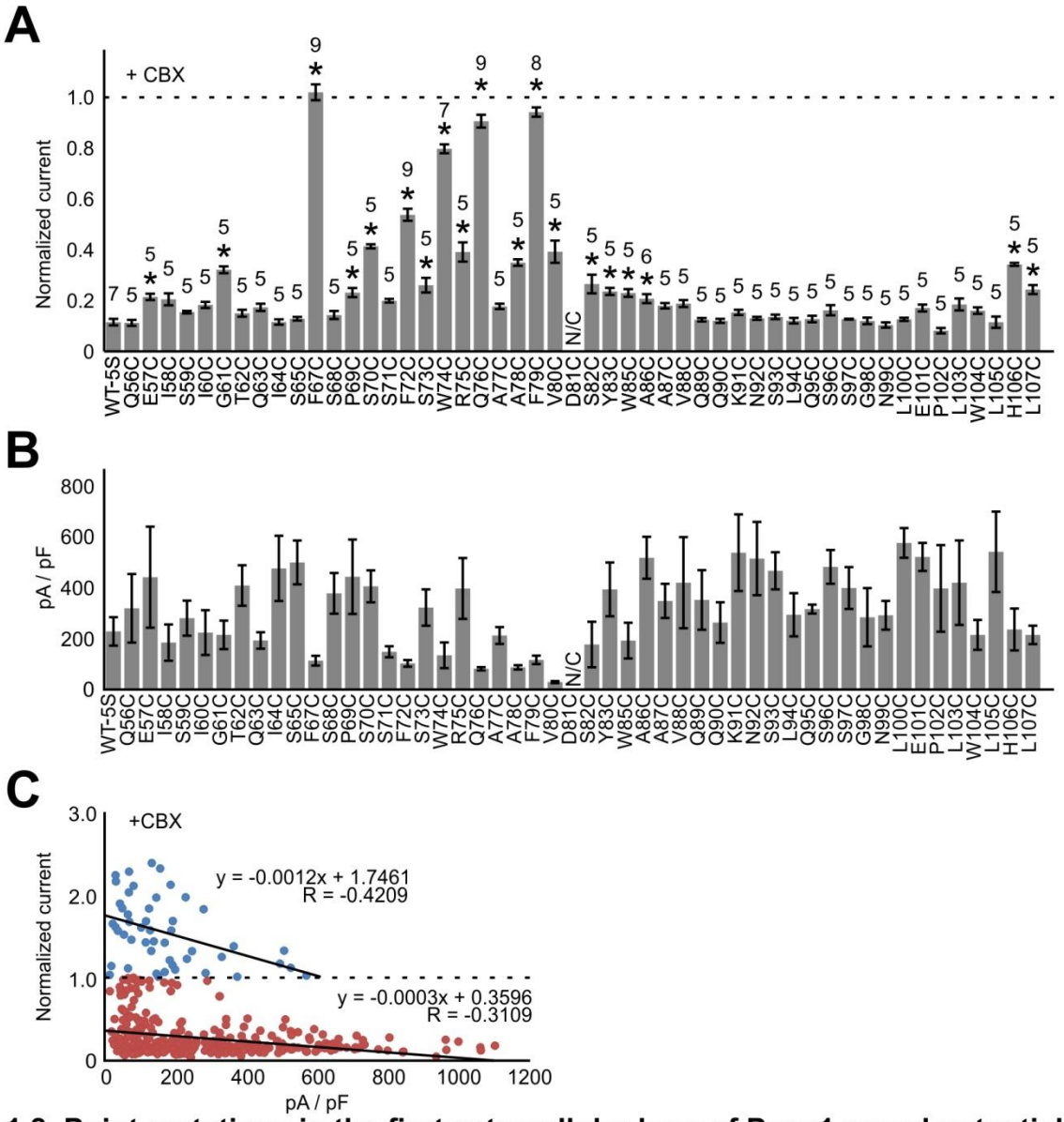

Figure 1.8. Point mutations in the first extracellular loop of Panx1 reveal potential residues that mediate CBX-dependent inhibition. (A) Quantification of whole cell currents triggered by voltage (100 mV) when treated with 100 μM CBX. Cysteine mutants were generated on a Panx1 construct where five internal cysteines were mutated to serine (WT-5S). Bars represent normalized mean currents, and error bars represent SEM. Numbers above the bars indicate the number of cells used for this study. Asterisks indicate significance with $P < 0.05$ determined by one-way ANOVA followed by Dunnett's test comparing WT-5S with each mutant. (B) Current densities of Cys mutants. Bars represent mean current density at 100 mV, and error bars represent SEM. N/C indicates no current. (C) Linear regression analyses comparing current density with normalized current in the presence of 100 μM CBX for all patches used in the present study (n = 396). Linear regression analyses were performed on cells that were potentiated upon CBX treatment (blue; n = 49) or patches that were inhibited by CBX (red; n = 347).

the current density and CBX-normalized current for the cells that are potentiated by

CBX (R = −0.42), the correlation and the slope (100 pA/pF difference would change the effect of CBX by ~10%) seem too weak to support the idea that activation by the drugs only happens in chimeras/mutants with small initial currents. Indeed, the channel activity of several constructs with >500 pA/pF current densities was enhanced by CBX.

Other Panx1 inhibitors also enhance the voltage-gated channel activity of the W74A mutant

We have demonstrated that a single residue at position 74 in the first extracellular loop can switch the polarity of CBX action on Panx1 channel activity, which strongly supports the idea that CBX functions as a gating modulator of Panx1. Do other Panx1 inhibitors function through a common modulation site? If they do, such Panx1 inhibitors may also enhance Panx1 channel activity when W74 is mutated to a nonaromatic residue. To test this idea, we compared voltage-activated currents of the W74A mutant with or without four different inhibitors, namely, glybenclamide (150 μM), ATP (10 mM), probenecid (3 mM), and disodium DIDS (200 μM). Because the EC_{50} of CBX on the loop1 chimera (~120 μM; Figure 1.2D) was ~40-times higher than the IC_{50} on Panx1 (~2 μM; Figure 1.2D), we decided to use at least a 10-times higher concentration of each inhibitor than its published IC_{50} value (45, 75), except for glybenclamide which was insoluble above a concentration ~3-times higher than its IC_{50}. Among these four inhibitors, glybenclamide, ATP, and probenecid enhanced the voltage-activated channel activity of W74A (Figure 1.9). In particular, probenecid enhanced the voltage-gated currents of W74A by ~3-fold, which was even stronger than the effect of CBX (~1.8-fold increase). DIDS, in contrast, did not alter the voltage-gated currents of W74A, suggesting that its mechanism of action may be different even

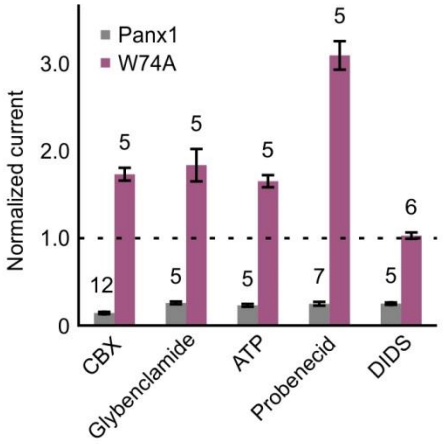

Figure 1.9. Several known Panx1 inhibitors also enhance voltage-activated currents of the Panx1 W74A point mutant. Bars represent mean currents in the presence of different inhibitors at 100 mV. Currents were normalized to those in the absence of inhibitors. Gray: Panx1; purple: Panx1 W74A. Concentrations used for each drug were as follows: 100 μM CBX, 150 μM glybenclamide, 10 mM ATP, 3 mM probenecid, and 200 μM DIDS. Numbers above the bars indicate the number of cells used for this study, and error bars represent SEM.

though it also relies on residue 74 to inhibit Panx1. In support of this idea, the off rate of DIDS was substantially slower than those of the other inhibitors, making the reaction almost irreversible at a high concentration (Figure 1.10). These results highlight that W74 is essential not only for CBX, but also for the other four Panx1 inhibitors to function. Furthermore, our results demonstrate that these inhibitors, except for DIDS, can positively modulate Panx1 through the first extracellular loop when tryptophan at 74 is mutated to alanine.

Probenecid can activate the W74A mutant without voltage stimulation

Given that the enhancing action of probenecid on the W74A mutant was remarkable (i.e., approximately threefold enhancement at 100 mV), we wondered whether probenecid alone could open W74A channels without voltage stimulation. When a cell expressing WT Panx1 was held at a resting membrane potential (−60 mV), probenecid did not give rise to inward currents, but instead, this drug attenuated the

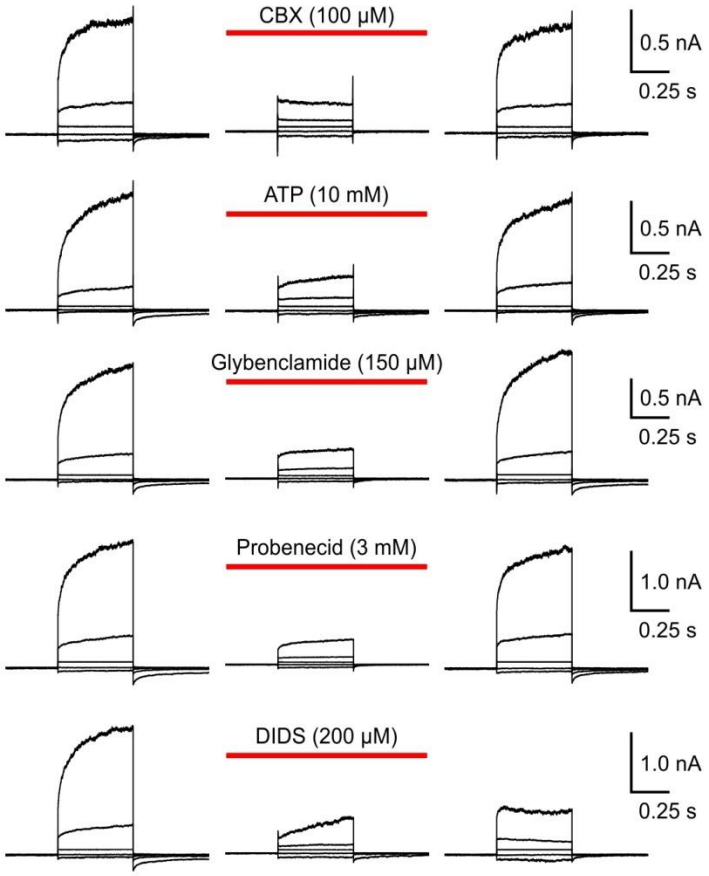

Figure 1.10. Whole cell recordings suggest that the inhibitory effect of DIDS is irreversible. Panx1 was activated by voltage steps (-100 to 100 mV, 50-mV increments) from a holding potential of -50 mV and exposed to an external buffer containing different Panx1 inhibitors at the following concentrations: 100 μM CBX, 10 mM ATP, 150 μM glybenclamide, 3 mM probenecid, and 200 μM DIDS. Control voltage steps before (left) and after (right) application of the inhibitor suggest that DIDS may irreversibly inhibit Panx1. Recordings were obtained after perfusing cells for 5–10 s with inhibitor solutions, and post-inhibitor recordings were obtained after a 20–25-s wash with external buffer.

leak currents to some extent (Figure 1.11A, top traces). Interestingly, inhibition of the leak current was transient, and removal of probenecid gave rise to a large tail current, suggesting that binding of probenecid trapped Panx1 in a nonresting closed conformation. This effect of probenecid was not an off-target artifact, as this drug has no effect on untransfected HEK293 cells (Figure 1.12). Though the exact mechanism is beyond the scope of this study, this result also supports the idea that probenecid functions as a gating modulator of Panx1. In contrast, both the loop1 chimera and the

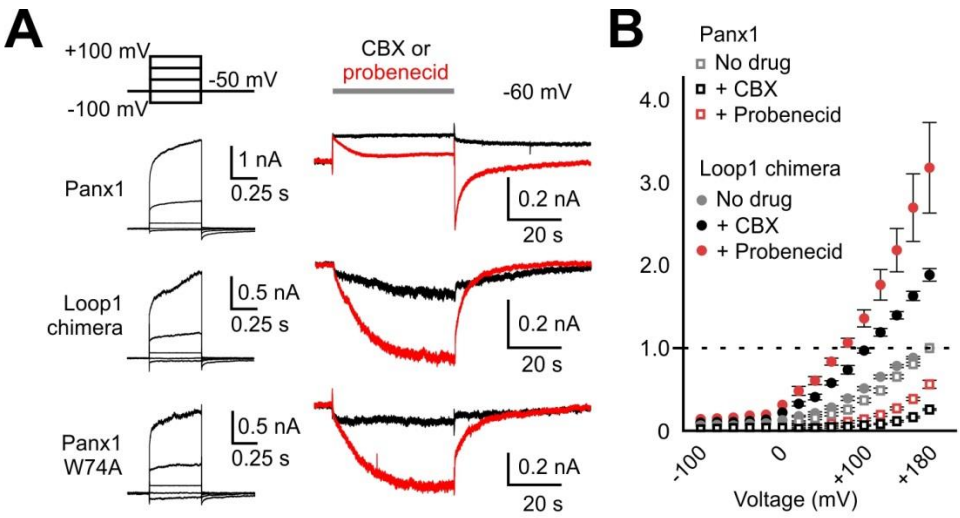

Figure 1.11. Probenecid can activate the Panx1 W74A point mutant at a resting membrane potential. (A) Whole cell recordings of Panx1 (top), loop1 chimera (middle), or W74A mutant (bottom) when exposed to 562 μM CBX (black) or 10 mM probenecid (red). Patches were held at −60 mV, and drugs were applied during the indicated length of time. Voltage-gated channel activity of each Panx1 construct is shown in the left traces. (B) G-V relationship of loop1 chimera (gray circles) and that in the presence of 100 μM CBX (black circles) or 3 mM probenecid (red circles). G-V relationship for WT Panx1 is shown as empty squares. Data were normalized to current without drugs at 180 mV. Each point represents the mean value, and error bars (shown only for points >0 mV) represent SEM (n = 5–10).

W74A mutant gave rise to inward currents upon probenecid application at −60 mV (Figure 1.11A, middle and bottom traces). These results indicate that probenecid can function as an agonist of the Panx1 channel if the tryptophan residue is replaced with a nonaromatic residue at position 74 in the first extracellular loop. Though the loop1 chimera did give rise to a current at −60 mV in response to CBX application, the current amplitude was much weaker than that triggered by probenecid (Figure 1.11A, middle traces). To what extent do probenecid and CBX contribute to the enhanced currents of the W74A mutant at positive voltages? If these drugs open the W74A mutant channel independent of voltage stimulus, the G-V relationship would simply shift upward throughout the voltage range. In contrast, if these drugs work synergistically with voltage stimuli, the G-V curve would shift leftward. To examine how probenecid and CBX affect voltage-activated activity of the loop1 chimera, we analyzed the G-V

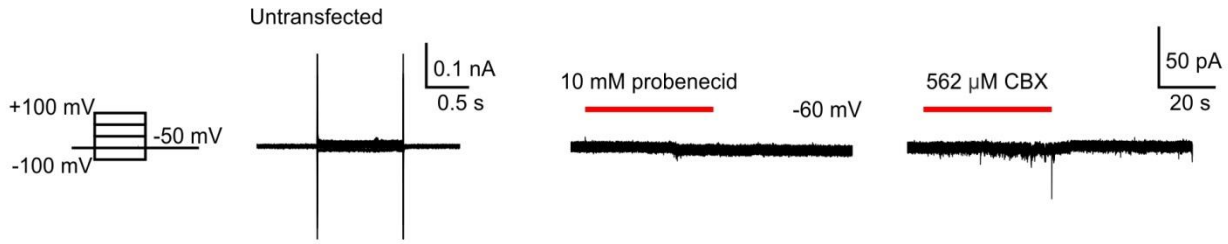

Figure 1.12. Probenecid and CBX have no effect on untransfected HEK cells. Whole cell current recordings of an untransfected HEK293 cell held at -60 mV when exposed to 10 mM probenecid or 562 µM CBX. Voltage steps (left) demonstrate no apparent voltage-gated channel activity from untransfected HEK293 cells.

relationship between −100 and 180 mV in the presence of probenecid or CBX. In both cases, the G-V curves exhibited a strong leftward shift and a weak upward shift (Figure 1.11B, closed red and black circles). Although the loop1 chimera in the absence of these drugs presented substantial voltage rectification (Figure 1.11B, gray circles), the large conductance at positive membrane potentials in the presence of these drugs cannot be explained as a simple addition of extra conductance equivalent to that observed at negative potentials. It is therefore likely that both probenecid and CBX potentiate voltage-gated channel activity of the loop1 chimera, supporting the idea that these drugs and voltage activate the loop1 chimera through a common gating mechanism.

Discussion

CBX has been widely used for inhibiting Panx1 and connexin gap junction channels; however, its mechanism of action remains unknown. In this study, we demonstrate that CBX inhibits Panx1 through modulation of the first extracellular loop, which likely plays a central role in Panx1 channel opening. Because a single mutation at position 74 in this loop does not merely abolish but actually reverses the inhibitory effect of CBX (Figure 1.6), a simple pore-blocking mechanism is highly unlikely. Also, our

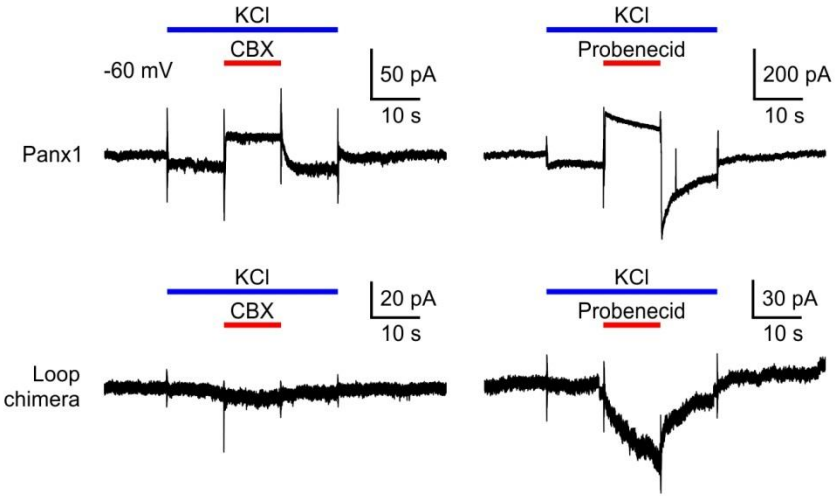

Figure 1.13. Effects of CBX and probenecid on the potassium-activated Panx1 currents. Whole cell patches of Panx1 (top) or the loop1 chimera (bottom) were held at -60 mV and exposed to an external buffer with high potassium (60 mM KCl and 87 mM NaCl). 100 μM CBX or 3 mM probenecid was applied during the KCl exposure.

cysteine-scanning mutagenesis experiments (Figure 1.8) revealed that multiple residues in the first extracellular loop mediate CBX-dependent Panx1 inhibition, supporting the idea that CBX interacts with residues in this loop. Though one may argue that binding of CBX in the first extracellular loop might increase the unitary conductance or alter ion selectivity for voltage activation of the W74A mutant channel, such mechanisms cannot fully explain how CBX (and probenecid) opens this mutant channel in the absence of voltage stimulation (Figure 1.11A). Furthermore, the synergistic potentiative effect of CBX on the voltage-gated activity of the loop1 chimera supports that CBX binding facilitates channel opening of the loop1 chimera (Figure 1.11B). Therefore, modulation of Panx1 gating machinery is the likely mechanism of action for CBX.

Given that CBX has been successfully used to inhibit Panx1 channels activated by diverse stimuli, conformational changes in the first extracellular loop likely play an important role in Panx1 channel gating. This idea is supported by previous studies where chemical modifications of introduced cysteines in the first extracellular loop reduced voltage-gated Panx1 channel activity (73). The fact that probenecid (and CBX

to a lesser extent) can open the W74A mutant channel in the absence of voltage stimulation and that each drug potentiates (i.e., synergistically stimulates) the voltage-activated channel activity of this mutant, it is possible that movement of the first extracellular loop is coupled with Panx1 channel opening. We attempted to assess whether probenecid synergistically stimulates the loop1 chimera with a high concentration of potassium, another Panx1 activation stimulus that leads to a large conductance open state (38). Under our experimental condition, however, a high concentration of potassium (60 mM) gave rise to only a tiny current (<50 pA) such that the analysis of synergism was technically challenging (Figure 1.13). Nevertheless, the loop1 chimera–mediated current was smaller than that of Panx1, suggesting that extracellular potassium may also act through the first extracellular loop. It would be interesting to investigate whether CBX potentiates the W74A mutant channel activity triggered by other stimuli, such as C-terminal cleavage by caspase and high concentration of intracellular calcium.

In this study, we used a chimeric approach to identify W74 as the central player for controlling the polarity of CBX action on Panx1 channel activity. The key discovery was that CBX actually potentiates, instead of simply not affecting, the voltage-gated channel activity of the loop1 chimera, which includes a W74A mutation. We therefore concluded that W74 actively drives the inhibitory action of CBX, whereas other residues support its function, possibly by mediating CBX binding. Indeed, our cysteine mutagenesis experiments demonstrate that most residues between 67 and 86 in the first extracellular loop play important roles in CBX-mediated inhibition of Panx1 (Figure 1.8). Interestingly, 9 out of 19 residues in this region are hydrophobic residues that may

directly mediate the binding of CBX, a glycyrrhetinic acid derivative harboring a steroid-like structure. Notably, previous studies also highlighted the importance of W74 in Panx1 inhibition mediated by several drugs, including ATP, probenecid, and CBX (to a lesser extent; 76; 77). However, these studies showed diminished inhibitory effect of CBX on the W74A mutant but not the potentiative effect that we observed in our experiments. Although the exact reason for this discrepancy is unclear, the previous studies used *Xenopus laevis* oocytes where Panx1 channel properties may be affected by cytosolic components or different membrane components.

In conclusion, our current study provides a much needed first clue for how CBX inhibits Panx1 channels. Although our study does not exclude a possibility that other parts of Panx1 may contribute to the action of CBX, the first extracellular loop seems to play a central role in CBX-mediated Panx1 channel inhibition. We expect that further investigations focusing on the movement and regulation of the first extracellular loop will provide valuable insights into the mechanism underlying Panx1 channel gating.

CHAPTER II - The amino terminus of pannexin1 is important for channel activation

Introduction

Pannexins are membrane channels found to control regulated ATP-release in vertebrates (37, 78, 79). Although originally characterized as a new family of gap junction proteins—indeed, pannexins share a similar membrane topology to the connexin and innexin families—more recent studies have established that pannexins form independent membrane channels (31, 30, 80). Attributed to their broad tissue distribution and unique channel properties, pannexins have been implicated in a number of physiological processes important for human health (60). For example, pannexin-1 (Panx1) expressed in vascular smooth muscle cells was found to regulate systemic blood pressure via downstream signaling of α_1-adrenergic receptor activation (56). Additionally, mutated forms of the Panx1 gene promote metastatic progression of breast cancer cells by enhancing cellular ATP-release during migration through microvasculature (81). More recently, Panx1 was demonstrated to mediate hyperalgesia in neuropathic pain (36). These examples, and more, have established the pannexin family as promising targets for treating diseases like hypertension, ischemia, cancer, and chronic pain (82, 83, 84).

Activation of Panx1 can be achieved by a number of mechanisms (63, 79). As an ATP-release channel, Panx1 is part of signaling pathways involving cell surface receptors. For example, a positive feedback loop occurs when P2X7 receptors are activated by extracellular ATP, which then stimulates opening of Panx1 channels to release additional ATP into the extracellular space (44, 75, 85, 86). In addition,

stimulation of N-methyl-D-aspartate receptors (NMDARs) has been shown to trigger Panx1 activation in hippocampal neurons (52, 54, 87, 53). Tyrosine phosphorylation of the Panx1 intracellular loop has also been shown to stimulate channel opening, resulting from phenylephrine activation of the α_1-adrenergic receptor (56). Finally, during apoptosis, caspase-mediated cleavage of the Panx1 C-terminus relieves the channel of its constitutive pore block, irreversibly activating the channel and releasing signals important for recruiting phagocytes (16, 49, 43). In addition to these activation stimuli, Panx1 has also been reported to sense intracellular Ca^{2+} , membrane stretch, and membrane potential (37, 25, 26, 68, 38). With such a diverse repertoire of stimuli that activate this protein, Panx1 must possess the intriguing ability to sense, respond, and coordinate channel opening through a variety of mechanisms.

Despite the growing collections of stimuli that activate Panx1, it remains unclear how the channel is structured and how it is gated. In one study, thiol-reactive reagents were used on systematically introduced cysteines in Panx1 to probe for pore-lining residues (73). The authors unexpectedly found that the residues likely surrounding the permeation pathway were located in the first extracellular loop and the very C-terminus, instead of the anticipated transmembrane domain. This is consistent with the proposed gating mechanism where unplugging of the inserted C-terminus from the pore irreversibly opens Panx1 channel (49). Notably, the unitary conductance of a caspase-activated Panx1 channel depends on the number of detached C-terminus, but not on the membrane potential itself (43). However, other gating mechanisms may also exist, as a number of studies show that the full-length Panx1 channel opens at a positive membrane potential (25, 44). In addition, other studies demonstrated that the

extracellular loops of Panx1 play important roles in channel gating, as binding sites for some channel inhibitors were mapped to these regions (75, 76). More detailed studies are needed to uncover molecular mechanisms of Panx1 channel gating.

To better understand how the Panx1 channel opens, we focused on the ability of the full-length channel to sense membrane potential. Voltage stimulation has long been used to study the activity of Panx1 in both mammalian cells and oocytes, but the mechanism of voltage sensing remains poorly understood (25, 44). Because Panx1 lacks charged amino acids within its predicted transmembrane domains, this channel may sense voltage through a domain that loops into the voltage field (i.e. somewhere within the lipid bilayer). This is the case for connexin channels, which exploit the non-transmembrane N-terminus for sensing membrane potentials (88, 89, 90, 91). The crystal structure of connexin 26 revealed that this domain actually surrounds the permeation pathway within the voltage field, supporting that voltage-dependent movement of the N-terminus regulates both gating and permeation properties (92). Though the primary sequence of Panx1 is unrelated to those of connexins, a similar membrane topology postulates an interesting possibility that the N-terminus of Panx1 plays crucial roles in voltage-sensing as well. In the present study, we investigate a potential role of the Panx1 N-terminus in voltage-dependent channel activity.

Materials and Methods

Chemicals and Reagents

All chemicals were purchased from Sigma-Aldrich unless otherwise noted.

Cell culture

HEK293 (CRL-1573) and CHO (CCL-61) cell lines were purchased from the American Type Culture Collection (ATCC), and therefore were not further authenticated. Mycoplasma contamination test was confirmed to be negative at ATCC. HEK293 cells were maintained in DMEM (Gibco) supplemented with 10% FBS (Atlanta Biologicals) and 10 μg/ml gentamicin (Gibco). CHO cells were maintained in F-12K media (Gibco) supplemented with 10% FBS and 10 μg/ml gentamicin. Cells were incubated at 37 °C with 5% CO_2 in a humidified incubator.

Molecular biology

DNA corresponding to the human pannexin-1 (hPanx1; NCBI Reference Sequence: NP_056183.2) was synthesized based on protein sequence. Mouse Panx1 (mPanx1; NM_019482) DNA was obtained from GenScript (OMu21951D). Panx1 constructs were cloned into the BamHI and XhoI sites of the pIE2 vector (Michalski and Kawate, 2016), the pIE2 vector modified with a C-terminal FLAG tag, the pCGFP-EU2, or the pNGFP-EU2 vectors. This cloning strategy resulted in insertions of two amino acids (GS) right after the first methionine and three amino acids (ASS) before the stop codon. To restore the native N-terminus, these linkers were removed by QuikChange mutagenesis (Agilent Technologies). Insertions, deletions, and point mutations were performed using overlapping PCR and QuikChange mutagenesis. To generate GFP tagged versions of constructs lacking the BamHI and XhoI sites, the respective constructs were digested with NdeI and PstI, gel purified, and ligated to a similarly digested pCGFP Panx1 EU2 vector. The NGFP C-FLAG Panx1 construct was generated by modifying the BamHI site (GGATCC to GGCTCC) of the pN-GFP-EU2 vector harboring the Panx1 gene,

introducing a new BamHI site after the start methionine of GFP, and subcloning the GFP-Panx1 fusion into the BamHI/XhoI sites of pIE2 harboring a C-terminal FLAG tag. All constructs were generated on the full-length Panx1 genes and verified by DNA sequencing.

Whole cell recording

Two days prior to recording, HEK293 cells were plated at low density onto 12-mm glass coverslips (VWR) in wells of a 6-well plate (Greiner). Cells were transfected after 24 hours with 300-800 ng plasmid DNA using FuGENE6 (Promega) according to the manufacturer's instructions, and used for whole cell electrophysiological recordings 16-24 hours later. For CHO cell recordings, cells were plated to high density into wells of a 6 well plate and transfected the next day with 2 µg plasmid DNA using FuGENE6 according to the manufacturer instructions. After 24 hours, cells were washed once with PBS, trypsinized, and plated onto glass coverslips at low density. Recordings were obtained within 2 hours of plating. Borosilicate glass pipettes (Harvard Apparatus) were pulled and heat polished to a final resistance of 1-6 MΩ and backfilled with (in mM) 147 NaCl, 10 EGTA, and 10 HEPES (adjusted to pH 7.0 with NaOH). Where noted, NaCl was replaced with 147 mM CsCl. Patches were obtained in an external buffer containing (in mM) 147 NaCl, 2 KCl, 2 $CaCl_2$, 1 $MgCl_2$, 13 glucose, 10 HEPES (adjusted to pH 7.3 with NaOH). A rapid solution exchange system (RSC-200; Bio-Logic) was used for recordings in which patches were perfused with drugs. Currents were recorded using an Axopatch 200B patch clamp amplifier (Axon Instruments), filtered at 2 kHz (Frequency Devices), digitized with a Digidata 1440A (Axon Instruments) with a sampling frequency

of 10 kHz, and analyzed using the pCLAMP 10.5 software (Axon Instruments). A Nikon Intensilight C-HGFI fluorescence lamp was used to visualize transfected cells. Recordings of Panx1 were obtained by performing voltage steps, in which cells were held at -60 mV and stepped between various voltages in 20 mV increments for either 1.0 s or 0.1 s. To obtain approximate EV_{50} and valence values for the hPanx1 mutants, average conductance values (n=3-10) were plotted over voltage and the resulting GV curves were fitted with the Hill equation using KaleidaGraph software (Synergy Software).

Single channel recording

CHO cells were plated onto glass coverslips and transfected 24 hours later with 600 ng total DNA at a 1:5 ratio of pIE2 hPanx1 construct:empty pIE2 vector. Recordings were performed 24 to 48 hours after transfection. The bath solution was the same as above, and the pipette solution contained (in mM) 110 CsCl, 37 tetraethylammonium chloride, 10 EGTA, and 10 HEPES adjusted to pH 7.0 with CsOH. After the outside-out configuration was obtained, the holding potential was increased to +60 mV or +120 mV, and total recording lengths ranged from 30 seconds to 6 minutes. Recordings were sampled at 10 kHz and filtered to 1 kHz prior to analysis.

Single channel data analysis

For hPanx1(-GS), raw traces were analyzed to obtain open probability (Po) and unitary conductance (g) using the idealization function of the QuB software suite (https://milesculabs.biology.missouri.edu/QuB.html). In patches that contained more

than one step currents, Po was calculated under the assumption that each step correlated with gating of an independent channel. Patches with more than 3 steps were not used to calculate Po. For hPanx1 (+GS), numerous sub-transitions between closed and open states made it difficult to resolve distinct conductance classes at +60 mV and +120 mV. Channel activity was therefore quantified for three independent current ranges (1.0-2.5, 2.5-4.5, and >4.5 pA) using the sum of the product of unitary current and current frequency.

Cell surface biotinylation

Constructs used in this assay were cloned into the pIE2 vector modified with a C-terminal FLAG tag or the N- or C-GFP EU2 vector. HEK293 cells were plated onto 6 well plates and transfected at 100% confluency with 2 μg DNA using JetPrime (Polyplus) following the manufacturer's instructions. After 24 hours, cells were suspended, transferred to a 2 ml centrifuge tube, and washed twice with 1 ml PBS (Fisher). Surface membrane proteins were biotin-labeled by resuspending cells in 2 ml PBS supplemented with 0.5 mg/ml sulfo-NHS-SS-biotin (Thermo Scientific) and rotated for 40 min at 4 °C. The reaction was quenched by washing cells twice with 2 ml PBS supplemented with 50 mM NH_4Cl, followed by a final wash with 1 ml PBS. Cells were lysed in 200 μL RIPA buffer (150 mM NaCl, 3 mM $MgCl_2$, 1% NP-40, 0.5% deoxycholate (Anatrace), 0.1% SDS, 20 mM HEPES pH to 7.4 with NaOH) supplemented with 1x protease inhibitor cocktail (Thermo Scientific) and rotated for 30 min. The lysate was clarified by centrifugation at 21,000 x g for 15 min and the supernatant was recovered. The "Input" samples were generated by mixing 30 μL of

lysate with 15 μL 3x SDS sample buffer supplemented with 60 mM DTT (Fisher). Streptactin sepharose high-performance resin (GE Healthcare) was equilibrated in RIPA buffer and 35 μL of 50% slurry was added to the remaining lysates and rotated for 2 hours and 30 minutes. Samples were washed 6 times by pelleting resin at 21,000 x g for 2 minutes and resuspending in 700 μL RIPA buffer. Biotinylated proteins were eluted by incubating resin with 50 μL of 1.5 x SDS sample buffer supplemented with 75 mM DTT for 30 min at 55 °C with intermittent vortexing. The supernatants were recovered after a final spin at 21,000 x g for 2 minutes and used as the "pull-down" samples. Samples were resolved on 9% SDS-PAGE gels and blotted onto nitrocellulose (Bio-rad). Membranes were blocked with TBS/0.1% Tween (Anatrace) supplemented with 5% milk (Bio-rad) and 1% BSA overnight, probed first with anti-GFP (1:2000; Clontech), anti-FLAG (1:2000; clone M2), or anti-actin monoclonal antibodies (1:2000; line AC-40), then with goat anti-mouse AP conjugate secondary antibody (1:2000; Bio-rad), and developed with colorimetric AP substrate (Bio-rad).

Cysteine accessibility assay

All constructs used in this assay were cloned into the pIE2 vector modified with a C-terminal FLAG tag. HEK cells were plated onto 6 well plates and transfected at 100% confluency with 2 μg DNA using JetPrime reagent according to the manufacturer's instructions. After 24 hours, cells were collected in 2 ml centrifuge tubes, and washed once with 1 ml PBS. Cells were lysed by resuspending in 500 μL hypotonic buffer (20 mM HEPES pH to 7.4 with NaOH) supplemented with 1x protease inhibitor cocktail for 30 minutes on ice, followed by 10 passes through a 22-gauge needle. Lysed cells were

split evenly between two thick-walled 1.5 ml ultracentrifuge tubes (Beckman) and centrifuged at ~200,000g for 20 minutes. The supernatant was discarded and the membrane pellet was suspended in 110 μL of PBS. Cysteines were labeled by mixing membranes with 10 μL water or 10 μL MAL-dPEG$_4$-(m-dPEG$_{12}$)$_3$ (MAL-dPEG; Quanta BioDesign) to a final concentration of 0.1 mM, vortexing briefly, and incubating for 30 minutes at room temperature. The reaction was quenched by adding 1 ml PBS supplemented with 10 mM cysteine, briefly vortexing, and centrifuging at ~160,000 x g for 20 minutes. The supernatant was discarded and the membrane pellet was solubilized in 25 μL solubilization buffer (PBS supplemented with 1% $C_{12}E_8$ (Anatrace)) overnight. Samples were centrifuged at 21,000 x g for 10 minutes and the supernatant was mixed with 5 μL 6x SDS sample buffer without reducing agent. Samples were loaded on 9% SDS-PAGE gels, blotted onto nitrocellulose, and blocked for 1 hour in TBS/0.1% Tween supplemented with 5% milk and 1% BSA. Panx1 was detected by probing with anti-FLAG antibody (1:2000) followed by goat anti-mouse AP conjugate antibody (1:2000), and developed with colorimetric AP substrate.

Fluorescent size exclusion chromatography (FSEC)

All constructs used for this experiment were cloned into the pNGFP-EU2 or pCGFP-EU2 vectors. FSEC experiments are performed as described previously (108). Briefly, HEK293 cells were plated onto 6-well plates and transfected at 100% confluency (usually next-day) using 2 μg DNA and JetPrime according to the instructions. After 24 hours, cells were suspended and transferred to a 2 ml centrifuge tube and centrifuged at 5000 x g for 5 min. Cells were washed with 1 ml PBS and centrifuged again at 5000

x g for 5 min. Cells were suspended in 150 µL solubilization buffer (1x PBS supplemented with 1% $C_{12}E_8$ and 1x protease inhibitor cocktail) and rocked for 30 min at 4 °C. Samples were centrifuged at 21,000 x g for 5 minutes at 4 °C. The supernatents were transferred to 1.5 ml ultracentrifuge tubes and centrifuged again at ~200,000 x g for 20 minutes. 50 µL of each supernatent was injected into a Superose 6 Increase 10/300 GL column pre-equilibrated with running buffer (1x PBS supplemented with 0.5 mM $C_{12}E_8$) using a flow rate of 0.5 ml/min. The eluate was monitored using a fluorescence detector (Shimadzu RF-20Axs; Ex: 480, Em: 508).

Results

N-terminally attached GFP abolishes Panx1 channel activity

Our initial interest in the function of Panx1 N-terminus arose serendipitously when we noticed differences in channel activity between N- and C-terminally tagged human Panx1 (hPanx1) with GFP. Whole-cell electrophysiology recordings of the C-terminally tagged hPanx1 expressed in HEK cells presented readily observable voltage-activated currents when depolarized with a voltage-step protocol (Figure 2.1A; left). In contrast, we did not observe voltage-dependent currents from the N-terminally tagged hPanx1, suggesting this fusion protein may not be activated by a voltage potential (Figure 2.1A; right).

To assess whether the N-terminal GFP tag interferes with trafficking of the channel to the cell membrane, we performed cell-surface biotinylation experiments. Using a membrane impermeable, amine-reactive biotin-conjugated molecule, we labeled and enriched for membrane proteins located on the surface of transfected HEK

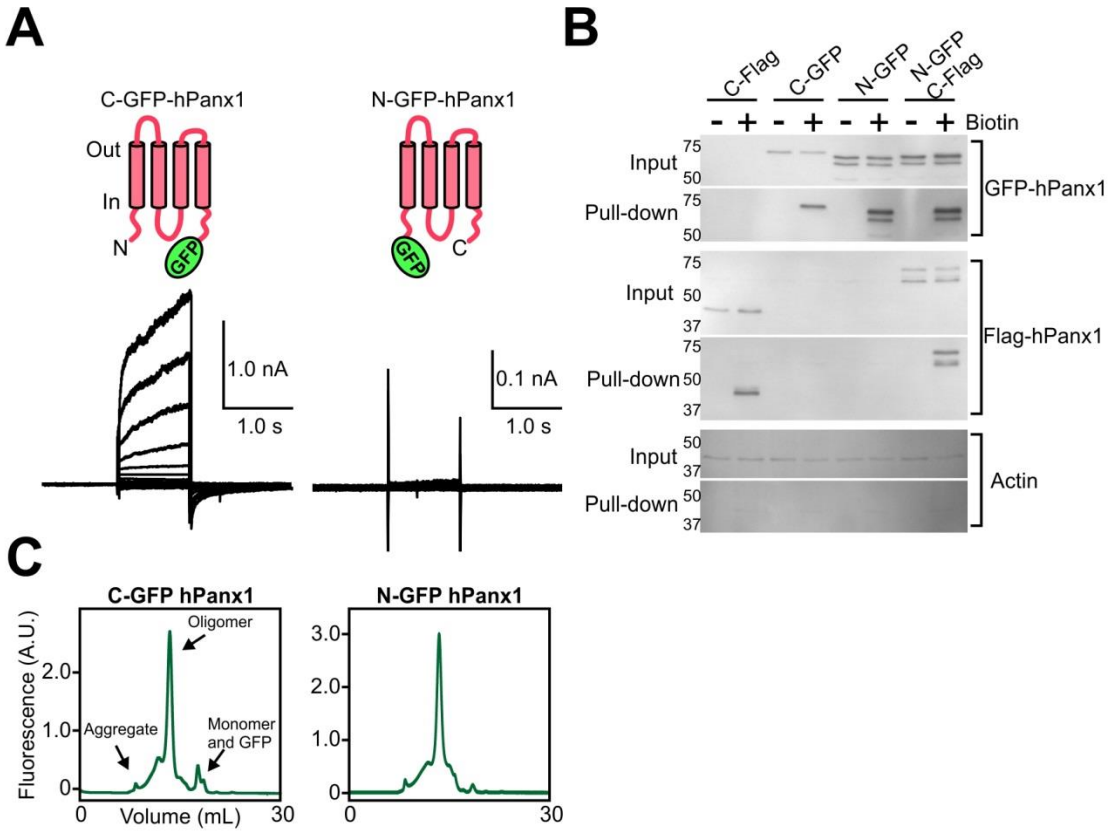

Figure 2.1. Panx1 is inactivated by tagging its N-terminus with GFP. (A) Whole cell recordings of wild-type human Panx1 or GFP-tagged Panx1 expressed in HEK293 cells. Cells were held at a resting membrane potential of -60 mV and stepped between -100 mV and +100 mV in 20 mV increments for 1 s. Shown are representative recordings from 5-7 cells. Pink cartoons represent a predicted Panx1 topology and GFPs indicate the tag position. (B) Surface biotinylation assay of Flag-Panx1, GFP-tagged Panx1, or N-GFP C-FLAG tagged Panx1. Panx1 constructs were transfected into HEK cells and treated with sulfo-NHS-SS-biotin. Biotin-labelled proteins were analyzed by SDS-PAGE and western blotting. Membranes were probed with GFP, FLAG, or actin antibodies. Representative blots from 3 independent experiments are shown. (C) FSEC elution profiles of N- or C- terminally GFP tagged hPanx1. Either construct was transfected into HEK293 cells, solubilized in detergent, and analyzed by size exclusion chromatography coupled to a fluorescence detector (Ex: 480, Em: 508).

cells and used western blots to identify hPanx1. Both N-GFP and C-GFP hPanx1 proteins could be identified in the pull-down samples, suggesting both fusion proteins traffic to the cell surface (Figure 2.1B). Actin could be identified in the protein lysates but not in the pull down samples, suggesting this assay specifically pulls down membrane proteins. We noticed that the N-GFP hPanx1 construct migrates faster than the C-GFP counterpart when resolved by SDS-PAGE, and, additionally, N-GFP hPanx1 appears as

a doublet compared to the single band observed for C-GFP Panx1. One possibility for this difference could be that the C-terminus of N-GFP hPanx1 gets cleaved by proteases before or during sample preparation. To test this possibility, we added a C-terminal FLAG tag to the N-GFP hPanx1 construct (N-GFP/C-FLAG hPanx1). We were able to pull down this doubly-tagged hPanx1 and identify both the N-terminal GFP tag and the C-terminal FLAG tag at similar molecular weights. This suggests that N-terminally tagged hPanx1 is not susceptible to proteases and has intact termini.

We next examined whether N-GFP hPanx1 is properly folded using fluorescence detection size exclusion chromatography (FSEC). This protocol enables one to characterize assembly, stability, and monodispersity of a detergent solubilized GFP-fusion protein based on the SEC elution profiles (108). The FSEC of both N- and C-GFP hPanx1 presented a major peak at a molecular weight corresponding to the size of a mature oligomer (6-7 mers), indicating that these proteins remained properly folded and assembled after solubilization in a detergent-containing buffer (Figure 2.1C). There was little aggregation (i.e. void peak) or dissociation (i.e. monomeric peak), suggesting that the majority of both N- and C-GFP hPanx1 were properly folded in HEK cells. We therefore conclude that hPanx1 tagged at the N-terminus with GFP is insensitive to voltage activation, and this is not due to poor membrane localization, unwarranted proteolysis, or misfolding of the channel.

Insertion of Gly-Ser at the N-terminus enhances Panx1 channel activity

The voltage-insensitive N-GFP hPanx1 proposed that the intact N-terminus may be required for voltage-triggered channel opening. To examine the relationship between

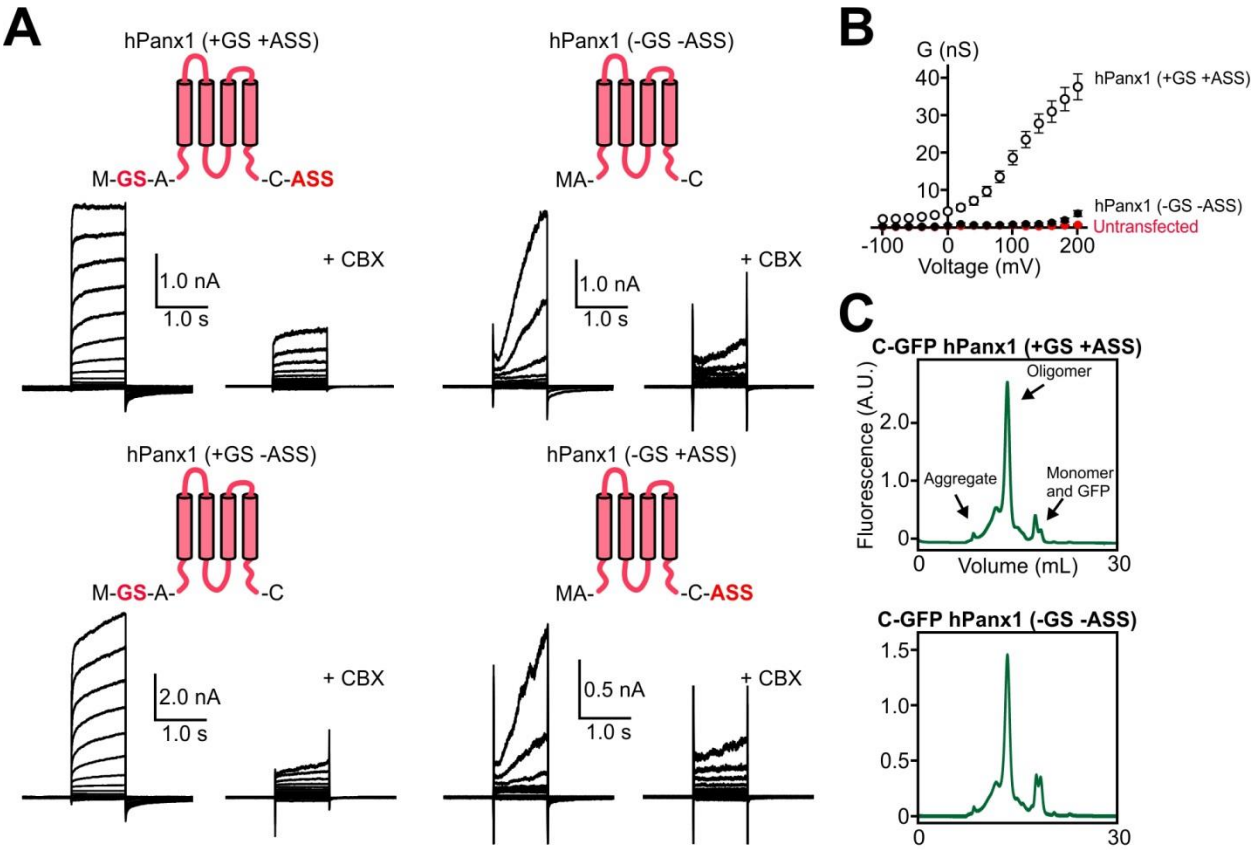

Figure 2.2. A short linker at the Panx1 N-terminus modifies channel activity. (A) Whole cell recordings of WT human Panx1 constructs with (top left) or without (top right) modified N- and C- termini. Recordings from Panx1 constructs with individual modifications to the N-terminus (bottom left) or C-terminus (bottom right) are also shown. Recordings were obtained from transfected HEK293 cells held at -60 mV and stepped between -100 mV and +160 mV in 20 mV increments for 1 s. CBX (50 μM) was applied through a rapid solution exchange system. Shown are representative recordings from at least 5 different cells. Pink cartoons represent the topology of Panx1 and the amino acids constituting the N- and C- termini for each construct. (B) G-V curves of WT hPanx1 with (open circles) or without (black) modified termini. Recordings from untransfected cells are shown in red. Recordings were obtained from HEK293 cells held at -60 mV and stepped between -100 mV and +200 mV in 20 mV increments for 0.1 s. Each dot represents the mean value and error bars represent SEM of 3-4 cells. (D) FSEC elution profiles of WT hPanx1 with (top) or without (bottom) modified termini. Panx1 was tagged at the C-terminus with GFP, transfected into HEK293 cells, solubilized in detergent, and analyzed by size exclusion chromatography.

N-terminal integrity and voltage-dependent channel activity, we first sought to characterize untagged hPanx1 using a whole-cell patch-clamp method. In our lab, hPanx1 constructs have been made using BamHI and XhoI restriction sites, which expedites subcloning processes into multiple vectors. As we demonstrated previously

(Chapter I), our full-length, wild type hPanx1 construct created in this way shows robust carbenoxolone (CBX)-sensitive channel activity at membrane potentials higher than +20 mV (Figure 2.2A; hPanx1+GS/+ASS). This cloning strategy, however, results in insertions of Gly-Ser residues right after the first Met and Ala-Ser-Ser before the stop codon (Figure 2.2A; hPanx1+GS/+ASS). We have overlooked these artificial insertions, as we assumed that additions of a few small amino acids at either terminus would not disrupt the local structure of hPanx1. To our surprise, however, when these artificially inserted residues were removed to restore the natural N- and C-termini, hPanx1 only weakly responded to voltage stimuli such that we observed detectable currents at voltages above +100 mV (Figure 2.2A and B; hPanx1 -GS/-ASS). This unexpected enhancement of hPanx1 channel activity was due to the N-terminally inserted Gly-Ser, as removal of the C-terminal Ala-Ser-Ser had no effect on voltage-dependent channel activity (Figure 2.2A). Importantly, these results are not limited to hPanx1 expressed in HEK cells, as we observed similar current enhancement from the mouse Panx1 (mPanx1) and Panx1s expressed in Chinese hamster ovary (CHO) cells (Figure 2.3A-C). We also confirmed using FSEC that an insertion of Gly-Ser at the N-terminus does not alter overall expression level or assembly status of hPanx1 (Figure 2.2C). These results indicate that the full-length, wild type Panx1 responds to only extreme membrane potentials (> +100 mV), whereas an N-terminal insertion of Gly-Ser substantially enhances the voltage-dependent channel activity.

To explore the nature of this unexpected gain-of-function by the N-terminal Gly-Ser, we performed single-channel recordings using outside-out patches pulled from hPanx1-expressing CHO cells. Consistent with the macroscopic observations (Figure

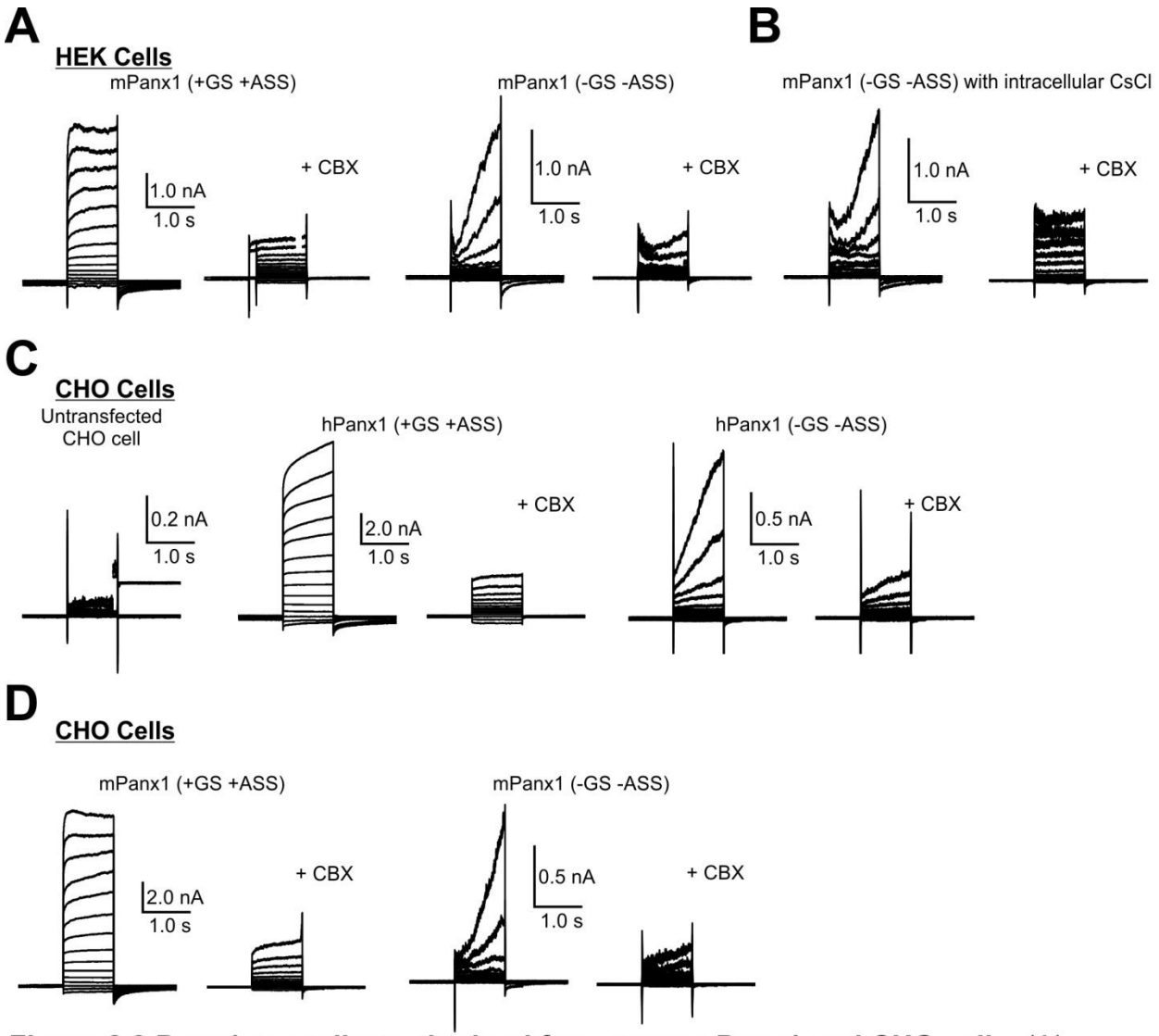

Figure 2.3 Panx1 recordings obtained from mouse Panx1 and CHO cells. (A) Representative whole cell recordings of WT mouse Panx1 with linkers on both termini (left) or WT mouse Panx1 without linkers (right). CBX (50 μM) was applied using a rapid solution exchange system. Recordings were obtained from HEK293 cells held at -60 mV and stepped between -100 mV and +180 mV for 1 s in 20 mV increments. (B) Mouse Panx1 recording obtained using a CsCl based intracellular solution. Shown are representative recordings from 4 cells of 1 s voltage steps from -100 to +180 mV with or without 50 μM CBX. (C) Representative whole cell recordings from CHO cells. Shown are recordings from an untransfected cell (left), WT human Panx1 with linkers on both termini (middle) and WT human Panx1 with no linkers (right). Recordings were obtained by holding cells at -60 mV and stepping between -100 mV and +160 mV for 1 s in 20 mV increments. CBX (50 μM) was applied using a rapid solution exchange system. (C) Representative whole cell recordings of mouse Panx1 with linkers (left) or without (right) from CHO cells. Cells were held at -60 mV and stepped between -100 mV and +180 mV for 1 s in 20 mV increments. CBX (50 μM) was applied using a rapid solution exchange system.

2.2A and B), hPanx1 with the natural N-terminus (hPanx1-GS) presented no channel

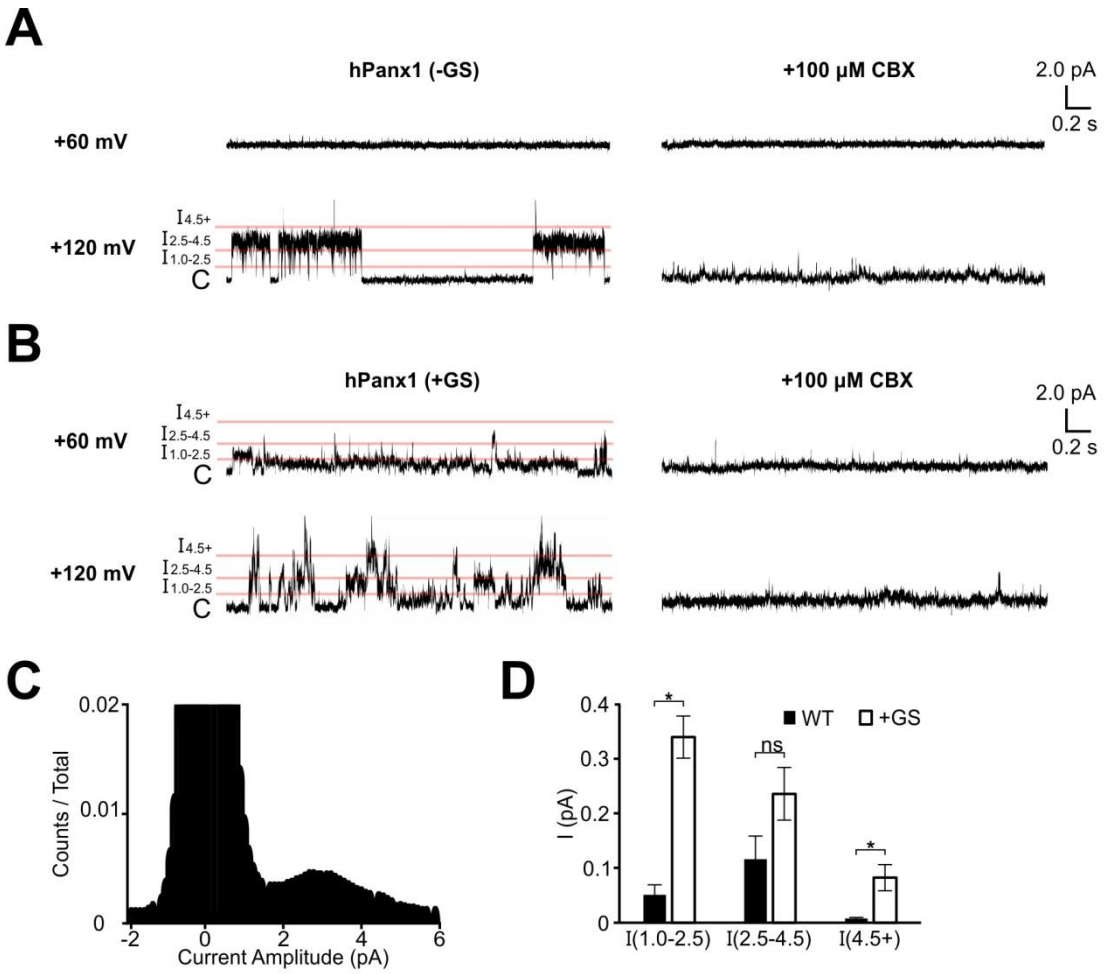

Figure 2.4. Single-channel recordings of hPanx1. (A) Representative outside-out recordings from hPanx1 (-GS) at +60 and +120 mV. Red horizontal lines define the current amplitude bins for each calculation of I (1.0-2.5, 2.5-4.5, and >4.5 pA). CBX (100 µM) was applied using a rapid solution perfusion. (B) Representative outside-out recordings from hPanx1 (+GS) at +60 and +120 mV. (C) All-amplitude histogram generated from single channel outside-out recordings of hPanx1 (-GS) at +120 mV. (D) Histogram of single channel activity, I, for each bin of hPanx1 (-GS) (n=4) and hPanx1 (+GS) (n=5). Asterisks denote significance ($p<0.05$) as determined by Student's t-test, while "ns" indicates no statistically significant difference.

activity at +60 mV (Figure 2.4A; +60 mV). On the other hand, hPanx1+GS showed conspicuous channel activity at +60 mV (Figure 2.4B; +60 mV). While we were able to observe some clear steps representing discrete unitary currents between 1 to 3 pA, it was difficult to assign specific unitary conductance to those steps, as many transient currents also existed and obscured the overall current histogram (Figure 3B and S2A). These suggest that the N-terminal insertion of Gly-Ser increases the open probability of

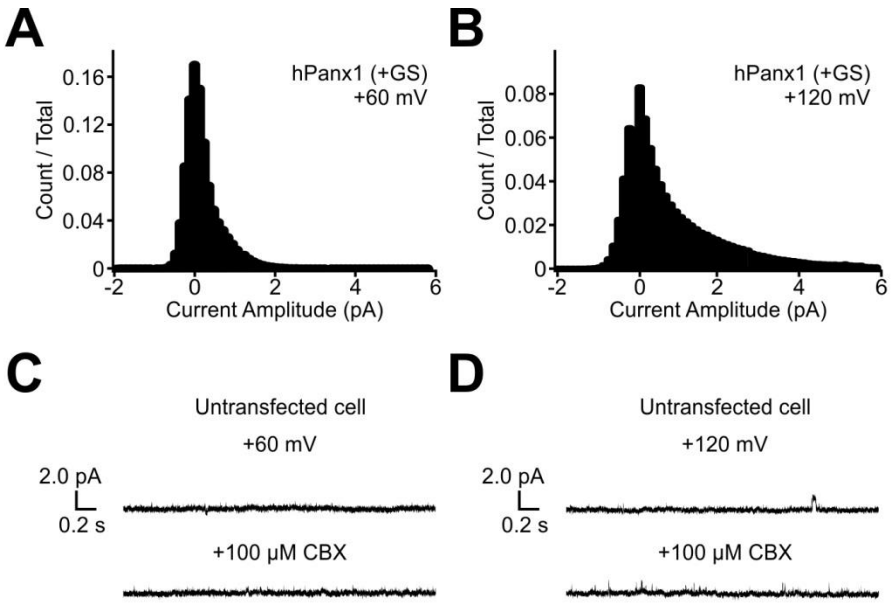

Figure 2.5. Single-channel data of hPanx1 (+GS) and untransfected cells. (A and B) All-amplitude histograms constructed from single-channel outside-out recordings of hPanx1 (+GS) at +60 (A) or +120 mV (B). (C and D) Representative single-channel recordings of untransfected CHO cells held at +60 (C) or +120 mV (D). CBX (100 µM) was applied using a rapid solution perfusion.

hPanx1 at this membrane potential. At +120 mV, hPanx1-GS showed a discrete unitary current at 3.2±0.5 pA (conductance g = 26.7±3.9 pS) with the open probability (Po) of 6.8±2.7% (Figure 2.4A and C). Like at +60 mV, hPanx1+GS presented indiscrete unitary currents at +120 mV (Figure 2.4B and 2.5B). We therefore divided the single channel activity in three different brackets (unitary current of 1.0-2.5, 2.5-4.5, and >4.5pA) and estimated the overall contribution of differently sized channels (Figure 2.4D). While the product of the current and its frequency in the I2.5-4.5 bracket showed no statistical difference between -GS and +GS, both the smaller (I1.0-2.5) and the larger (I4.5+) current brackets showed significant increase with Gly-Ser. This analysis suggests that the N-terminal Gly-Ser generates extra channel open states with both smaller and larger conductances. In particular, more frequent opening of the smaller channel seems to contribute to the enhanced channel activity in hPanx1+GS. Rapid

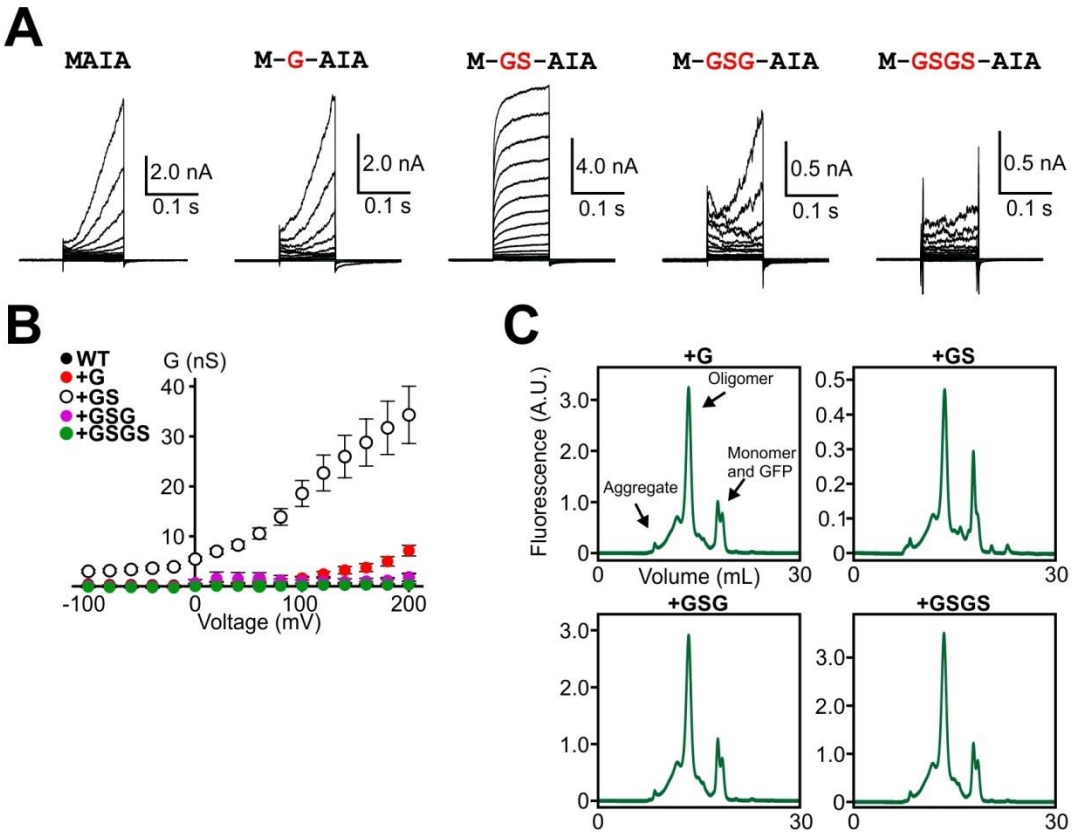

Figure 2.6. Length of the N-terminal insertion is sensitive to voltage-dependent channel activity. (A) Whole cell recordings from HEK293 cells transfected with hPanx1 with increasing N-terminal modification length. Recordings were obtained from transfected cells held at -60 mV and stepped between -100 mV and +260 mV in 20 mV increments for 0.1 s. Shown are representative recordings from at least 4 different cells. Sequences above each construct correspond to the amino acid sequence of the N-terminus of human Panx1, where black text represents the native sequence and red text identifies the insertion. (B) G-V curves of the constructs shown in (A). Each point represents the mean value, and error bars represent the SEM of at least 4 different cells. (C) FSEC analysis of the constructs shown in (A). Constructs were tagged C-terminally with GFP, transfected into HEK293 cells, solubilized in detergent, and analyzed by size exclusion chromatography.

perfusion of 100 μM CBX confirmed that all the recorded single channel activity came from hPanx1. Untransfected CHO cells did not show any channel activity (Figure 2.5C).

Insertion of other amino acid(s) at the N-terminus also enhances Panx1 channel activity

We next varied the length of the inserted residues at the N-terminus and examined voltage-dependent channel activity using a whole-cell patch clamp method. Insertion of one residue (Gly) did not affect hPanx1 channel activity (Figure 4A and B). In contrast, insertion of either three (Gly-Ser-Gly) or four (Gly-Ser-Gly-Ser) residues reduced the voltage-dependent channel activity of hPanx1 (Figure 2.6A and B). The FSEC experiments showed that all those constructs were properly assembled in HEK cells (Figure 2.6C). These data suggest that the length of N-terminal insertion is sensitive to channel activity and the insertion of two residues (Gly-Ser) most effectively enhances voltage-dependent hPanx1 activation.

To assess whether enhancement of Panx1 channel activity depends on the types of inserted amino acids, we tested six different single amino-acid insertions after the first Met residue. Faster and slightly stronger channel activity especially at higher voltages was observed for the insertions of Ala, Ser, or Asp (Figures 2.7A and B). When a Thr residue was inserted, a marked current increase was observed beyond +120 mV (Figure 2.7A and B). Likewise, insertion of Trp showed much larger currents (Figure 2.7A and B). However, this Trp inserted construct activated even at +20 mV, suggesting that this mechanism of current enhancement is different from that of the Thr insertion. We also noticed that channel activation and inactivation kinetics substantially vary depending on the kind of amino acid inserted at this position (Figure 2.7A). We next tested three different double amino acid insertions after the first Met residue. To our surprise, insertion of Ser-Gly residues did not affect the voltage-dependent channel activity of hPanx1 (Figure 2.7A and B). On the other hand, insertions of either Ala-Ala or Trp-Trp enhanced the channel activity like Gly-Ser. All these insertions did not interfere

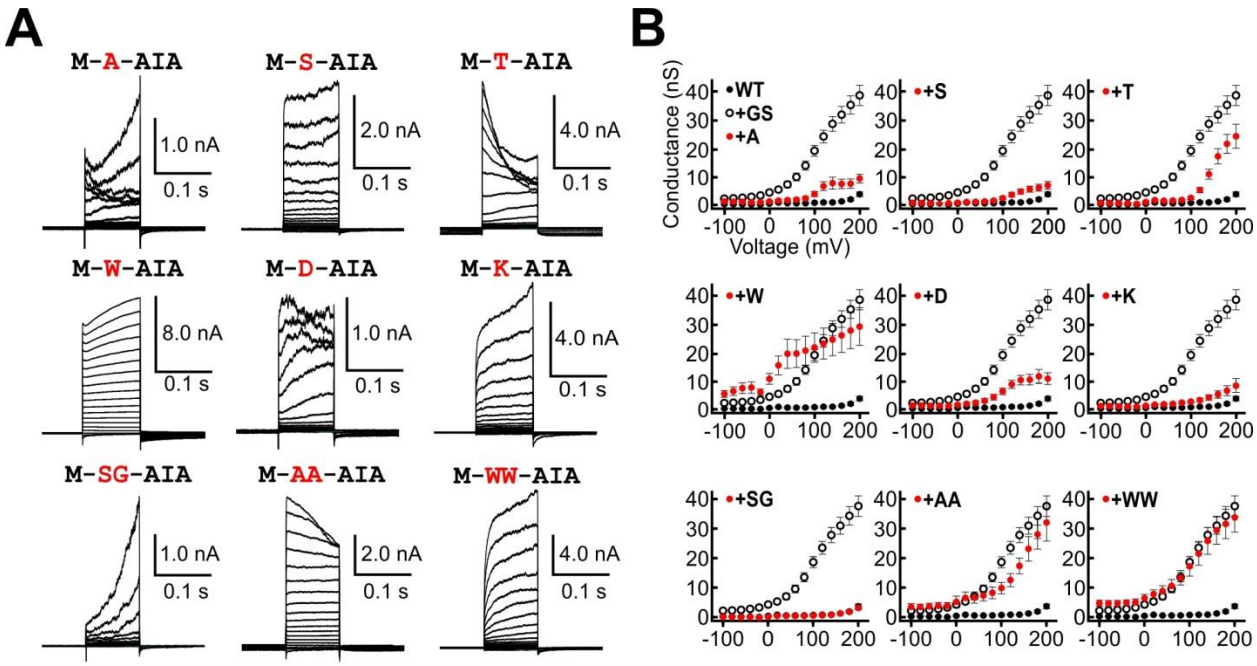

Figure 2.7. Amino acid identity inserted into the Panx1 N-terminus determines channel properties. (A) Whole cell patch clamp recordings of hPanx1 with various amino acids inserted immediately following the start methionine. Recordings were obtained from HEK293 cells transfected with each construct. Cells were held at -60 mV and stepped between -100 mV and +260 mV for 0.1 s in 20 mV increments, with the exception of the "A" and "D" insertions which were stepped maximally to +220 mV and +200 mV, respectively. Sequence above each recording corresponds to the amino acid composition of the very N-terminus of human Panx1 in black text, and red text identifies the amino acid insertion. (B) G-V plots of the recordings from Panx1 channels shown (A). Each point represents the mean conductance at each voltage and error bars represent the SEM of at least 4 different cells.

with hPanx1 folding in HEK cells judged by the FSEC profiles (Figure 2.8). Altogether, these data suggest that the very tip of the N-terminus is sensitive to modifications and even a single amino acid insertion (e.g. Trp) can substantially enhance the channel activity.

N-terminal residues leading to TM1 is important for Panx1 assembly

We next assessed whether the rest of the N-terminal domain plays a role in controlling Panx1 channel activity. We rationalized that insertion of a short, unstructured peptide constituted of Gly and Ser (GSGSG) into a critical position of the hPanx1 N-

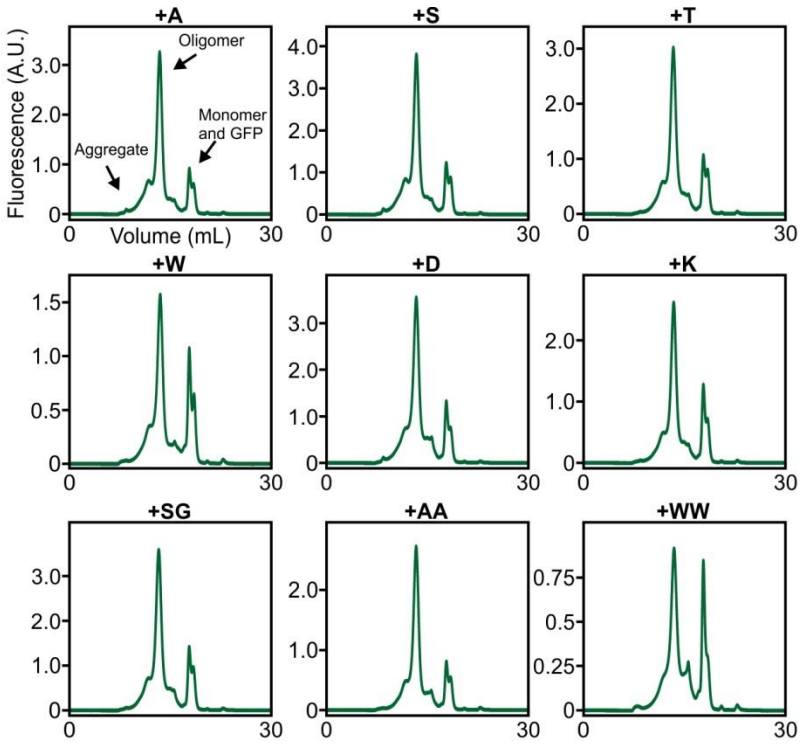

Figure 2.8 FSEC analysis of human Panx1 constructs with various amino acids inserted immediately after the start methionine. Each Panx1 mutant was tagged C-terminally with GFP, transfected into HEK293 cells, solubilized in detergent, and analyzed by size exclusion chromatography.

terminus would locally disrupt the structure and diminish voltage-triggered channel activation. To facilitate the finding of a loss-of-function construct, we inserted the short peptide into hPanx1+GS that gives rise to much stronger voltage-dependent channel activity than wildtype. Using this strategy, we found that this peptide had variable effects on channel activity depending on the location of where it was inserted. As we expected, we did not observe voltage-dependent currents from Panx1 harboring the insertion located immediately after Met1 (Figure 2.9A-C; GS1), confirming that this region plays a critical role in channel gating. Likewise, we did not observe currents from a construct containing the insertion after Lys36 (Figure 2.9A-C; GS4). In contrast, we readily observed voltage-activated currents from the constructs in which the same peptide was inserted after Phe12 (“GS2”) or Phe25 (“GS3”). Notably, the FSEC experiments showed

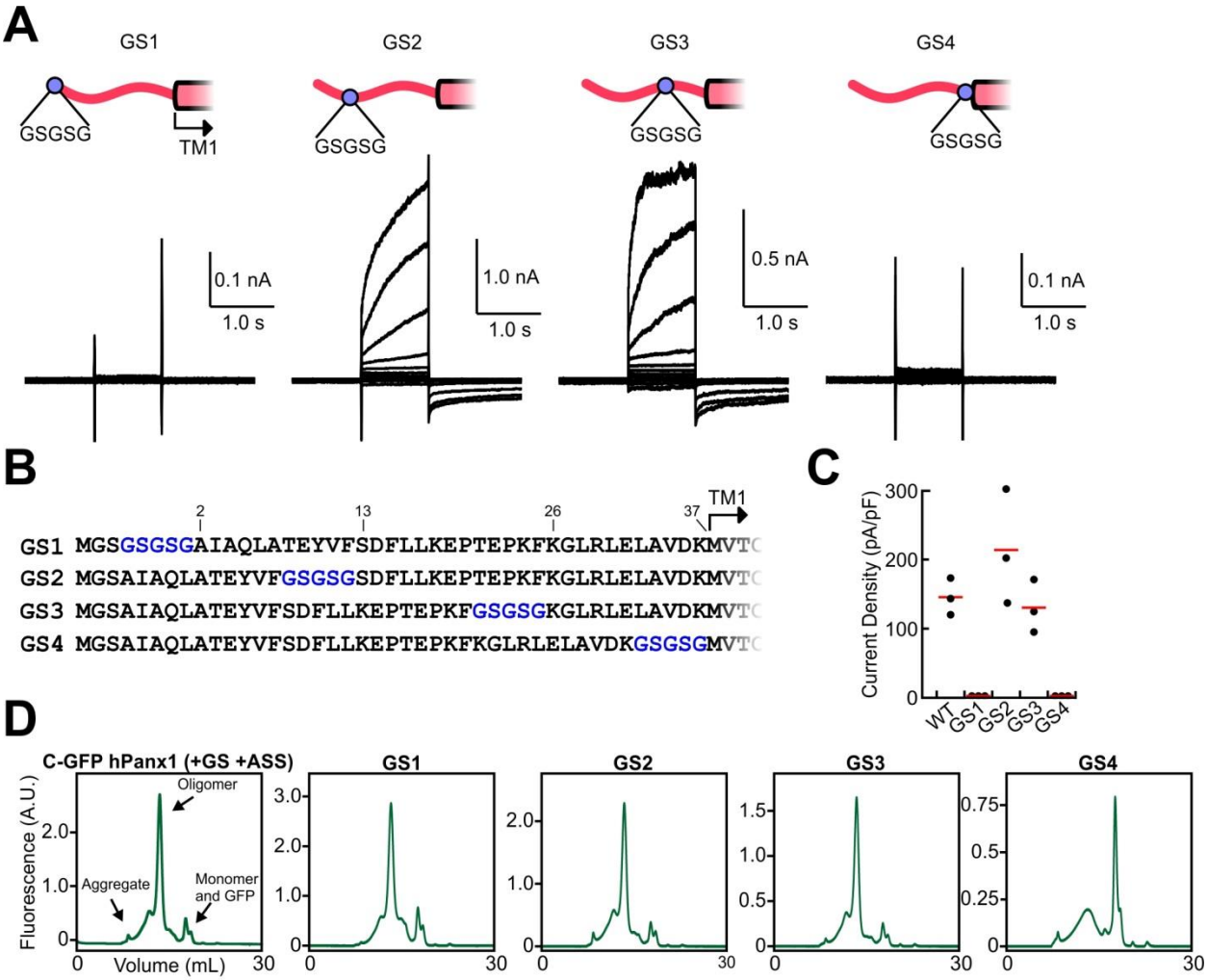

Figure 2.9. Modifying the Panx1 N-terminus with a short peptide positionally inactivates the channel. (A) Whole cell recordings of modified human Panx1 constructs (+GS and +ASS) which harbor a short peptide (GSGSG) inserted at positions along the N-terminus. Recordings were obtained from HEK293 cells held at a membrane potential of -60 mV, and stepped between -100 mV and +100 mV with 20 mV increments. Shown are representative recordings from 3-4 different cells. Pink cartoons represent the Panx1 N-terminus displaying the relative position of the peptide insertions. (B) Sequence of the human Panx1 N-terminus. Locations of the inserted peptide are shown in blue text for each construct. (C) Current densities of WT Panx1 (+GS +ASS) and constructs shown in (A). Points represent an individual measurement, and red bars represent the mean value of 3 different cells. (D) FSEC analysis of constructs shown in (A). Each Panx1 was tagged C-terminally with GFP, transfected into HEK293 cells, solubilized in detergent, and analyzed by size exclusion chromatography.

that GS1-3 are properly assembled in HEK cells, but GS4 is likely misfolded, as the oligomeric species substantially diminished (Figure 2.9D). These results suggest that the N-terminal residues immediately prior to the predicted first transmembrane helix are

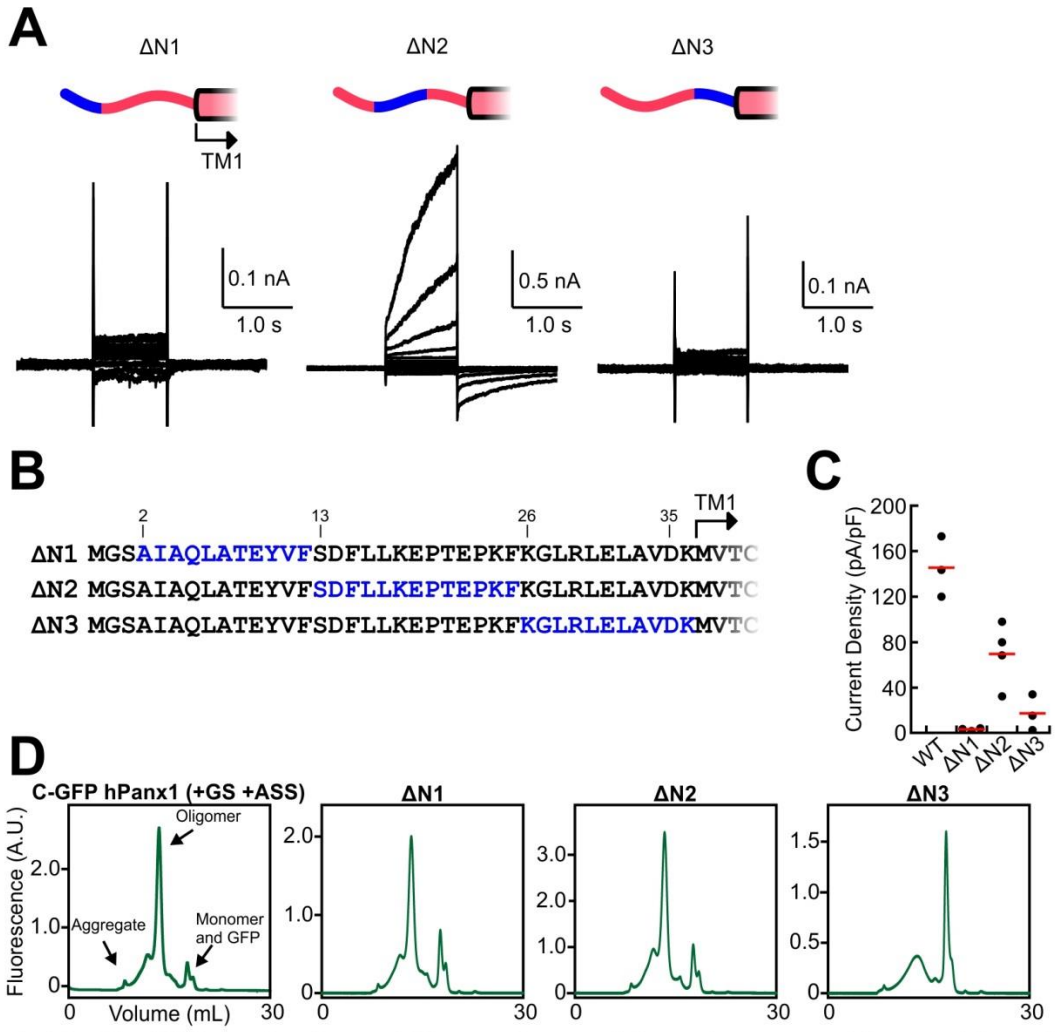

Figure 2.10. Modifying the Panx1 N-terminus with a short peptide positionally inactivates the channel. (A) Whole cell recordings of modified human Panx1 constructs (+GS and +ASS) which harbor a short peptide (GSGSG) inserted at positions along the N-terminus. Recordings were obtained from HEK293 cells held at a membrane potential of -60 mV, and stepped between -100 mV and +100 mV with 20 mV increments. Shown are representative recordings from 3-4 different cells. Pink cartoons represent the Panx1 N-terminus displaying the relative position of the peptide insertions. (B) Sequence of the human Panx1 N-terminus. Locations of the inserted peptide are shown in blue text for each construct. (C) Current densities of WT Panx1 (+GS +ASS) and constructs shown in (A). Points represent an individual measurement, and red bars represent the mean value of 3 different cells. (D) FSEC analysis of constructs shown in (A). Each Panx1 was tagged C-terminally with GFP, transfected into HEK293 cells, solubilized in detergent, and analyzed by size exclusion chromatography.

important for Panx1 channel assembly, but the middle region seems to be dispensable for voltage-triggered channel activity.

To further explore which regions of the N-terminus contribute to voltage sensing, we designed and tested three deletion constructs in which portions of the N-terminus were removed. We were unable to observe hPanx1 currents through channels which lack residues 2 to 12 (ΔN1) or channels which lack residues 26 to 36 (ΔN3) (Figure 2.10A-C). Like the insertion of a short peptide at this site (i.e. GS4), ΔN3 seemed to be misfolded as indicated by the FSEC trace (Figure 2.10D). Notably, we observed hPanx1 currents from channels in which residues 13 to 25 (ΔN2) were deleted. FSEC experiments showed that ΔN2 is properly folded (Figure 2.9D). These suggest that the amino acids removed in the ΔN2 construct are not important for channel activation, and agrees with data from our insertion constructs. Because the ΔN2 construct was designed arbitrarily, we were curious about the precise number of amino acids that could be removed from the N-terminus while still maintaining voltage-dependent activity. We designed a series of additional deletions where extra amino acids were removed from the ΔN2 parent construct and each was tested for channel function. Interestingly, none of these extended deletion constructs presented voltage-activated currents (ΔN2.1 - ΔN2.6) (Figure 2.11A-C). This suggests that ΔN2 harbors the maximum number of amino acids that can be deleted from the N-terminus while still maintaining channel activity.

N-terminus seems to form a structural domain within the voltage field

Our experiments so far have focused on which segments of the N-terminus are important for voltage-dependent Panx1 channel activity. One possibility that could explain our findings is that the N-terminus acts as a voltage-sensing motif, and that

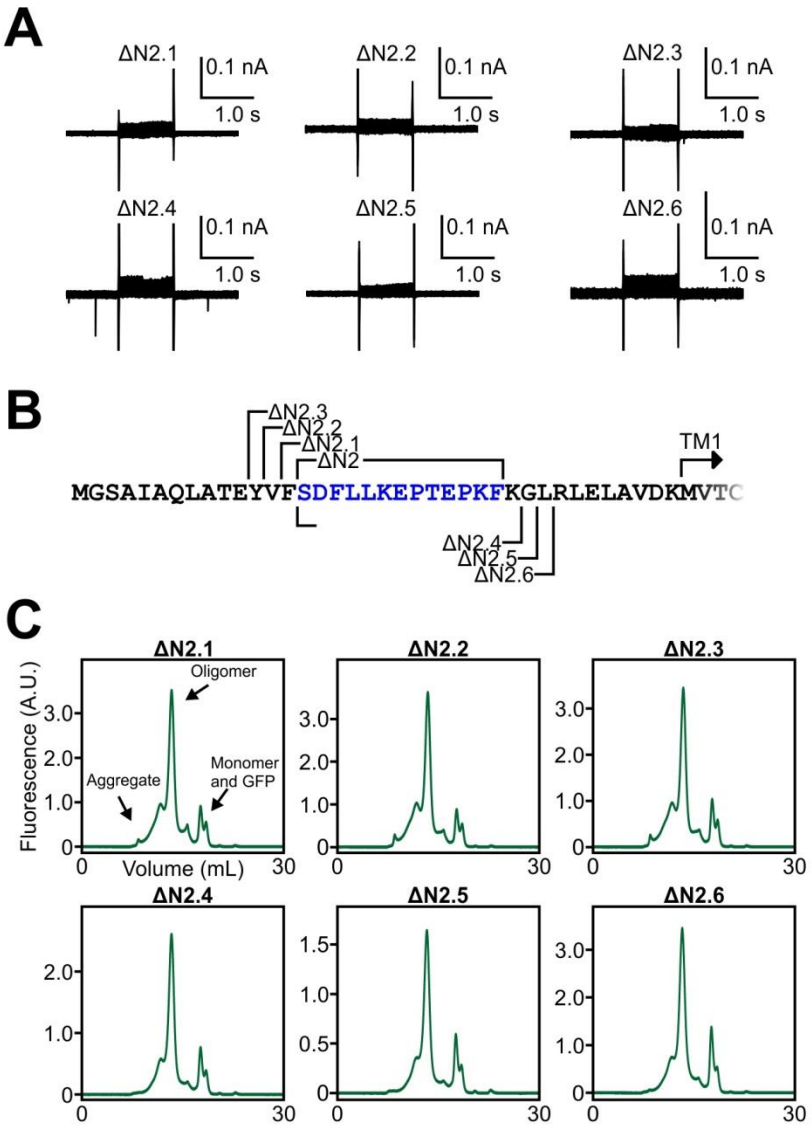

Figure 2.11. Whole cell recordings of Panx1 with longer ΔN2 truncations. (A) Recordings were obtained from transfected HEK293 cells held at -60 mV and stepped between -100 mV and +100 mV in 20 mV increments for 1 s. (B) Sequence of the hPanx1 N-terminus. Shown in blue is the region corresponding to the ΔN2 deletion, and marked are the locations of the additional deletions tested in (A). (C) FSEC analysis of ΔN2.1-ΔN2.6. Each construct was tagged with GFP at the C-terminus, transfected into HEK293 cells, solubilized in detergent, and analyzed by size exclusion chromatography.

manipulating this domain results in a non-functional voltage sensor. If this is the case, we would anticipate two criteria: 1) portions of the N-terminus are within the plane of the lipid bilayer and not accessible to solvent, and 2) charged residues found within the plane of the membrane may act as voltage sensors. To test whether amino acids in the

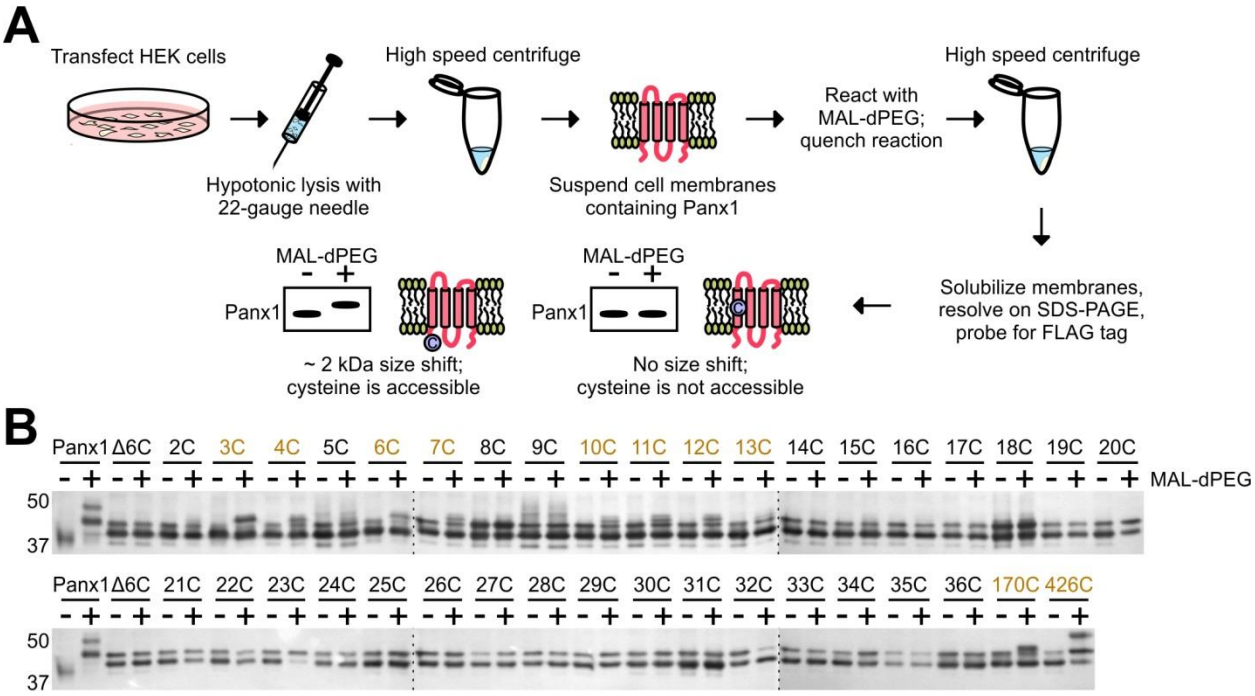

Figure 2.12. The majority of the Panx1 N-terminus is protected from a thiol-reactive agent. (A) Schematic representation of the assay used to probe the accessibility of the Panx1 N-terminus. (B) Western blots probe the accessibility of the Panx1 N-terminus using MALd-PEG. HEK293 cells transfected with wild-type Panx1, Panx1 lacking 6 native cysteines (Δ6C), or Δ6C with single cysteines introduced to each position of the N-terminus were broken and membranes were collected. Membranes were reacted with water (-) or MALd-PEG (+), solubilized in detergent, and proteins were analyzed by SDS-PAGE followed by western blots probed with FLAG antibody. Molecular weights are shown in kDa and dashed lines indicate separate gels. Mutants colored in orange display reactivity towards MALd-PEG. All samples were prepared concurrently; gels on the top row were blotted onto the same membrane, and gels on the bottom row were blotted onto a second membrane. Shown are representative blots from 3 independent experiments.

N-terminus are located inside or outside of the plane of the lipid bilayer, we designed a cysteine reactivity-based assay (Figure 2.12A). We first generated a "Δ6C" construct based on hPanx1+GS by mutating 5 native cysteines from the intracellular loop and the C-tail of hPanx1 to serines, and by mutating one native cysteine in the first transmembrane domain to alanine (C136S, C170S, C216S, C347S, C422S, and C40A). We confirmed the voltage-dependent channel activity of Δ6C was similar to that of the parent hPanx1+GS (Figure 2.13A). We then introduced cysteines into every position of the N-terminus and tested each cysteine mutant for reactivity to MAL-dPEG, a water

soluble, thiol reactive compound that tags exposed cysteines with a ~2 kDa moiety. Using western blots against the FLAG-tag attached to the hPanx1 cysteine mutants, we could then determine which positions in the N-terminus are exposed to solution (Figure 2.12A). For positive controls we reintroduced native C170 located on the intracellular loop or C426 found on the C-terminus, which are regions of hPanx1 we predict to be exposed to the cytoplasm. As validation of this technique, we could detect a noticeable increase in molecular weight as detected by western blots from hPanx1+GS, Δ6C/170C, and Δ6C/426C, but not from Δ6C alone. This affirms that MAL-dPEG specifically labels cysteine residues that are accessible to the cytoplasm (Figure 2.12B).

Using this assay we found that a number of positions in the N-terminus react with MAL-dPEG (Figure 2.12B). Interestingly, the only positions that reacted to MAL-dPEG are found within the first 13 amino acids, including 3, 4, 6, 7, and 10-13. These results suggest that the N-terminal segment (residues 2-13) is partially exposed to solvent, while the other region appears not to be exposed to solution. Such a region may be partially hidden by secondary structure or located within the lipid bilayer. We anticipated that some cysteine mutants generated for this assay might not form voltage sensitive channels, and thus, may not represent a native conformation of hPanx1. To rule out this possibility, we tested several cysteine mutants for channel activity (Figure 2.13B). Of the mutants tested, all showed hPanx1 currents as evidenced by voltage-dependent currents, suggesting the mutants used in this assay do not disrupt channel function. Altogether, this experiment suggests that the N-terminus of hPanx1 is only partially exposed to the cytoplasm, with the majority of this domain being inaccessible.

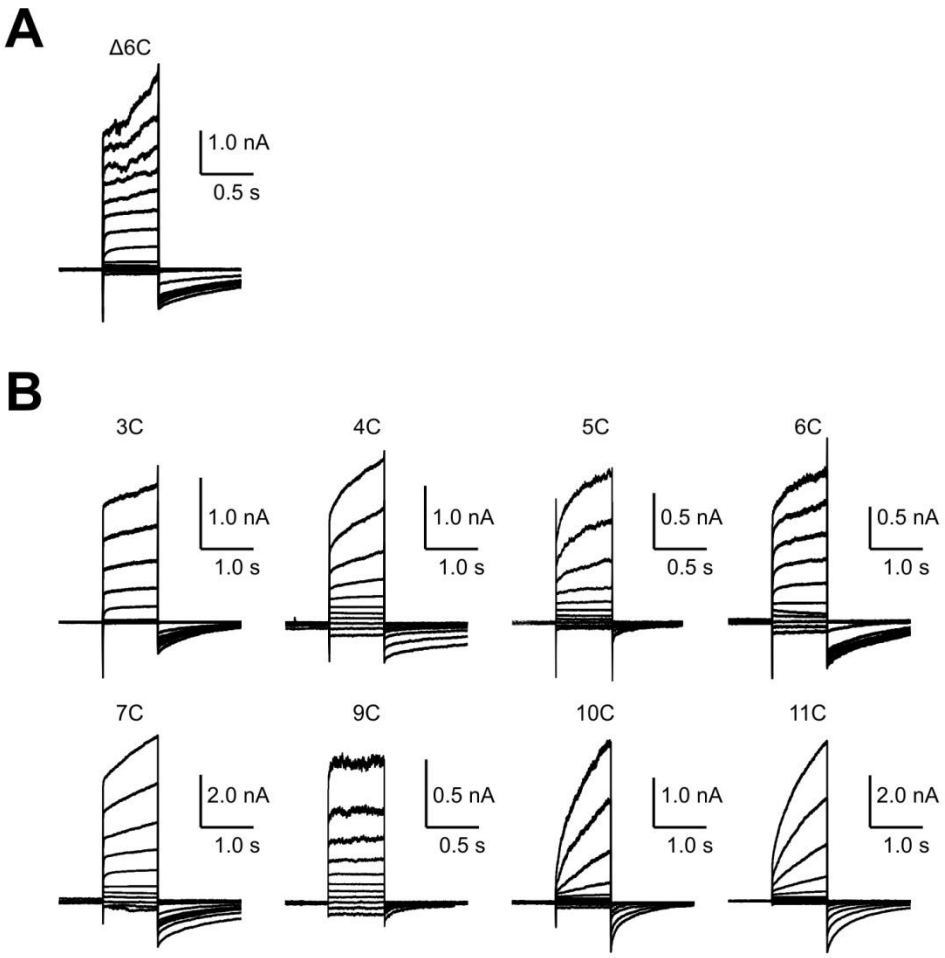

Figure 2.13 Whole cell recordings of HEK cells expressing the Δ6C construct and single cysteine derivatives. (A) Representative whole-cell recording of an HEK cell expressing the Δ6C variant. The cell was held at -60 mV and stepped between -100 and +160 for 0.5 s in 20 mV increments. (B) Single cysteine mutants were tested for voltage-gated Panx1 activity by a series of voltage steps from -100 mV to +100 mV for 1.0 s or 0.5 s in 20 mV increments from a holding potential of -60 mV.

E9 may play a role in regulating voltage-dependent channel activity

All charged residues in the N-terminus (E9, D14, K18, E19, E22, K24, K26, R29, E31, D35, and K36; Figure 2.14A) were inaccessible to solvent, which is consistent with the idea that these residues may be located in a domain embedded within the voltage field. To test the possibility that some of these positions are directly involved in voltage sensing, we mutated these charged residues to alanines on the hPanx1+GS parent construct. We tested each alanine mutant for voltage-dependent channel activity, with

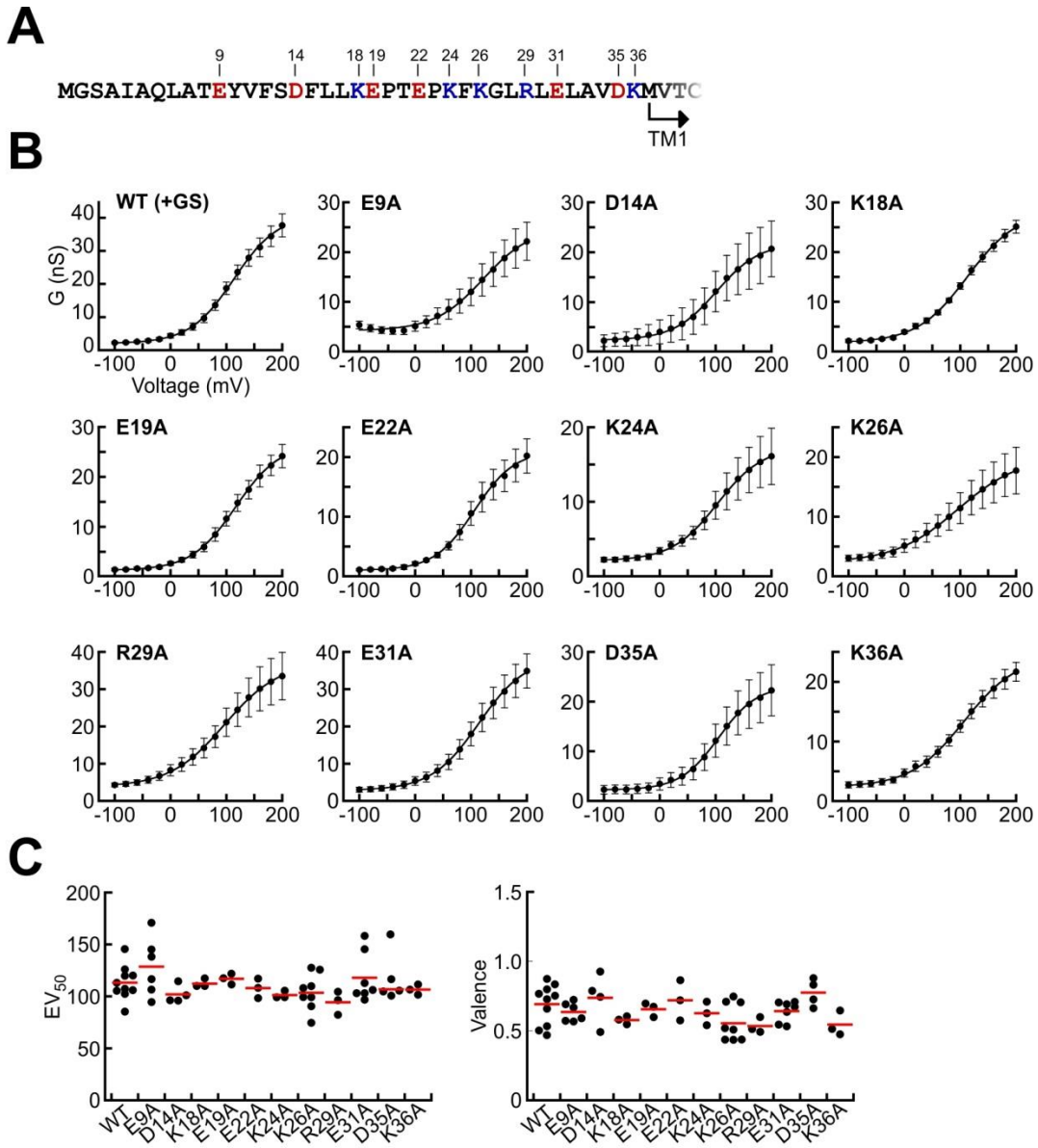

Figure 2.14. Charged amino acids do not contribute to Panx1 voltage sensing. (A) Sequence of the human Panx1 N-terminus colored to show the location of the acidic (red) and basic (blue) amino acids. (B) G-V curves of alanine mutants of the charged amino acids found within the N-terminus. HEK293 cells were held at -60 mV and stepped between -100 and +200 mV in 20 mV increments for 0.1 s. (C) EV50 and valance analysis of the G-V curves presented in (B). Each point represents an individual measurement and red bars represent the mean value of 3-10 cells.

the expectation that some of them may drastically reduce voltage-sensing capabilities.

All alanine mutants seemed to be assembled properly in HEK cells and gave rise to robust currents triggered by positive membrane potentials (Figures 2.14B and 2.11). To crudely evaluate the effect of each alanine mutation on voltage-sensitivity, we fit the

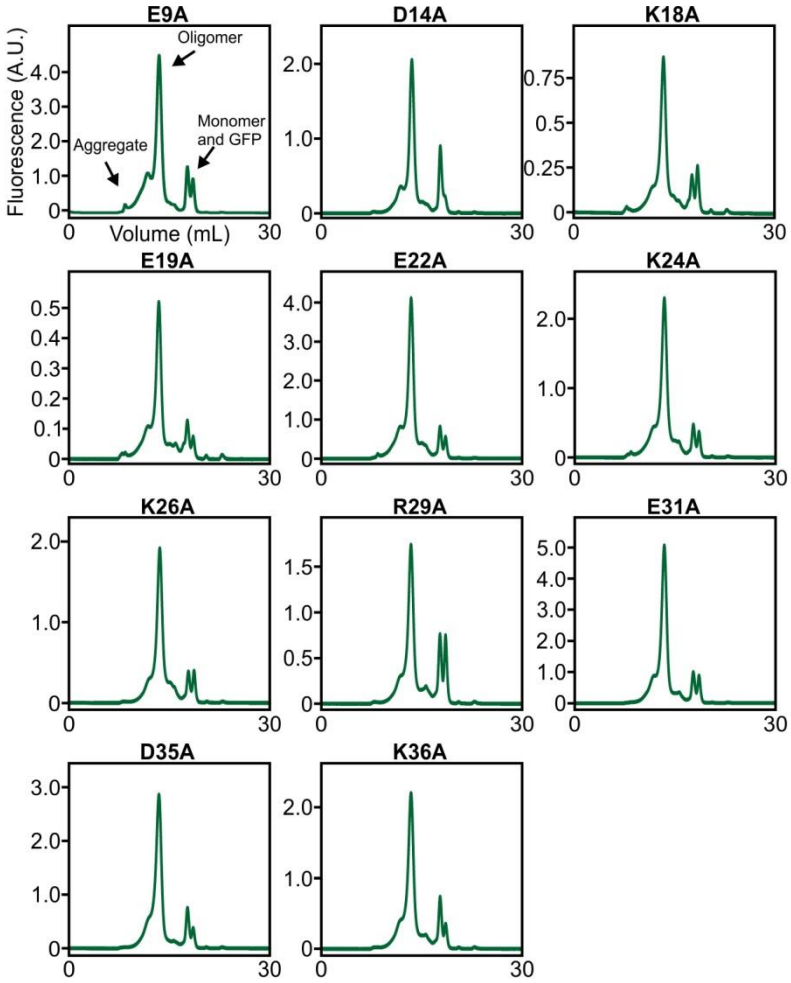

Figure 2.15. FSEC analysis of N-terminal alanine mutants. Each mutant was tagged with GFP at the C-terminus, transfected into HEK293 cells, solubilized in detergent, and analyzed by size exclusion chromatography.

conductance-voltage (GV) plot with the Boltzmann's equation and compared the valence and the voltage required to achieve 50% of the maximal response (EV_{50}). Though the GV relationship of the parent hPanx1+GS construct did not saturate even at +200 mV, the fit was reasonable (R=0.999; Chisq=2.693) and showed the average EV_{50} value of 113 mV and the valance of 0.69 (n=11). These numbers are consistent with the very weak voltage sensitivity of hPanx1. Notably, the eleven alanine mutants also showed similar EV_{50} and valence values (Figure 2.14C) and no statistically significant difference was detected by one-way ANOVA and Dunnet's test (P>0.05). These

mutants also did not alter the assembly status of hPanx1 (Figure 2.15). These data suggest that none of the single charged residues play a major role in voltage sensation.

Interestingly, we noticed that the E9A mutant is also activated at negative potentials and gave rise to strong currents especially below -100 mV (Figure 2.16A). Given that the voltage-dependent activation of E9A between -100 mV and +200 mV was similar to that of the parent hPanx1+GS (Figure 2.16B), the inward currents observed below -100 mV are probably not due to a reversed polarity in voltage sensitivity. A conservative mutation at this position (i.e. E9D) showed almost the same voltage-dependent channel activity to hPanx1+GS (Figure 2.16B). Likewise, a positively charged amino acid at this position (i.e. E9K) showed a slightly weaker, but similar voltage-response to hPanx1+GS (Figure 2.16B). The E9A mutation was generated on the +GS hPanx1 construct to analyze this mutation for changes in EV50 and valence. However, to understand if this mutation is sufficient to achieve channel activity at negative potentials of the wild-type protein, we made the E9A variant without the GS. This construct displayed relatively weak outward currents and had a constitutive leak current compared to the wild-type channel, perhaps suggesting E9 is directly involved in regulating pore permeation (Figure 2.16C). Channel activation was observed at negative potentials similar to the +GS version (Figure 2.16C and D). This suggests the channel influence of the E9A mutation is independent from the GS insertion, and that the effects of both are complementary. Together, these data suggest that E9 may play a positive role in closing or decreasing the conductance of the Panx1 channel at negative potentials.

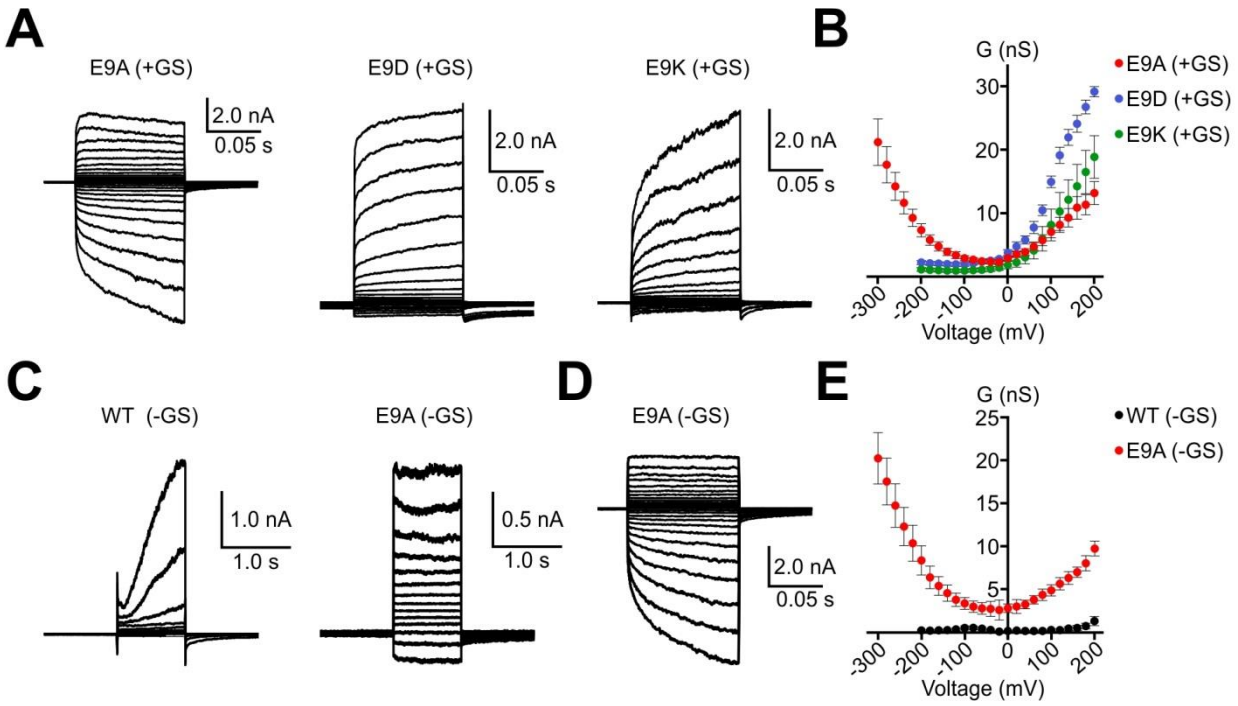

Figure 2.16. E9A results in inwardly rectifying currents. (A) Whole cell recordings of HEK293 cells transfected with the E9A (+GS), E9D (+GS), or E9K (+GS) Panx1 mutants. Cells were held at -60 mV and stepped between -300 mV and +200 mV in 20 mV increments for 0.1 s (E9A), or between -200 mV and +200 mV (E9D and E9K). Shown are representative recordings of 4-6 cells. (B) G-V curves were generated by plotting mean conductance at each voltage, and error bars represent SEM. (C) Whole cell recordings of WT hPanx1 (-GS) and the E9A (-GS) mutant. Cells were held at -60 mV and stepped between -100 mV and +160 mV for 1 s. Shown are representative recordings from at least 4 cells. (D) Whole cell recording of the E9A (-GS) mutant. Recording was obtained by holding the cell at -60 mV and stepping between -300 mV and +200 mV for 0.1 s. Shown is a representative of 4 different cells. (E) G-V curves were generated by plotting mean conductance at each voltage, and error bars represent SEM.

Discussion

In this study, we demonstrate that the Panx1 N-terminus plays a pivotal role in voltage-dependent channel activity. We found that addition of one or two specific amino acid(s) right after the first Met substantially enhances Panx1 channel activity. In contrast, insertion of more than two amino acids or deletion of a few residues at this position diminish the channel activity. Importantly, such N-terminal manipulations do not seem to affect Panx1 channel folding or assembly. We also show that the first half of

the N-terminus is partially exposed to solvent, while the last half is protected from chemical modifications. These are consistent with the idea that Panx1 N-terminus is not merely hanging in the cytoplasm, but rather forms a structured domain, potentially within the permeation pore, like seen in connexin or innexin channels.

How does the N-terminus regulate voltage-dependent channel activity of Panx1? One possibility is that this domain acts as a voltage sensor. Given that 1) the counterpart domain in connexin channels harbors a voltage sensor (91) (Harris and Contreras, 2014) and 2) Panx1 does not possess charged residues in the transmembrane helices, this idea sounds reasonable. However, we observed no change in EV_{50} or valence values from any of the 11 single alanine mutants of the charged residues in the N-terminus (Figure 2.14). These results are in contrast to the N-terminal mutants of connexin channels, which exhibit remarkably altered voltage responses (93, 94, 95). While it is still possible that multiple charged residues work together to achieve sufficient voltage-sensitivity, our data suggest that the Panx1 N-terminus regulates voltage-dependent channel activity in a different way from that of connexins.

Another possibility is that the N-terminus is not directly involved in voltage-sensing but governs other channel properties such as ion selectivity or conductance. If this is the case, voltage is somehow sensed by the transmembrane or other unfound domains in the voltage field. Movement of the voltage sensor then triggers rearrangement of the N-terminus, which could alter the electrostatic surface potential or physical diameter of the permeation pore, allowing more ions to flow. Interestingly, manipulation of a connexin N-terminus, which lies within the pore lumen, also alters ion

permeation properties (92, 91). Combined with our accessibility assays, the N-terminus of Panx1 may also fold up into the channel cavity and form part of the permeation pathway. This could explain why deletions, insertions, or tagging GFP to this terminus leads to loss of channel activity, as the permeation pathway could easily be disrupted by these modifications.

We found in this study that an insertion of Gly-Ser at the N-terminus substantially enhances the voltage-gated channel activity of Panx1. This is an excellent tool for studying Panx1, as voltage stimulation is convenient and easily controlled. But how does +GS enhance Panx1 channel activity? Our single channel recordings revealed that +GS elevates the apparent open probability of hPanx1 channels, which normally open only at an extremely high membrane potential (i.e. >+120 mV). This N-terminal manipulation also gave rise to a wide range of unitary currents, which do not seem to exist in the wild type hPanx1. One potential mechanism is that the natural N-terminus contributes to keep the channel closed under normal conditions, rendering it insensitive to voltages up to +120 mV. Notably, we found that the E9A mutant gives rise to strong voltage-dependent currents at negative membrane potentials (<-100 mV; Figure 2.16). Considering that hPanx1 channel is normally closed at negative potentials, this gain-of-function phenotype suggests that an unknown voltage sensor tries to push the channel open at negative potentials but such a structural rearrangement may be blocked by E9 in the native N-terminus. Addition of GS may delocalize the N-terminus, which could lead to a wobbly pore that opens more frequently and less uniformly at positive membrane potentials (channel remains closed at negative potentials with intact E9). Because a Gly residue at the 2nd position could get co-translationally myristoylated

(96), the N-terminus of hPanx1+GS may be rearranged due to lipidation. This idea explains why insertion of Ser-Gly had no effect on hPanx1 and insertions of a hydrophobic residue such as Trp or a phospholipid-interacting residue like Lys mimicked the effect of Gly-Ser (Figure 2.7). Importantly, deletions or insertions of a few amino acids near the first transmembrane helix disrupts the hPanx1 channel assembly (Figures 2.9 and 2.10). These suggest that the N-terminus does not function merely as a pore-plug but rather forms a tight structural domain that controls ion permeation.

We and others have reported that Panx1 channels give rise to conspicuous voltage-dependent currents (25). We found in this study, however, that the wildtype hPanx1 with its native N-terminus responds to voltages only beyond +100 mV. This unusually weak voltage-dependent activity might be a reason why some groups failed to record voltage-activated hPanx1 currents (58). Notably, we found that the mouse Panx1 (mPanx1) also responds to voltage very weakly and its activity is remarkably enhanced by the addition of Gly-Ser (Figure 2.3). This is not limited to our experimental conditions, as we also observed similar activities from CHO cells (Figure 2.3) and in a recording buffer commonly used to show strong voltage-dependent activity (Figure 2.3B; (Romanov et al., 2012)). These results are inconsistent with previous studies which showed robust and perhaps constitutive channel activity from mPanx1 (58, 40). Though the actual reason for this discrepancy is unclear, it is possible that mPanx1 with an unintentionally altered N-terminus might be used in those studies. Alternatively, different degrees of post-translational modifications, which could be due to various passage numbers or different culture conditions, may result in inconsistent mPanx1 channel

activity. Indeed, phosphorylation and S-nitrosylation have been shown to modulate Panx1 channel activity (50, 54, 60)..

Our single channel recordings revealed that hPanx1 opens a channel at +120 mV with a unitary conductance of ~20-40 pS. This is less than half of the channel activated by C-terminal cleavage or by α1-adrenoceptor (43). We suspect that only a subset of the C-termini move out from the hPanx1 pore at +120 mV. Unfortunately, we could not test whether unitary conductance becomes larger at higher voltages, as single channel patches did not survive at those membrane potentials. An alternative explanation is that the mode of channel opening at such a high voltage substantially differs from other modes, which are normally tested at membrane potentials up to +80 mV.

In conclusion, we demonstrate that Panx1 hardly opens at a positive membrane potential, but its activity redoubles when a couple of specific amino acids (GS in particular) are inserted at the N-terminus. While this is an artificial way to promote Panx1 activity, a natural facilitation mechanism may exist. For example, posttranslational modification or interaction with the other cytoplasmic domains at N-terminus may enhance the channel activity. Involvement of the N-terminus in Panx1 channel gating/ion permeation supports that pannexins may be structural analogues of connexins and innexins.

CHAPTER III – Towards obtaining a structure of a pannexin channel

Introduction

A high resolution structure of pannexin would be paramount for understanding properties of the channel and mechanisms surrounding channel gating. Often times, crystal structures of membrane proteins reveal unanticipated biophysical properties or protein nuances that were otherwise overlooked or which previous experiments incorrectly characterized. For example, biochemical and biophysical methods for determining the oligomeric state of large multimeric ion channels are not particularly efficacious, and are often corrected years later when a structure is solved. Examples of this are seen in the Orai, bestrophin, and innexin fields. Cross-linking and photobleaching experiments originally suggested that Orai, a calcium channel, formed a tetramer (97). Four years later, the orai crystal structure revealed this channel forms a hexameric assembly (98). Similarly, the chloride channel bestrophin-1 was determined to be a tetramer by single-molecule photobleaching but was later crystallized and revealed to be pentameric (99, 100). Finally, speculations had originally assumed that innexins formed hexameric channels and a later cryo-EM structure determined it then to be octomeric (101, 102). Many of the techniques used to characterize these multimeric channels have also been applied to the pannexin family. Photobleaching and crosslinking currently support Panx1 being hexameric and crosslinking suggests Panx2 as a putative octomer (43, 103). It would be enlightening to verify the literature and to know whether subunit stoichiometry is consistent within the pannexin family or if perhaps they oligomerize in unique ways.

In addition to subunit stoichiometry, ion channel crystal structures can reveal novel pharmacological insights including unanticipated antagonist binding sites and unusual ligand binding pockets. An example of this is observed in the P2X field. These channels activate upon ATP binding but primary sequence analysis originally failed to identify any canonical ATP binding pocket in the P2X family that shared homology to other known ATP-binding proteins. Mutagenesis was successful in localizing the ATP binding site to a handful of residues, but the architecture of this site was still a mystery (104). Successful crystallization of P2X channels later revealed the unique ATP binding sites which are located at the interfaces between subunits of this trimeric receptor (105, 106). Inhibition of the P2X7 receptor by small molecules has also been a subject of controversy. A handful of compounds have been developed to inhibit this receptor but their mechanisms of action were disputed. Some inhibitory molecules were characterized as competitive antagonists and others as non-competitive. Crystal structures of a P2X7 receptor in complex with these antagonists revealed that all compounds bind to a novel allosteric ‘drug binding site’ located in the upper turrets of the receptor, distal from the ATP binding site (107). These compounds do not prevent ATP from binding to the ATP binding site, but prevent protein movements necessary for channel opening. Essentially, these drugs lock the receptor into a closed conformation. Several compounds have been characterized as Panx1 inhibitors and their mechanisms of action are likewise controversial. Although we have mapped putative binding residues for Panx1 inhibitors, the location of these sites in relation to the channel pore is undefined. Additionally, there are currently no high specificity or high affinity

antagonists against Panx1, and solving an inhibitor-bound Panx1 structure would open the field to structure-based drug design.

Given the complexity of pannexin activation and regulation, a direct visualization of this channel would expose valuable insights. There is currently a deficit of information regarding some basic pannexin properties which would undoubtedly be revealed in light a high resolution structure. For example, the ion permeation pathway and pore-lining helix have still not been identified. Along these lines, details about ion selectivity could be explained if the permeation pathway was defined. Perhaps the most interesting is that mechanisms surrounding channel gating – including activation and inhibition – could be clarified to truly understand how pannexin channels operate in physiology. What is the structure of the C-terminus and how does it block the pore? How does phosphorylation of intracellular motifs correlate with channel opening? Why does addition of 2 amino acids to the N-terminus drastically change channel activity? In light of these seductive questions, we sought to obtain a structure of a pannexin channel by x-ray crystallography.

Materials and Methods

Reagents

All chemicals were purchased from Sigma-Aldrich unless described otherwise.

FSEC screening

Pannexin constructs were synthesized based on protein their protein sequence (GenScript). To facilitate cloning, all constructs included a BamHI site immediately after the start Met (GGATCC) resulting in the insertion of a GS, and an XhoI site immediately before the stop codon (GCCTCGAG) resulting in the addition of ASS after the final amino acid of each protein. Constructs were subcloned into the BamHI and XhoI sites of the pC-GFP-EU2 or pN-GFP-EU2 vectors (108). Fusion constructs were transfected into HEK cells previously plated in wells of a 6-well plate at ~80-100% confluency using 2 µg DNA and 5 µL FuGENE6, as described by the manufacturer. After 2 days, cells were collected in 2 mL centrifuge tubes, washed with 1 mL cold PBS, and lysed in solubilization buffer (1% $C_{12}E_8$, 1x PBS, 1x protease inhibitor cocktail) for 30 minutes at 4 °C with rocking. Lysates were spun 21,000 x g for 5 minutes at 4 °C, then 70,000 rpm (TLA100.3 rotor) for 20 minutes at 4 °C. A sample of supernatant (50 µL) was injected into a Superose 200 10/300 column equilibrated with 1x PBS supplemented with 0.5 mM $C_{12}E_8$ at 0.5 mL/min and the elution was monitored for GFP fluorescence (ex: 480, em: 508).

Bacmid and virus generation

frPanx1 constructs (1 µl) in various fast-bac vectors (described in 107, 110) were mixed with 20 µl DH10Bac competent cells on ice for 30 minutes. Cells were heat shocked for 45 second at 42 °C, put back on ice, and 500 µl SOC media was added followed by shaking at 37 °C for 2-4 hours. Cells (~50 µl) were directly plated onto LB/Bac plates containing 50 µg/ml kanamycin, 6.8 µg/ml gentamicin, 10 µg/ml tetracycline, 100 µg/ml

Bluo-gal, and 40 µg/ml IPTG and incubated at 37 °C for 2 days. White colonies were inoculated into 7 mL of LB/Bac media containing 50 µg/ml kanamycin, 6 µg/ml gentamicin, and 10 µg/ml tetracycline and grown overnight at 37 °C.

Bacmid DNA was isolated by spinning cultures at 3500 rpm for 10 minutes, suspending cells in 250 µl Solution 1, followed by 250 µl Solution 2, followed by 350 µl Solution 3. Lysates were clarified by centrifugation at 21k x g for 10 minutes. 700 µl clarified lysate was mixed with 700 µl phenol:chloroform:isoamyl alcohol, vortexed briefly, and centrifuged at 21k x g for 2 minutes. The top layer was retrieved and added to 700 µl chloroform, vortexed briefly, and centrifuged again. The top layer was mixed with 1.4 mL 100% ethanol, vortexed briefly, and chilled at -20 °C for 20 minutes. DNA was pelleted by centrifugation at 21k x g for 15 minutes at 4 °C, and the supernatant was aspirated. Pellets were washed with 1 mL of 70% ethanol, centrifuged again, and dried in a vacuum desiccator for 1-2 hours. Finally, pellets were dissolved in 50 µl sterile water.

Sf9 cells were plated to a density of 80 x 10^4 cells/well on a 6-well plate and media was exchanged to SFM-900 III. Transfection mixtures were prepared with 100 µl SFM-900 III media, 5 µl bacmid DNA, and 15 µl PEI (1 mg / ml pH 7.4). Following brief mixing and incubation at room temperature for 15 minutes, mixtures were added to cells and incubated for 7 days at 27 °C, with occasional rocking to mix.

P1 virus was harvested by collecting the supernatant, which was stored with 1x pen/strep at 4 °C until use. In some cases, P1 was amplified by adding 100 µl to a 6-well plate containing ~200 x 10^4 cells/ml in 2 ml media for 4 or 5 days. P2 was

generated by infecting 150 ml Sf9 cells at a density of $100x10^4$ cells/ml with 75 µl P1. Cell density was checked every day for 3 or 4 days to monitor the infection. After 4-7 days, cells were collected in 50 ml conical tubes, centrifuged at 4000 rpm for 10 minutes, and the supernatant (20 ml) was used to infect 1 L cultures at densities of ~250-350 x 10^4 cells/ml.

Protein purification

After 48 hours infection, cells were collected (4000 rpm JA4.2), washed once in PBS (5000 rpm JA-14), and then lysed by nitrogen cavitation at 750 psi for 20 minutes in PBS supplemented with PMSF, pepstatin, aprotinin, and leupeptin. Lysate was centrifuged at 9.1k rpm (JA-14) for 10 minutes and the supernatant was centrifuged 32k rpm (Ti-45) for 40 minutes. Membrane pellets were collected, dounce homogenized in PBS, and solubilized in solubilization buffer containing PBS, 1% $C_{12}E_8$, and 7.5% glycerol. After 40 minutes, insoluble material was removed by centrifugation at 32k rpm (Ti-45) for 40 minutes. The clarified lysate was incubated with 4 mL strep resin for ~30-40 minutes, collected on a column, and washed until the flow-through has an A280 = 0 with 1x wash buffer supplemented with 0.5 mM $C_{12}E_8$ and 7.5% glycerol (typically, 25 mL wash buffer per 2 mL resin). Protein was eluted with 1x elution buffer supplemented with 0.5 mM $C_{12}E_8$ and 15% glycerol, concentrated to 1 mL, and treated with EndoH 1:40 overnight. Protein was spun in the TLA100.3 rotor 70k rpm for 20 minutes, and 500 µl was injected onto a Superdex Increase 10/300 column equilibrated with 150 mM NaCl, 10 mM Tris pH 8.0, 15% glycerol, and 0.5 mM DDM at 0.2 mL/min flow rate.

Peak fractions were pooled, concentrated to ~15 mg/ml, spun at 70k for 20 minutes, and used for crystallography at 6-15 mg/ml.

Antibody production, screening, and complex formation

frPanx1 “74A2” (frPanx1 residues 1-357 containing the N257A glycosylation knockout and the RDI intracellular loop motif (residues 152-154) replaced with a single alanine) was purified as described using $C_{12}E_8$ using a C-terminal strep tag, and protein was reconstituted into liposomes. Monoclonal antibodies were obtained as generally described in (109) by the Monoclonal Antibody Core at OHSU. Briefly, a mouse was immunized with Panx1 containing proteoliposomes, spleen cells were fused with mouse myeloma cells, and ELISA screening identified clonal cell lines producing Panx1-binding antibodies.

ELISA positive hybridoma culture media supernatants were obtained and mixed with ~3 µg C-GFP frPanx1 74A2 supplemented with additional $C_{12}E_8$. 10 µL of the mixture was injected onto a 3 mL Superdex 200 Increase 5/150 GL column (GE) at a flow rate of 0.2 ml/min and the elution was monitored for GFP fluorescence (ex: 480, em: 508).

Western blot screening was performed by resolving 1 ug frPanx1 74A2 with a C-terminal Strep tag on denaturing 10% SDS-PAGE gels. Gels were blotted onto PVDF membrane, blocked in 5% milk, and incubated in 10 mL 5% milk with 10 µL each hybridoma supernatant for 1 hour. Blots were washed, incubated with 10 mL 5% milk with 5 µL goat α-mouse-AP conjugate antibody for 1 hour, washed, and developed with

colorimetric substrate. Suitable antibodies bound to intact Panx1 (determined by size shift on exclusion chromatography) but did not bind denatured Panx1 (determined by no western blot signal), and were purified from larger cultures (performed by OHSU).

Fab fragments were obtained by digesting purified antibody (1 mL at various concentrations) with papain (1:100) in a final volume of 1.5 mL and a final buffer composition of 100 mM sodium phosphate, 10 mM EDTA, 10 mM cysteine, pH 6.3 for 2 hours at 37 °C. Digestion was quenched by adding iodoacetamide to 30 mM final concentration, and the mixture was applied to a 30 kDa centrifugal unit and washed with ~20-30 volumes of ion exchange buffer (either 10 mM sodium citrate pH 5.5 or 10 mM tris pH 8.0) followed by concentration to ~3 mL. Fabs were isolated by applying the mixture to a 1 mL HiTrap Q HP or HiTrap SP FF (GE) column followed by washing with ~5 column volumes of ion exchange buffer. In some cases the flow-through contained the fab. In other cases the fab was eluted with ion exchange buffer supplemented with NaCl to form a salt gradient from 0-250 mM NaCl over 30 minutes while collecting 1 mL fractions.

For crystallography, isolated fab was pooled and mixed with purified frPanx1 at a 1:1.2 (Panx1:fab) ratio on ice for 30 minutes before concentration to 500 µL and isolation of the complex by size exclusion chromatography.

Panx1 Crystallography

Crystals were grown with 1 µl reservoir (not diluted with glycerol) + 0.5 µl protein (6-15 mg/ml) equilibrated over a reservoir containing 1 M ammonium formate, 0.1 M tri-

sodium citrate pH 5.2, 9.8 – 10.8% PEG 1500, then diluted to 15% glycerol (425 µl solution + 75 µl glycerol for 500 µl total). Microseeding is performed ~24 hours later using a hair from Toshi's head. Crystal dehydration is performed at 4 °C by increasing PEG 1500 to 26% in 2.5% increments for ~1 hour each step, then letting crystals soak in the final solution overnight before freezing.

Results and Discussion

Crystallization trials require large amounts of stable, high quality protein. Often times, membrane proteins are challenging to purify due to instability in detergents and poor expression. Many of these challenges can be overcome using the high-throughput screening technique known as fluorescent size exclusion chromatography (FSEC), which reveals information about a proteins behavior in detergent. The result of an FSEC experiment is a set of chromatography profiles where the peaks can be analyzed for symmetry (protein monodispersity), height (protein expression), and elution volume (oligomeric size). Proteins which fail to display good characteristics are triaged, and those which show promising profiles are further explored by purification attempts.

Although human Panx1 would be the most physiologically relevant protein to study, it is not necessarily the best candidate to pursue for crystallography. To have the highest chance of obtaining a pannexin structure, we started with a broad screen of potential crystallization candidates that share some homology with human pannexins. We obtained a library of Panx1, Panx2, and Panx3 proteins from various vertebrate organisms. Each candidate was tagged at the N- or C- termini with GFP, expressed

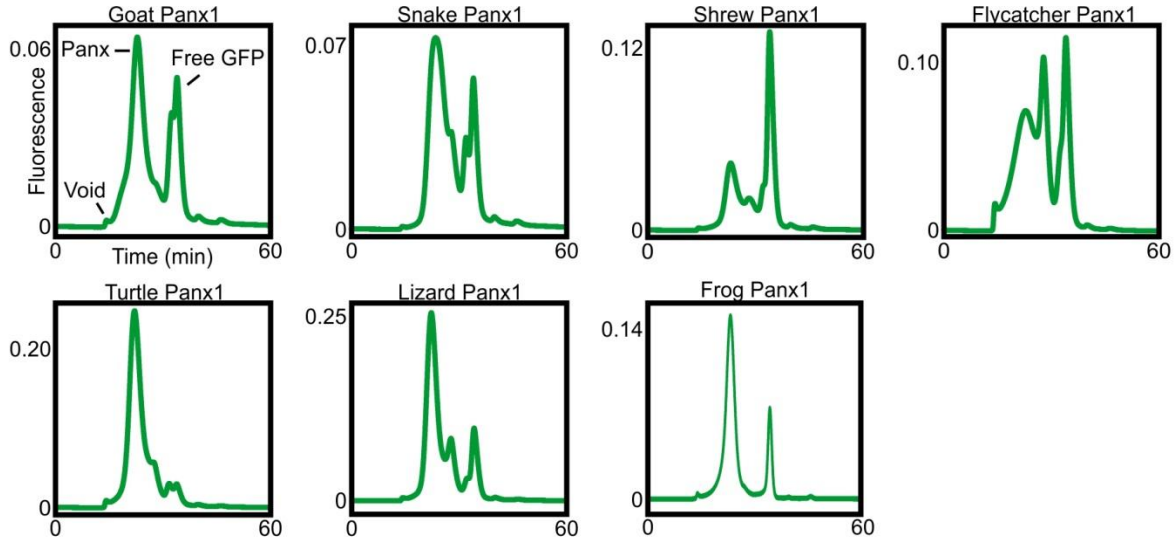

Figure 3.1. Frog panx1 is stable in detergent. FSEC chromatograms of various pannexin-1 orthologs. Full-length proteins were tagged C-terminally with GFP, expressed in insect cells, and detergent solubilized extracts were analyzed by size-exclusion chromatography on a superose 10/300 column. The eluent was monitored for GFP fluorescence (ex/em 480/508).

with baculovirus in Sf9 cells, solubilized in detergent, and analyzed by size-exclusion chromatography. The eluate was monitored for GFP fluorescence over time which results in a chromatography profile reflective of the solution behavior of each protein species.

The behavior of ~40 pannexin candidates was analyzed (Figure 3.1). In general, Panx1 proteins behaved significantly better and had more promising profiles than their Panx2 and Panx3 brethren. Virtually no Panx2 proteins displayed positive chromatography profiles, with most orthologs displaying high amounts of aggregate and dissociated species. (Interestingly, removal of the giant Panx2 C-terminus vastly improved the behavior of several orthologs, which may facilitate purification of this family member.) A few Panx3 proteins appeared to have attractive profiles, including cow Panx3 and human Panx3. However, the overall expression of these orthologs was

significantly weaker than Panx1. Nonetheless, they could be considered viable candidates to pursue for future work.

Among the Panx1 collection, although only 7 are shown for brevity, there was a range of protein behaviors (Figure 3.1). Goat and snake Panx1 show broad peaks with a significant amount of dissociated or monomeric species, suggesting these are not stable in detergent. Shrew Panx1 displayed very weak expression while flycatcher Panx1 had a large aggregate peak. Turtle and lizard Panx1 have promising profiles, with dissociated species comprising only a small fraction of the total protein. Many other orthologs mimicked the behaviors of the representative proteins shown here. Superseding all others was frog Panx1 (frPanx1), which showed a single sharp, symmetric peak. This is indicative of a protein stable in detergent since there is virtually no aggregated protein or dissociated species. Based off these results, we pursued frog Panx1 as our crystallization target.

Typical purification schemes for membrane proteins usually involve an affinity purification step followed by a size-exclusion chromatography step. Where can frog Panx1 be tagged to facilitate affinity purification? The literature suggests the C-terminus of Panx1 sticks up into the channel and acts as an autoinhibitory domain. Likewise, our previous experiments suggest that the extreme N-terminus is critical for proper channel activity. Based off this, tagging either termini with a short affinity peptide might disrupt the channel structure into a non-native conformation. I hypothesized that we could circumvent this by placing the affinity tag at an internal position – the intracellular loop. This region of the protein is predicted to be flexible and disordered, and could probably be mutated to harbor an internal Strep II tag which is relatively

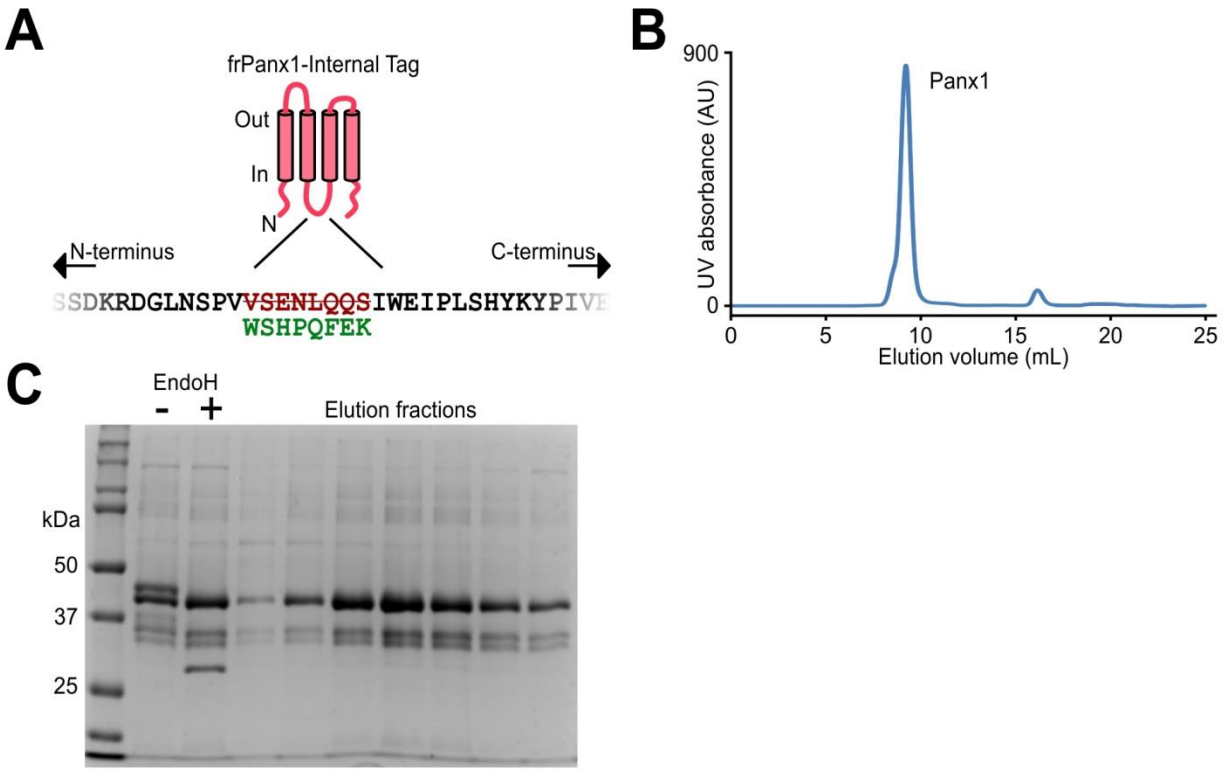

Figure 3.2. Full-length frog Panx1 purifies as a heterogenous mixture of oligomers. (A) Schematic diagram of the frog Panx1-Internal Tag construct. Pink cartoon represents the putative topology of Panx1. Below is the amino acid sequence of the intracellular loop. Amino acids crossed out in red were replaced with the Strep II tag sequence, shown below in green. (B) Size-exclusion chromatography of purifed frPanx1-Internal Tag. Proteins were treated with EndoH overnight and separated on a Superdex 10/300 Increase, with 0.5 mM C12E8 in the running buffer. (C) SDS-PAGE behavior of purified frPanx1-Internal Tag. Proteins eluted from the Strep column were treated with (+) or without (-) EndoH overnight. Peak elution fractions from (B) were assessed for purity.

amphipathic (Figure 3.2A). Most importantly, this construct has completely preserved N- and C- termini, suggesting it represents a near-native conformation of Panx1.

This construct could be successfully isolated from Sf9 cells using streptactin resin, suggesting the intracellular loop is exposed and that this strategy could facilitate pannexin purification (Figure 3.2). Of particular importance is the size exclusion chromatography (SEC) profile, which measures the solution behavior of the purified protein and separates good quality protein from aggregates and dissociated species (Figure 3.2B). The behavior of frPanx1-Internal Tag is quite good, displaying a single

sharp, relatively monodisperse peak. This is indicative of a stable protein species and validates the results from our previous FSEC screen.

However, SDS-PAGE analysis of the SEC fractions suggests otherwise (Figure 3.2C). When separated on a gel, frPanx1-Internal Tag is clearly not homogenous – the "elution fractions" all show 3 major bands. The predicted molecular weight of this construct is 49.2 kDa which probably corresponds to the heavier ~42 kDa species (it is not uncommon for membrane proteins to run at size different from their nominal molecular weight). Two other major bands run at ~35 and ~33 kDa and are contaminating. Although it's impossible to completely know what these bands represent, we hypothesized that they might be versions of frPanx1 that have been cleaved by proteases during purification. One clue that supports this is found when comparing protein treated with and without EndoH to remove post translational sugars. Treatment with EndoH reduces the size of one band of the major "doublet", consistent with the idea that only some of the Panx1 subunits receive glycosylation moieties. However, the same trend is observed for the contaminating species, where a faint 37 kDa band disappears after treatment with EndoH. This suggests the smaller species is likely to be Panx1 running at a lower molecular weight. Interestingly, the size difference between the full species (42 kDa) and the smaller species (35 kDa) roughly corresponds to the size of the distal non-conserved region of the Panx1 C-terminus (~7 kDa). We therefore hypothesized that the 'full length' Panx1 protein actually purifies as a mixture of full length protein and cleaved protein, likely resulting in heteromeric oligomers.

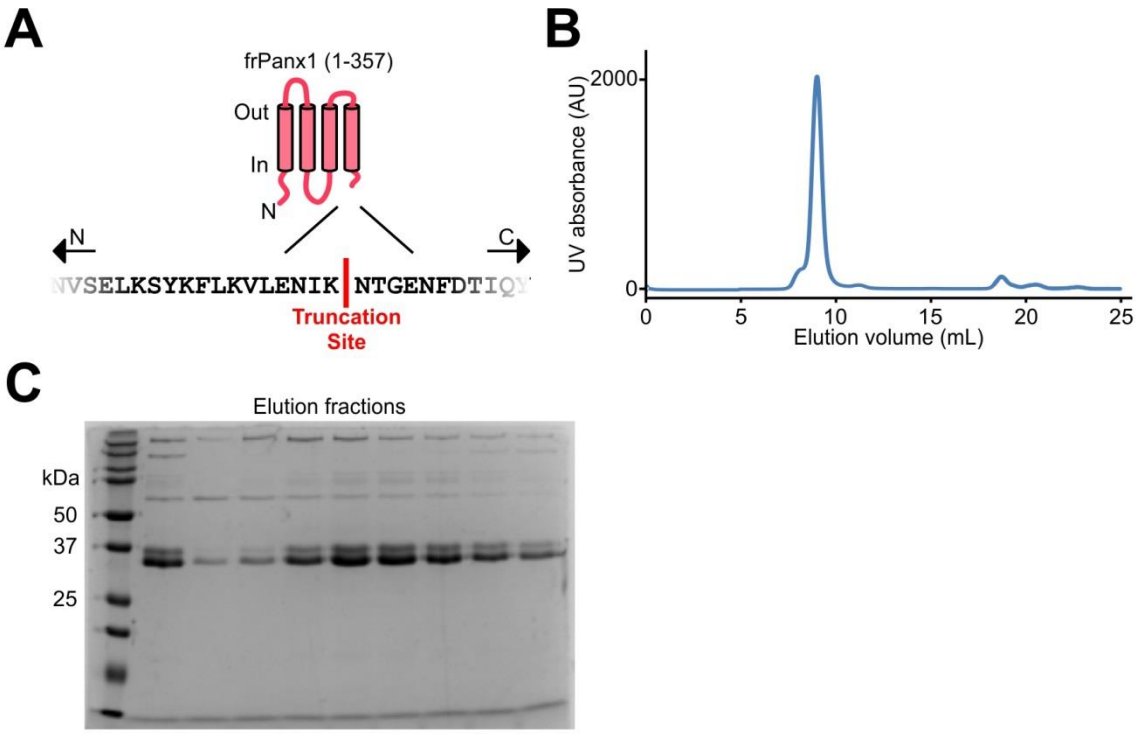

Figure 3.3. C-terminally truncated frPanx1 purifies as a singe species. (A) Schematic diagram of the frog Panx1 (1-357) construct. Pink cartoon represents the putative topology of Panx1. Below is the amino acid sequence of the C-terminal domain. The truncation position is indicated by the red line. (B) Size-exclusion chromatography of purifed frPanx1 (1-357). Proteins were treated with EndoH overnight and sperated on a Superdex 10/300 Increase, with 0.5 mM C12E8 in the running buffer. (C) SDS-PAGE behavior of purified frPanx1 (1-357).

To resolve this, we generated frPanx1 constructs with genetically truncated C-termini. Because the C-terminus is no longer preserved as in the native protein, we also moved the Strep affinity tag to the end of the truncated C-terminus. Initially a screen was performed to identify how much of the C-terminus could be removed without reducing expression or protein stability. This data is not shown, but frPanx1 could be truncated by ~70 amino acids, resulting in “frPanx1 1-357” (Figure 3.3A). This protein could be purified using identical strategies as the full length protein. The SEC profile of this truncated protein looks roughly similar (Figure 3.3B), suggesting the distal C-terminal region has no consequence on overall protein integrity. Interestingly, SDS-PAGE of the resulting elution fractions clearly shows fewer contaminants (Figure 3.3C).

Of particular importance, the previously seen higher molecular weight 42 kDa species has been removed, resulting in just the two lower molecular weight species. This result suggests, as previously hypothesized, that the full C-terminus of frPanx1 is susceptible to proteases which resulted in a heterogenous protein sample. Artificially truncating this part of the protein results in a higher quality sample.

frPanx1 1-357 purifies to homogeneity and displays reasonably good characteristics. We therefore used this protein for crystallization trials, mostly using protein solubilized in C12E8. Unfortunately we were unsuccessful at obtaining any protein crystals, suggesting something about this protein is not conducive to crystallization.

Given that the C-terminus of frPanx1 is predicted to be disordered and is not conserved between species, it is unsurprising to find that removing this part of the protein was beneficial. Sequence alignments identify a second region where conservation between species is low: the intracellular loop. We hypothesized that artificially deleting part of this loop might decrease flexibility of the overall protein, resulting in better crystallographic behavior. Initially, a random screen was performed to determine approximately how much of the intracellular loop could be removed without negatively impacting protein behavior. Out of 14 loop deletion constructs tested, one appeared to stand out in terms of protein behavior while also having a sizeable deletion. This particular construct had a total of 21 amino acids removed from the intracellular loop, and was dubbed “LD11” (for “loop deletion 11”).

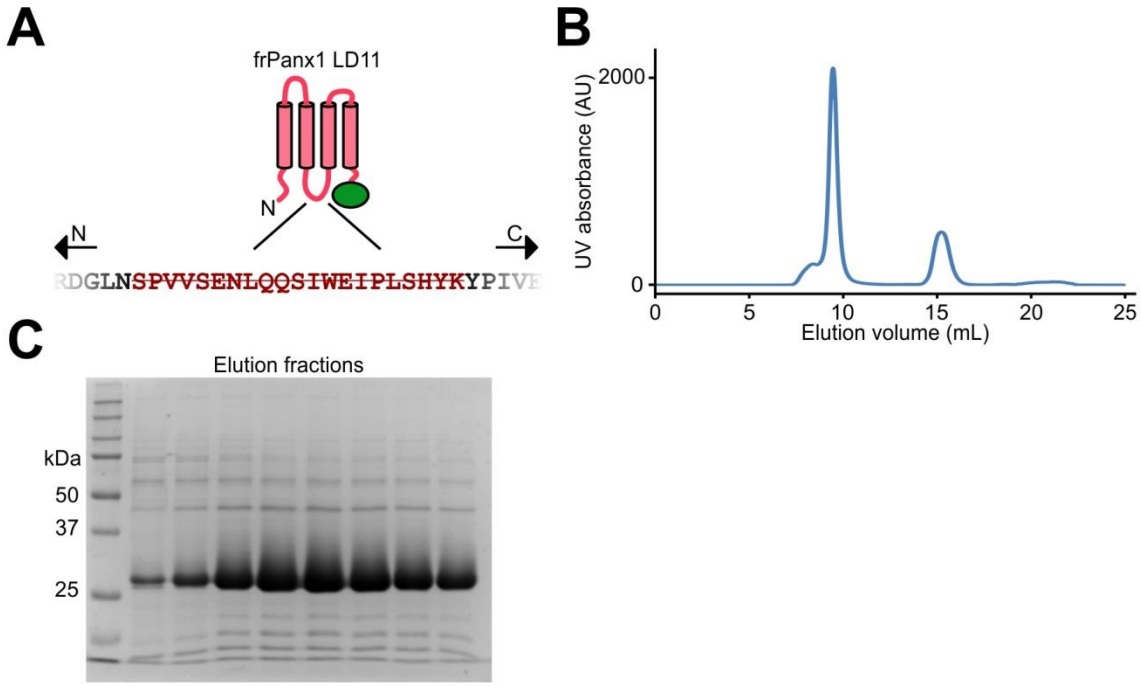

Figure 3.4. C-GFP frPanx1 LD11 purifies to homogeneity. (A) Schematic diagram of the frog Panx1 LD11 construct. Pink cartoon represents the putative topology of Panx1. Below is the amino acid sequence of the intracellular loop. The deleted amino acids are colored red and crossed out. (B) Size-exclusion chromatography of purifed frPanx1 LD11. Proteins were treated with EndoH and thrombin overnight and sperated on a Superdex 10/300 Increase, with 0.5 mM DDM in the running buffer. (C) SDS-PAGE behavior of purified frPanx1 LD11.

One modification was made to the purification scheme. The C-terminus of LD11 was tagged with GFP-Strep instead of just Strep (Figure 3.4A).

SEC elution fractions of LD11 were separated on SDS-PAGE (Figure 3.4C). The main protein species began running considerably lower than its predicted molecular weight (39 kDa predicted vs. ~28 kDa observed). This might reflect how this Panx1 protein is less flexible and may be more compact, thereby running faster on PAGE. We also began noticing recurring contaminating bands, especially at low molecular weights. These were later confirmed to be off-target proteolysis by thrombin (used to liberate frPanx1 from the GFP tag).

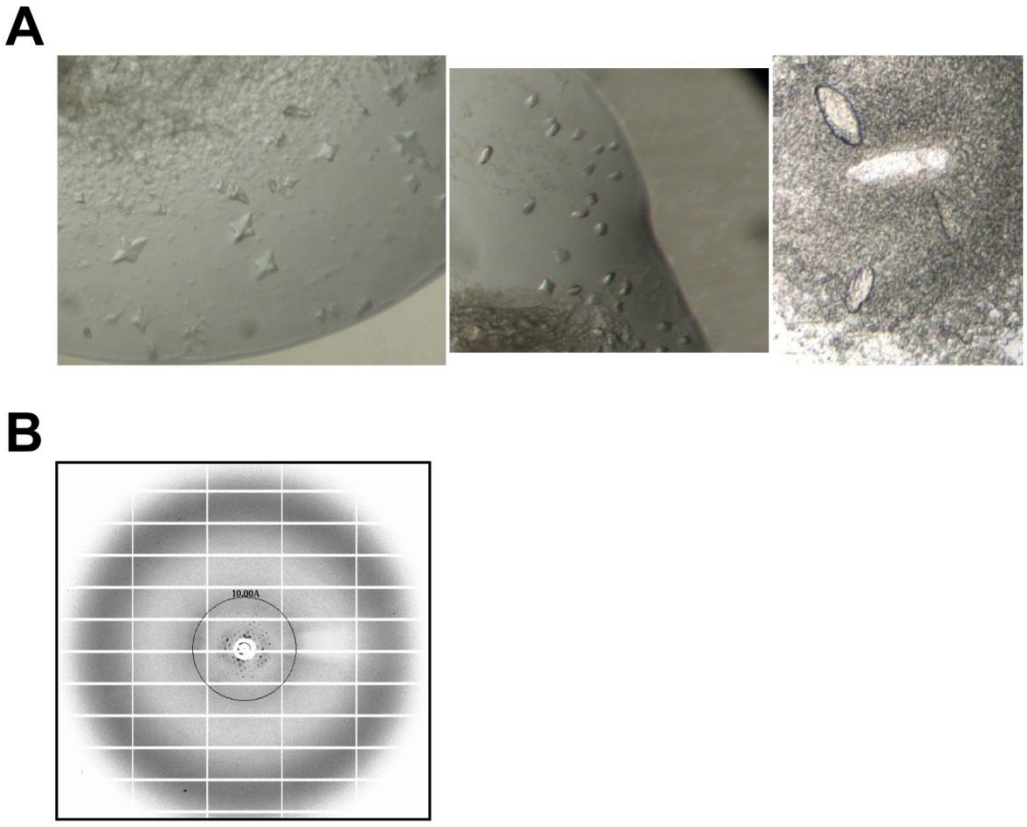

Figure 3.5. LD11 crystallizes in bicelles. (A) Examples of crystals of frPanx1 LD11 grown using bicelles. Proteins were reconstituted into DMPC/CHAPS/Cholesterol bicelles to 8% final concentration. Crystals appeared after several days. (B) Diffraction of bicelle-grown crystals. Crystals were scooped, frozen directly in liquid nitrogen, and analyzed for diffraction at CHESS.

This protein was subjected to crystallization trials. We were successful in obtaining our first pannexin crystals using bicelles as a crystallization media (Figure 3.5A). Bicelles are a mixture of lipids and detergents that form planar discs which can help facilitate crystallization of some membrane proteins. Strangely, bicelle-grown crystals could only be found if SEC was performed using C12E8, suggesting this detergent was required for crystal growth. Crystals that appeared followed no obvious trend in regards to conditions they grew in, with most growing between 10 – 15% PEG 4000 in a variety of salts and at any pH. Crystal shape was also highly variable, ranging

from small rectangles to stars to oblong ovals to chunky circles. Nonetheless, obtaining our first protein crystals indicated that we had improved our protein significantly.

LD11 crystals grown in bicelles were analyzed for diffraction at CHESS. Most crystals displayed poor diffraction quality, with most diffracting sub 15 Å. Sparsely reproduced were a handful of crystals that diffracted to 10 Å (Figure 3.5B). This was a promising start and we were hopeful that these crystals could be improved by optimizing growth conditions. Over the next 1.5 years I made many attempts to improve the growth conditions and quality of these bicelle-grown Panx1 crystals. Variables included different bicelle compositions, different SEC detergents, with or without Panx1 inhibitors, protein concentration, and crystal growth temperatures. I routinely failed to improve diffraction and growth, and continuously grew small, sad, misshapen crystals.

As an alternative avenue to pursue, we developed monoclonal antibodies against frPanx1 to use as crystallization chaperones. High affinity fab fragments have been successfully used to crystallize several recalcitrant membrane protein crystallization targets by binding to and forming a complex. This provides more exposed surface area which may facilitate new crystal contacts. Some fab fragments can also be conformational specific and lock dynamic membrane proteins into a single defined conformation, which vastly improves crystallogenesis. We obtained 59 potential monoclonal antibodies which were screened in two ways. We first checked for binding efficacy to purified frPanx1 by looking for a molecular weight shift measured by size exclusion chromatography. If an antibody binds to frPanx1 it will increase the mass of the complex considerably, whereas antibodies that do not bind will not increase the complex mass. We performed this screening on two constructs: the construct injected

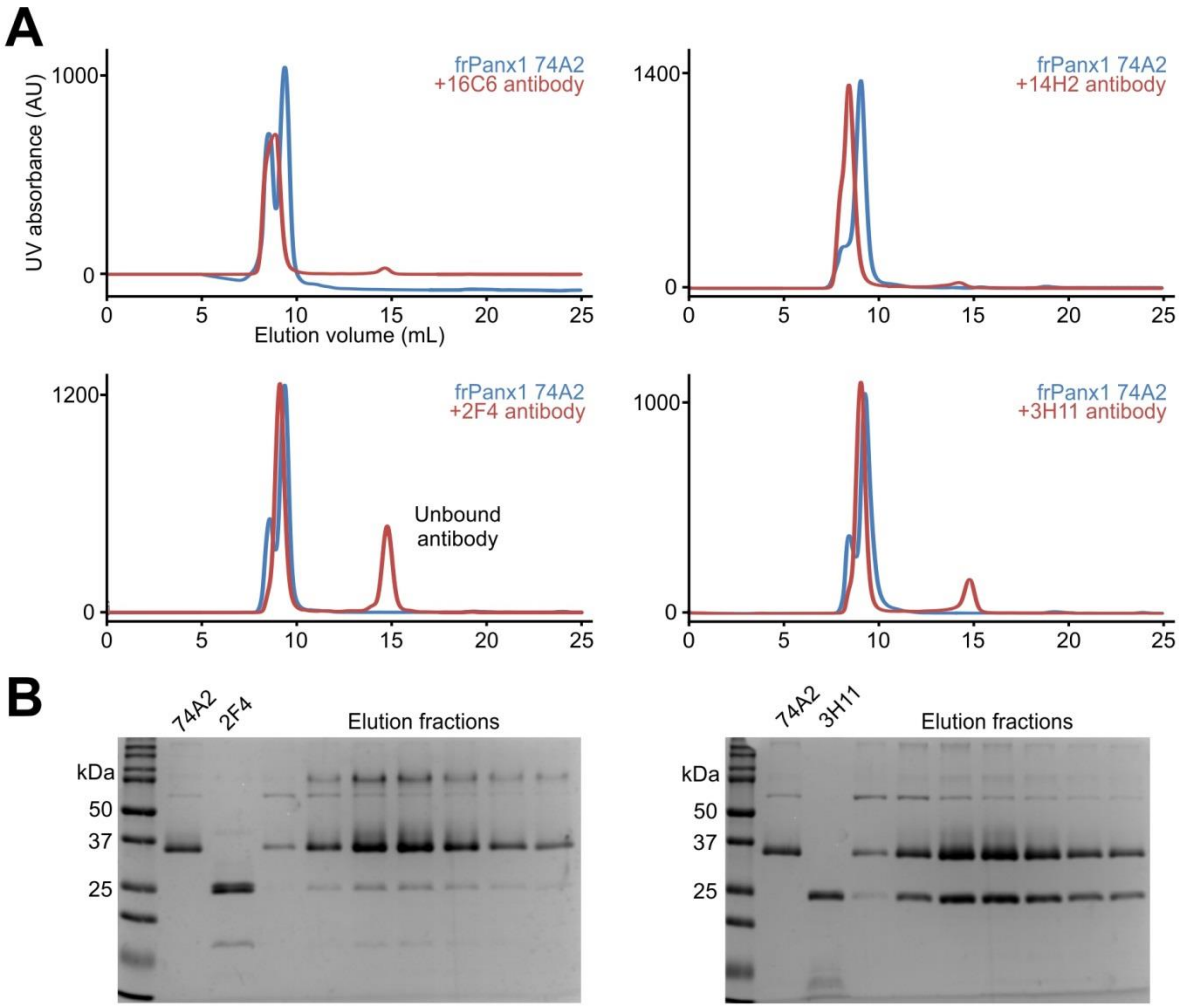

Figure 3.6. Complexes between 74A2 and various fabs. (A) Size exclusion chromatography profiles of frPanx1 74A2 complexed with (red) and without (blue) different fab fragments. Peak fractions of purified 74A2 in C12E8 were mixed with fabs at a 1:1.2 ratio of pannexin:fab, concententrated, and seperated again. (B) SDS-PAGE analysis of complexes formed between 74A2 and 2F4 (left) and 3H11 (right). Presence of pannexin and fab in the elution fractions indicates complex formation.

into mice used as the antigen known as “74A2” (frPanx1 1-357 with the intracellular loop motif “DIKD” replaced with “A” plus the glycoslyation mutation N257A) and frPanx1 1-357 LD11. Interestingly, 39 antibodies bound to 74A2 (66%) and only 14 bound to LD11 (24%). This suggests a rather large structural change in LD11 prevented many antibodies from recognizing this protein or that residual glycosylation on LD11 prevented binding of these. The second screening strategy deciphers whether antibodies can bind to a specific structural motif on 74A2 or if they only recognize

Table 1. Mutations tested to reduce surface entropy and surface charges.

K24A + K26A + R29A
D81A
E9A + D14A
K91A + D97A
D167A + K168A + R169A + D170A
R303A + K309A
D153 to D156 replaced by A

denatured protein. Guided by FSEC-positive antibodies, 34 western blots using denatured protein were performed using each monoclonal antibody as the primary antibody. Of these, 22 were incapable of binding to denatured protein, suggesting they recognize the intact frPanx1 74A2 multimer. The remaining 12 bind to unstructured or nonspecific pieces of the protein and were triaged. Of the 22 positives, we selected 4 to use as crystallization chaperones.

We originally screened complexes formed with LD11 and each of the 4 fab fragments. Unfortunately, complexes were heterogeneous in size after the final SEC step. There was an obvious size shift indicating a higher molecular weight complex was forming, but the SEC profile indicated 2 to 3 different species were forming. To mediate this, we formed complexes with the frPanx1 74A2 construct which was originally used as the antigen for these antibodies. Of the 4 fabs, 2 showed misshapen SEC profiles (16C6 and 14H2), suggesting heterogeneous complexes were forming, while 2 showed reasonably symmetric profiles (2F4 and 3H11) (Figure 3.6A). This indicates some kind of difference between LD11 and 74A2 in regards to complex behavior when bound to a fab fragment. SDS-PAGE analysis confirms fab binding to pannexin (Figure 3.6B).

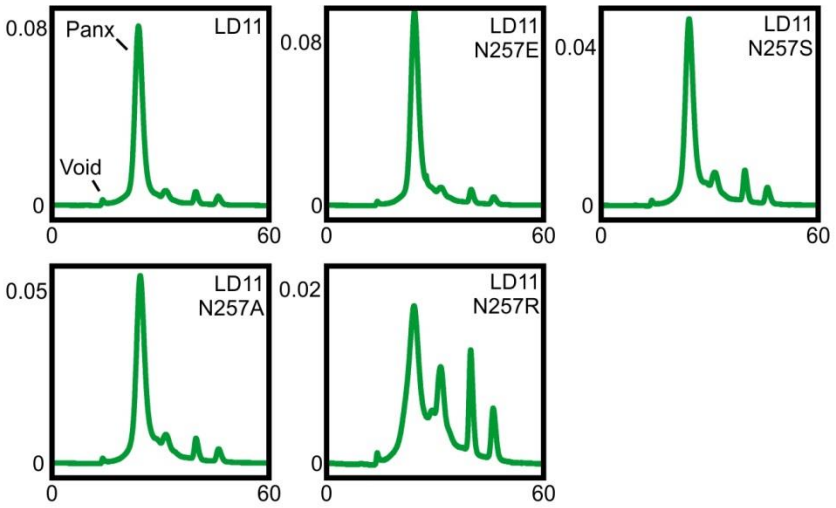

Figure 3.7. Glycosylation mutants are mostly stable. N257 was mutated to amino acids with varying properties and tested for behavior by FSEC. Constructs were expressed in insect cells, solubilized in C12E8, and analyzed on a Superose 10/300 column.

Regardless of SEC profile shape, all fab-Panx1 complexes were subjected to crystallization trials but none successfully formed crystals.

We decided to revisit LD11 and make further attempts to improve this protein. Down one path, I mutated charged amino acids which were putatively exposed to solution and may contribute to high surface entropy (Table 1). By neutralizing these charges we would remove amino acids that could prevent crystal formation. I generated 7 new constructs in which clusters of charged amino acids were replaced by alanines, distributed evenly across different domains of the protein. All constructs could be expressed, suggesting these mutations did not adversely affect protein structure. However, crystal growth was not observed, suggesting these mutations did not improve protein quality.

A second hypothesis involved the Panx1 glycosylation site. frPanx1 is subject to post translational modification in the form of sugar groups attached to N257 located in the second extracellular loop. When purified, protein is typically treated with EndoH to

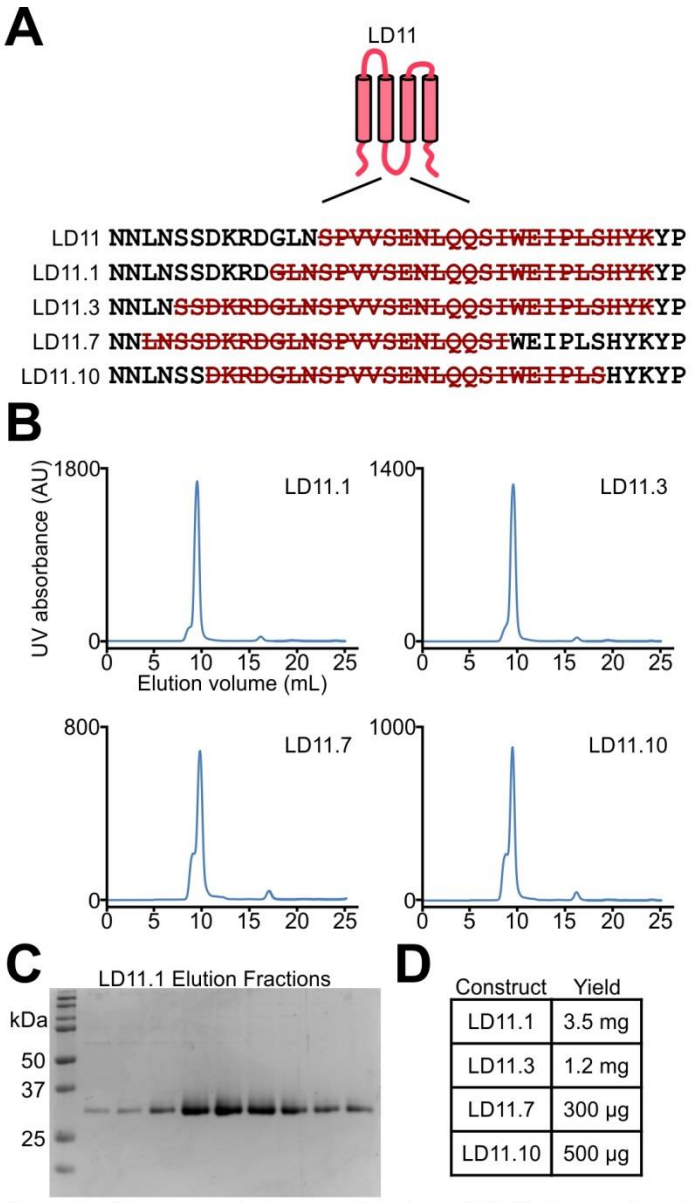

Figure 3.8. LD11.1 is a better crystal candidate. (A) Schematic diagram of frPanx1 and the deletions tested. Below is a section of amino acids corresponding to the intracellular loop. Deletions within the loop are depicted in crossed out red font. (B) Size-exclusion chromatography profiles of LD11.1, 11.3, 11.7, and 11.10. Protein was treated with EndoH overnight then separated in buffer containing 0.5 mM C12E8. (C) SDS-PAGE analysis of SEC fractions from LD11.1. (D) Yield comparisons between each loop deletion from 6L cells.

truncate this branched carbohydrate chain, leaving a single N-acetylglucosamine residue linked to the asparagine, resulting in a more homogeneous sample. It is feasible to think that the small remaining modification may inhibit crystal growth. To this end, I generated N257 mutants and tested each for expression by FSEC (Figure 3.7).

Of the four mutants, only the N257R mutant showed reduced expression and increased amounts of protein dissociation. N257E and N257A were purified and used for crystallization trials, but crystal quality did not improve compared to the EndoH treated protein.

A third path concerned the loop deletion in LD11. In this construct, 21 amino acids were deleted from the intracellular loop, but we had never determined if this was the most optimal deletion. We designed a screen to make very minor changes to the LD11 loop deletion to test if deleting more amino acids could improve crystal behavior. This is not an outlandish idea considering the LD11 deletion was required to find bicelle crystals in the first place. A total of 10 potential “loop deletions” were generated with deletion sizes ranging from 21 to 32 amino acids. FSEC screening indicated all deletions expressed normally, suggesting the intracellular loop can actually accommodate significant deletions. Of these, 4 were selected to be screened by purification and crystallizability: LD11.1, LD11.3, LD11.7, and LD11.10 (Figure 3.8A). All constructs were purified with a C-terminal Strep tag (without GFP). SEC profiles of LD11.1 and LD11.3 showed a reasonably monodisperse peak, suggesting those loop deletions are well-tolerated (Figure 3.8B). LD11.7 and LD11.10 displayed a significantly larger amount of aggregate shoulder, suggesting deletions in these constructs are not tolerated as well. Additionally, we were able to recover greater amounts of LD11.1 and LD11.3 (2 mg and 1.2 mg, respectively) from 6 L of starting culture compared to LD11.7 and LD11.10 (300 and 500 µg), suggesting the latter do not express as strongly, which may correlate with the stability of these two proteins (Figure 8D).

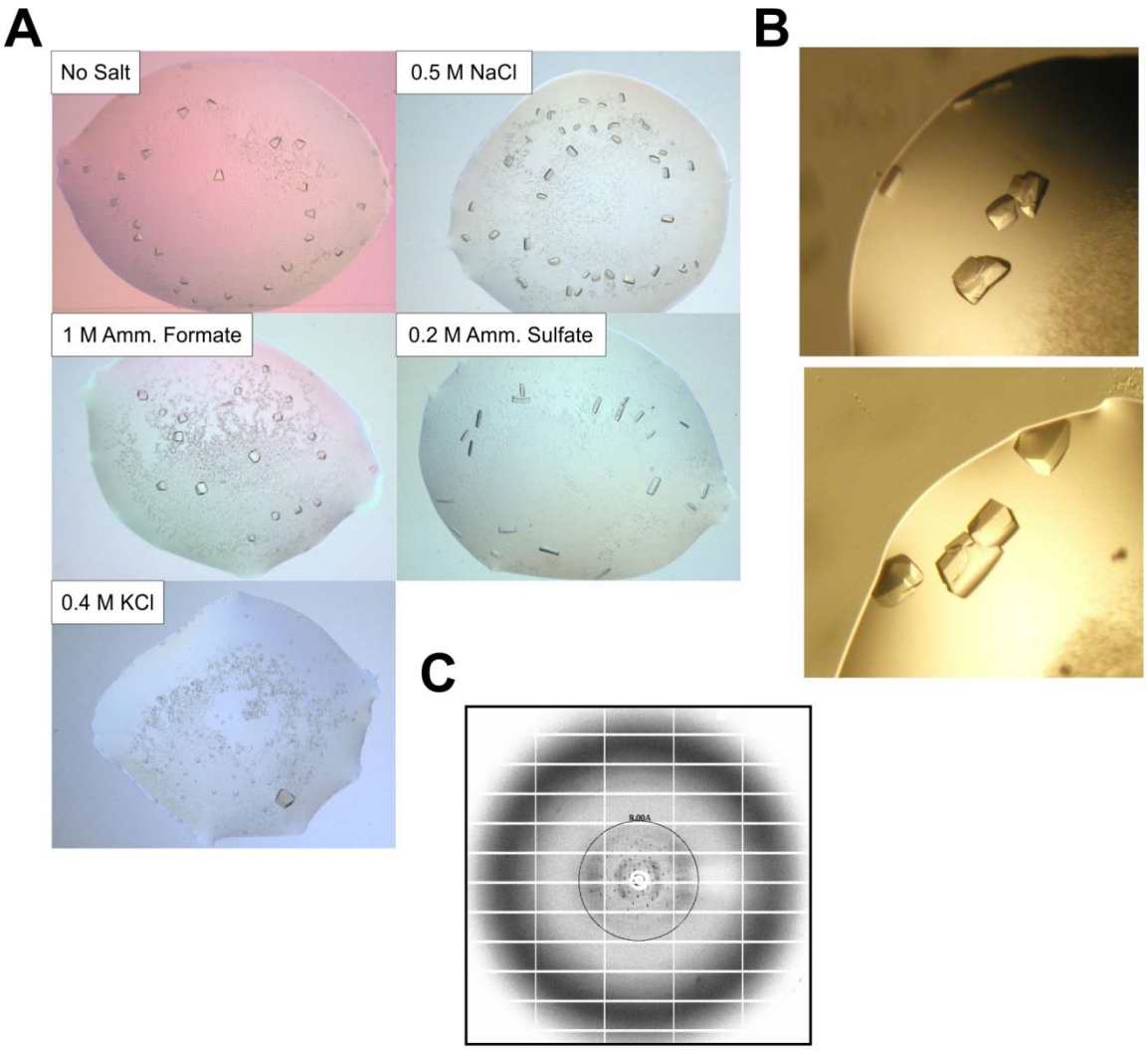

Figure 3.9. LD11.1 crystallizes in several conditions. (A) Initial crystal hits of LD11.1 grown on 96-well formats. Crystals appeared when mixed 1:1 in each condition with the indicated salt, plus 10% PEG 4000 with 0.1 M citrate pH 5.5. (B) Examples of crystals grown on 24 well plates, mixing 2:1 reservoir to protein. (C) Diffraction of crystals shown in (B). Crystals were frozen directly, and the ring represents the 8 Å resolution limit.

We mimicked my previous crystallization attempts with LD11 using bicelles and prepared 96-well trays for these 4 new constructs. We were successful in obtaining many crystal hits for LD11.1, only a few hits were for LD11.3, and very few hits for LD11.7 and LD11.10. This experiment suggests LD11.1 might be the most favorable construct to pursue, which shows a markedly clean purification (Figure 3.8C). Although this construct is only 3 amino acids shorter than the parent LD11, it had hopes of

diffracting better. Crystals of LD11.1 grown in bicelles did not have improved diffraction (~10 Å). We therefore sought to grow crystals in detergent.

At this time, we started routinely performing SEC using DDM in the running buffer. The rationale behind this is that, while pannexins seem extremely stable in the industrial detergent C12E8, this detergent garners very little attention in the literature as a 'good' crystallography detergent. In contrast, DDM is highly regarded as the gold standard detergent to start using when beginning a membrane protein crystallography venture. In contrast to previous SEC profiles, LD11.1 purified into a DDM containing buffer has a markedly sharper peak compared to C12E8. Also, the main peak separates better from the minor aggregate species, whereas in C12E8 both species overlap significantly. This is likely due to DDM forming a smaller micelle, reducing the overall mass of the protein-detergent complex.

LD11.1 purified in DDM was able to form crystals (Figure 3.9A). Crystals appeared 2-3 days after setting up trials and grew in a number of conditions and in different shapes. For example, bars appeared in ammonium sulfate and sodium chloride, while cubic shapes appeared in potassium chloride, ammonium formate, and no salt. There was a common theme between these conditions. Crystals appeared only under conditions of mild acidity (pH 5.5) with 10% PEG 4000 (polyethylene glycol with a MW of ~4000 Da). This might suggest that pH and PEG content are major factors governing frPanx1 crystallization.

Having obtained crystals on the 96-well format, we made attempts to reproduce these crystals on a larger scale. Unfortunately, we were only able to reproduce crystals

A

PEG	1000	1500	2000	4000	6000	8000
				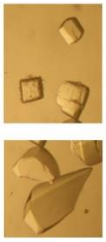		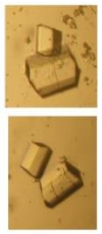
Max Å	8.5	6.5	8.2	7.2	8.8	8.0

B

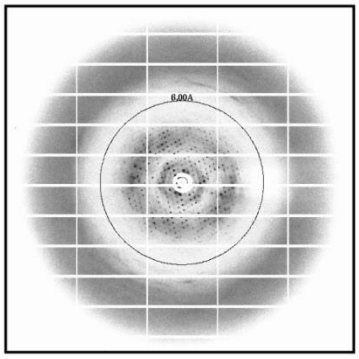

Figure 3.10. Crystals grown in PEG 1500 are improved. (A) Images of crystals grown in different PEG sizes ranged from 1000 to 8000 Da. Below is the diffraction limit of each crystal. (B) Diffraction image of a crystal grown in PEG 1500 and dehydrated. The ring represents a diffraction limit of 6 Å.

grown in ammonium formate (Figure 3.9B). When grown on a larger scale, these crystals were non-uniform in shape and crystals would often nucleate out of each other, leading to crystal aggregates. One thing we learned during this time was that crystals only grow in a narrow condition window, typically between a pH of 5.0 and 5.5 and a PEG concentration of 9-12%. This trend has been observed continuously when working with pannexin crystals. Nonetheless, we were able to separate and analyze several individual crystals by x-ray diffraction and found diffraction up to 8 Å, which was a significant improvement over the previous bicelle-grown crystals.

Optimization of these crystals involved screening various PEG sizes, which is a precipitant that can grossly effect crystal growth. We were successful in obtaining crystals using PEG of various sizes ranging from 1000 to 8000 Da (Figure 3.10A). Crystals typically crew as rectangular prisms (PEG 4000, 6000, 8000), curved rectangles (PEG 1000 and 2000), or as squarish-diamondy shapes (PEG 1500). Dehydration is a common technique used to remove water from protein crystals to help protein molecules pack together, and is routinely used to improve diffraction. We dehydrated a set of crystals grown in each PEG and also kept some hydrated. Upon diffraction analysis, we found that dehydrated crystals grown in PEG 1500 diffract the best, reaching about 6.5 Å (Figure 3.10B).

Crystals grown in PEG 1500 were typically small in size (70 – 90 µm), and we sought ways to coax them to grow bigger. We found that switching the incubation temperature from 4 °C to 12 °C reduces nucleation and generally results in bigger crystals. Combined with a more thorough dehydration protocol, we could achieve crystal diffraction to 5.5 Å.

A final improvement to these crystals was made by using microseeding. We noticed that crystals tended to nucleate and grow on the 'edge' of the crystal drop or on the air-water interface. This often resulted in flat crystals that were thin in their third dimension. To prevent this from occurring, and to make these crystals thicker, we began microseeding using crystal seeds obtained from similar conditions. This strategy was very successful in increasing crystal size and thickness, and we were able to obtain crystals up to ~400 µm in length (Figure 3.11A). These crystals were still smaller in the

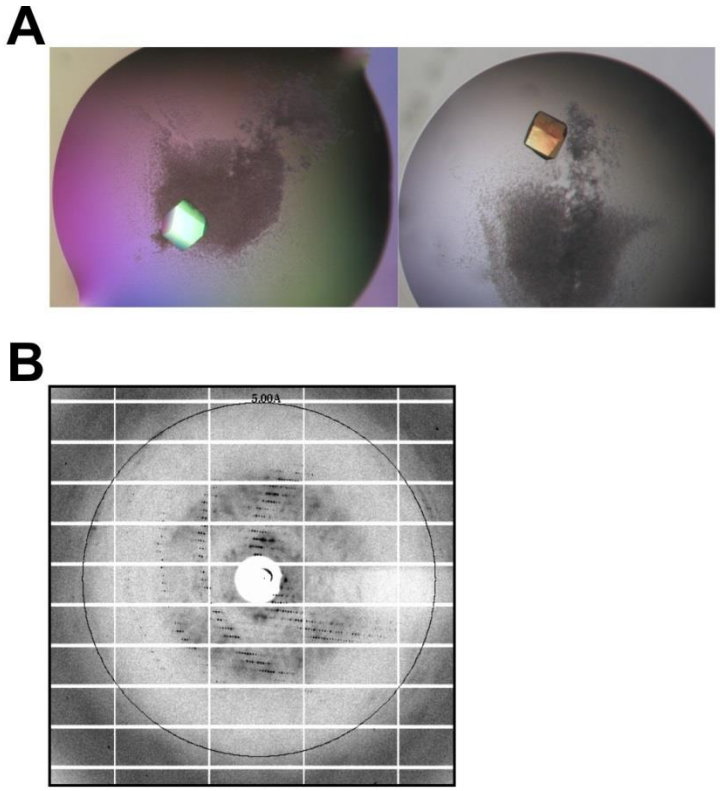

Figure 3.11. Microseeding improves crystal size and diffraction. (A) Images of crystals grown with microseeding. Crystals grown in similar conditions were collected, crushed, and diluted. Seeds were streaked through new crystal drops using a hair. (B) Diffraction image of seeded crystals also dehydrated. The ring represents a diffraction limit of 5 Å.

3rd dimension, with a maximum overall size of approximately 400 x 400 x 200 µm. Diffraction of these crystals were better, but were limited to about 4.9 Å (Figure 3.11B).

From here, we have tried a variety of strategies to improve diffraction of these crystals but all have generally failed. We will briefly overview our attempts to improve diffraction.

One of our first ideas was to make attempts at acquiring any kind of phase information which could be used to solve a low resolution frPanx1 structure. A common strategy to do this is to soak protein crystals in solutions containing heavy metal-containing compounds. Certain heavy metals can bind to exposed amino acids, resulting in an anomalous signal that can be used to calculate phases. We soaked

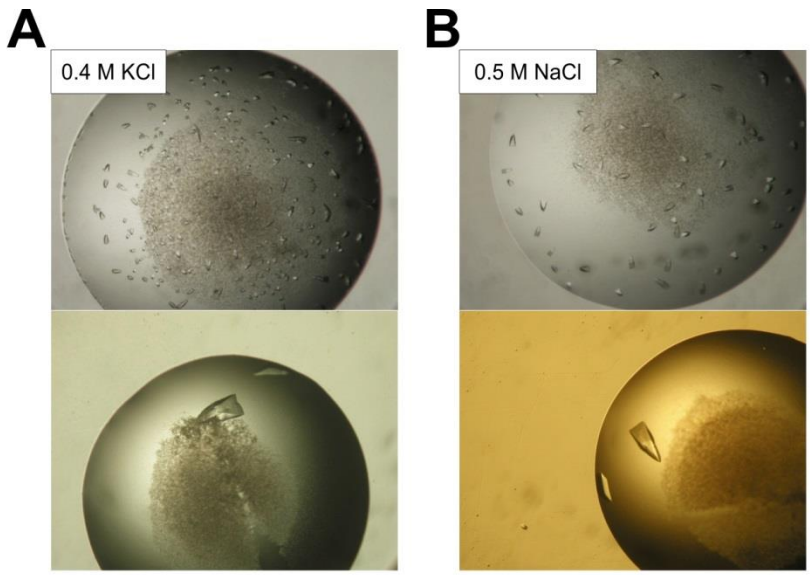

C

Ammonium Formate

Axis	Length (Å)
a	155
b	167
c	317
Space Group	C222

Potassium Chloride

Axis	Length (Å)
a	154
b	168
c	315
Space Group	C222

Figure 3.12. Crystals grown in new conditions are in the same space group. (A) Crystals grown with NaCl as the major salt (top) were small and used to make seeds. Microseeding resulted in much larger crystals (bottom). (B) Crystals grown in KCl (top). Microseeding promoted crystal growth (bottom). (C) Unit cell information comparing crystals grown in ammonium format (left) and potassium chloride (right).

crystals in 0.5 mM of 25 different heavy metal-containing solutions for 1 hour, 4 hours, or 24 hours, and used the tunable wavelength x-ray beam at APS for crystal analysis. Unfortunately we were unable to acquire meaningful heavy atom signals, suggesting these compounds were not binding in our protein crystals. A second attempt was made using higher concentrations of a select number of compounds (1 mM or 5 mM overnight), all which also failed to show a heavy atom signal. One interesting finding was that addition of the compound $TlCl_3$ marginally improved diffraction quality to ~4.7

Å. To date, our best diffracting crystal was dehydrated / soaked in solutions which contained trace amounts of $TlCl_3$, suggesting this may be a beneficial additive..

On another front, we realized we had only been obtaining crystals grown in the same condition – PEG 1500 with ammonium format at pH ~5.2. Now with expertise and experience on how to grow frPanx1 crystals, we wanted to revisit some broad screens to identify other crystallization conditions. In particular, we used screens comprised solely of PEG 1500, as that was one of the positive developments we had found. Using these screens, we identified at least 2 new conditions which could be reproduced on 24 well formats, one using sodium chloride and a second using potassium chloride (Figure 3.12A and B). Microseeding also proved to be useful in increasing the size of these crystals. As per our previous experience, these crystals were dehydrated and tested for diffraction. Unfortunately, crystals grown in both conditions diffracted maximally to ~6.0 Å. We were able to index data acquired from crystals grown in potassium chloride and found that the unit cell dimensions and space group were identical to crystals grown in ammonium formate (Figure 3.12C). This suggests both conditions promote growth of the same crystal lattice. Since crystals grown in both conditions diffract poorly, it is likely that this space group is not amenable to acquiring high resolution diffraction (at least, from this Panx1 construct). We would hypothesize that forming crystals in a different space group might improve diffraction.

With no knowledge of how our proteins are packed in the C222 lattice, there is no way to rationally design mutations to promote crystallogenesis in a new space group, although this is a common strategy if a low resolution structure is obtained. We reasoned that attempting to crystallize Panx1 proteins chimeric between human and

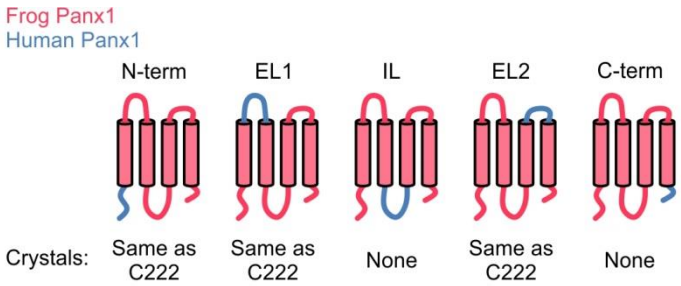

Figure 3.13. Chimeric constructs tested to break the C222 space group. Cartoon representations of pannexin where pink corresponds to sequences from frog Panx1 and blue corresponds to sequences from human Panx1.

frog might overcome this. Human and frog Panx1 are about 70% identical, and feature regions of low-conservation in their intracellular loops and C-termini. By replacing domains on frPanx1 with their humanPanx1 counterparts, we might be able to disrupt the C222 contact sites or introduce new crystal contact sites.

Five chimeric pannexins were generated, purified, and tested for crystallization (Figure 3.13). Crystals could be found for the N-term, EL1, and EL2 chimeras. Unfortunately, crystals appeared in conditions that were identical to previous conditions (PEG 1500 at pH 5.5, with ammonium formate, NaCl, and KCl), and crystal shape likewise looked similar to previously obtained crystals. Although these were not tested for diffraction, it is highly likely they are also in the C222 space group. This result is not surprising, given that the N-terminus and both extracellular loops are strongly conserved between human and frog pannexins. The IL and C-term chimeras did not crystallize in any conditions. This suggests that they might be important for mediating crystal contacts in the LD11.1 construct, and that these chimeras successfully broke those contacts. However, the human counterparts substituted into these chimeras may not be suitable for forming crystals in a new space group, explaining why no crystals appeared.

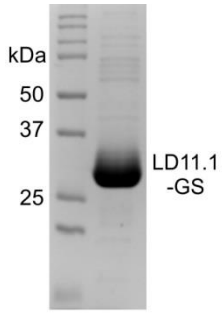

Figure 3.14. frPanx1 LD11.1 -GS purifies well. Protein was concentrated after SEC and ~6 µg was separated and stained on SDS-PAGE.

Another protein engineering idea we had involves our recent discovery regarding the +GS insertion into the Panx1 N-terminus. All frPanx1 constructs used for crystallography included these two additional amino acids, suggesting the proteins we've purified may easily adopt an open conformation. This may be inhibitory to obtaining high resolution data if channels are mixed (or fluctuating) between open and closed states. We hypothesized that removing the GS may increase diffraction simply by making channels more homogeneous in conformation. LD11.1 -GS expresses ~20% stronger than the parent LD11.1 (+GS) construct and purifies well (Figure 3.14). Crystals of this new protein, unsurprisingly, grow in the exact some conditions previously found with the exact same morphology. Unfortunately, diffraction of these crystals was roughly similar to constructs containing the GS insertion. Only a small handful of crystals were screened, but diffraction to at least ~6.5 Å was observed, suggesting that exclusion of the GS does not phenomenally improve crystal quality.

A final protein engineering attempt involved the first extracellular loop. This domain harbors a short stretch of ~13 amino acids that are not conserved between species. We hypothesized that this unconserved region may contribute negatively to crystal quality if it is disordered. Constructs were designed to test varying lengths of deletions in this region (Figure 15A). All deletions were FSEC positive, meaning they

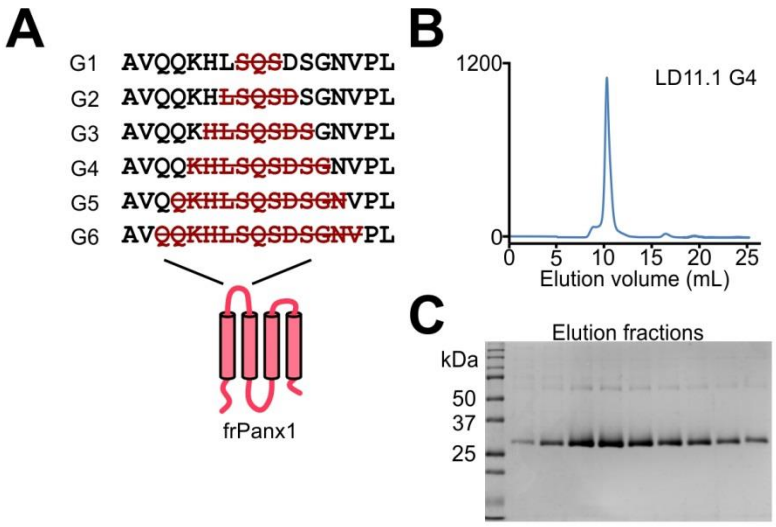

Figure 3.15. Deletions in the first extracellular loop are amenable to purification. (A) Cartoon representation of frPanx1. Shown is a segment amino acids from the first extracellular loop, and deletions in each construct are marked with red font. (B) SEC profile of the LD11.1 G4 construct. Protein was purified into buffer containing 0.5 mM DDM. (C) SDS-PAGE analysis of fractions eluted from (B) indicate the protein is pure.

expressed and formed stable oligomers. Of these, we selected the G4 deletion to attempt crystallization trials. 11.1 G4 could be successfully purified (Figure 3.15B and C) and it crystallized in conditions nearly identical to what was previously found to support growth of frPanx1 crystals. Crystal diffraction was poor, with the best diffraction reaching only 6 Å. This suggests that while this extracellular loop can tolerate significant deletions without impact protein stability, these deletions do not improve crystal quality.

In addition to the above strategies, quite a few crystallization attempts were aimed at finding a detergent amenable to high quality diffraction. When performing crystallography of membrane proteins, detergent choice is a nontrivial factor. One of the most important detergent properties is the micelle size it forms around transmembrane domains. Detergents with long alkyl chains and big hydrophilic head groups form large micelles (for example, C12E8 or C12M), and those with small alkyl

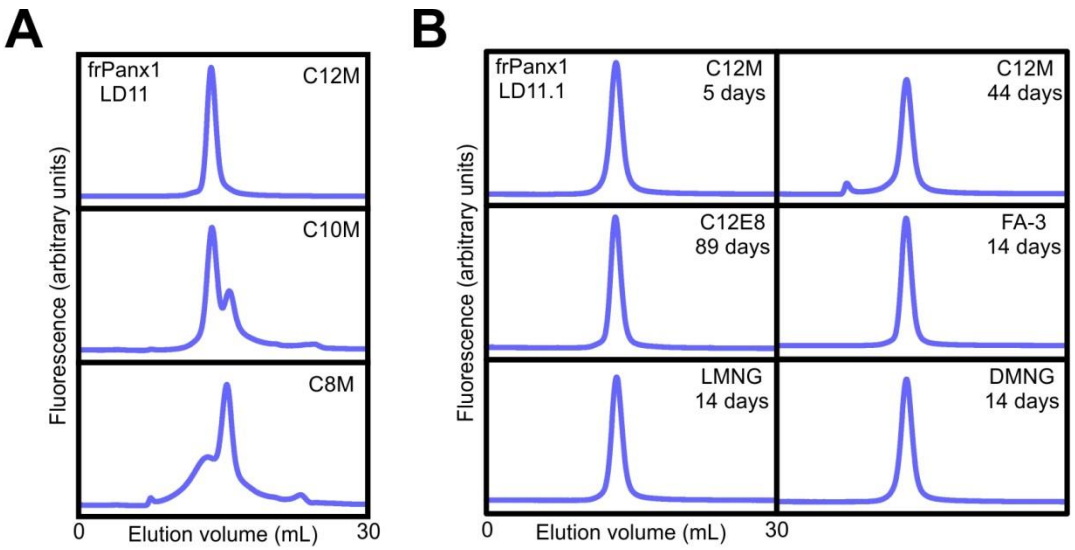

Figure 3.16. Profiles of frPanx1 purified into various detergents. (A) LD11 was purified into C12M then diluted into buffer containing an excess (~2-3 times the detergent CMC) of new detergent. After 24 hours, samples were analyzed on a Superose 10/300 column. (B) frPanx1 LD11.1 was purified by SEC into each different detergent and left at 4℃ for the indicated number of days before analysis by SEC. chains and small head groups form smaller micelles (like octyl-glucoside).

Reconstituting a protein into a detergent with a smaller micelle size is advantageous to expose more protein surface for crystal contacts and to allow tighter packing of neighboring proteins within the crystal lattice.

Frog Panx1, unfortunately, is tractable only in detergents that form large micelles (Figure 3.16A). LD11 is stable in dodecyl-maltoside (C12M, top chromatogram), but reducing the detergent alkyl chain size by just 2 carbons (C10M, middle chromatogram) results in dissociation of the pannexin oligomer. This is even more prominent when an additional 2 carbons are removed from the detergent (C8M, lower chromatogram), in which nearly all protein has dissociated. We explored whether frPanx1 is stable in long chain detergents other than C12M (Figure 16B). As briefly discussed previously, C12E8 incontestably remains the best detergent for stabilizing pannexins – a sample of "leftover" protein was still stable 89 days post-purification. In contrast, protein purified in

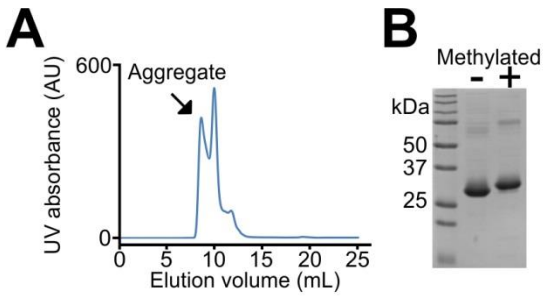

Figure 3.17. Methylation of LD11.1 -GS results in aggregated protein. (A) LD11.1 -GS was treated thrice with 20 mM DMAB and 40 mM formaldehyde each for 2 hours at 4 ˚C while protected from light, before a final treatment with 10 mM DMAB overnight 4 ˚C. Protein was separated on a Superdex 10/300 Increase column in the morning. (B) SDS-PAGE analysis of untreated and methylated protein. The higher molecular weight after treatment suggests the reaction has occurred.

C12M is generally stable, but after 44 days, has started to aggregate. LMNG, DMNG, and FA-3 are also capable of stabilizing frPanx1 LD11.1 (Figure 3.16B). Given the shape of the symmetry and monodispersity of proteins purified into these detergents, one would anticipate finding crystals. Unfortunately, LD11.1 is generally unable to form crystals in detergents other than C12M. We were able to find small crystal nucleations in FA-3 and LMNG, but optimization of these was unsuccessful. Although not included in the figure, fluorinated octyl-maltoside was also a good detergent for stabilizing frPanx1, but crystals never formed.

Two final avenues we pursued included protein methylation and lipidic cubic phase. In line with our previous idea of removing charged amino acids from the surface of frPanx1, protein methylation seeks to improve crystallization by neutralizing surface charges. Borane dimethylamine complex quenches the charge on lysines and arginines by methylating amine groups. Treated protein can then be used for crystallization trials, and has successfully improved the diffraction of membrane proteins, such as DHHC20. When performed on frPanx1, a minor increase in molecular weight is observed by SDS-PAGE indicating that the reaction has occurred (Figure 3.17B). However, size-

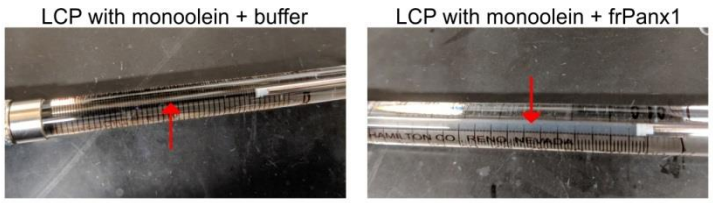

Figure 3.18. Reconstituting frPanx1 into LCP lipids results in precipitated protein. Buffer (left) or protein (right) was mixed with monoolein at a ratio of 60:40 (monoolein:sample) and mixed at room temperature with air-tight twin syringes. The transparent cubic phase emerged with buffer (left). All attempts using pannexin (right) resulted in a transparent but cloudy cubic phase, indicative of precipitated protein.

exclusion chromatography of the methylated protein indicates a high degree of aggregation, suggesting the methylated protein is not stable (Figure 3.17A). Although crystal screens were prepared, no hits were identified.

Lipidic cubic phase has risen in popularity for its success in facilitating the crystallization of small membrane proteins like GPCRs. This technique works by reconstituting protein into lipids, which then spontaneously assemble into a bicontinuous cubic phase. Although the details explaining how this promotes crystallogenesis are unclear, membrane proteins reconstituted into this system will preferentially make type I crystal contacts, with protein-protein contacts mediated between transmembrane helices. This is in constrast to type II contacts which are mainly mediated by extramembrane domains of detergent solubilized protein.

Reconstituting pannexins into LCP was not favorable. Upon mixing protein into monoolein, a perfectly transparent looking solution should result. However, with pannexin, the mixture always had a cloudy blue-tinged appearance (Figure 3.18). We were routinely successful at forming transparent cubic phase using buffers lacking protein or buffer saturated with a soluble protein like BSA, just adding pannexin appeared to disrupt the system. The amount of “cloudiness” depended on protein

concentration, suggesting the monoolein cubic phase might not support pannexin reconstitution, resulting in precipitated protein. The lipid curvature of the cubic phase is a strong determinant of crystallogenesis. We screened several commonly used alternative lipids that form a cubic phase with curvatures different from monoolein to test for successful pannexin reconstitution. In addition to 9.9 MAG (monoolein), we tested 11.9 MAG, 11.7 MAG, and 9.7 MAG. While we were successful in creating LCP with each different lipid using just buffer, pannexin always precipitated. Regardless, crystal trays were prepared with each lipid, but no crystal hits were ever observed.

It is maybe not surprising that frPanx1 fails to crystallize or reconstitute into LCP. This crystallography strategy typically favors membrane proteins with small membrane footprints. As an example, GPCRs have 7 transmembrane helices and are ~40 kDa in size. The full Panx1 complex should have 24 transmembrane helices and is at least 200 kDa in size. It is likely that the bicontinuous cubic phase has dimensions that cannot accommodate such a large membrane protein, perhaps explaining why this protein precipitates. Additionally, structures of oligomeric ion channels solved using LCP are severely underrepresented in databases, suggesting that this general class of proteins may not be compatible with forming crystals in LCP.

Solving the crystal structure of frPanx1 remains a challenging task. It's impossible to predict what subtle change may improve the diffraction limit of our current crystals from ~4.7 Å to sub- 4.0 Å resolutions. Perhaps some combination of additive screening and protein engineering might be required. Given that our current construct, LD11.1, is stuck forming crystals only in one space group, we imagine that something

that drives lattice formation into a better space group may be required to obtain high quality crystals.

Looking towards the future, cryo-electron microscopy has seen a surge of popularity in solving membrane protein structures, and has rapidly marched to the forefront of structural biology. While this technique was originally only successful in visualizing large >300 kDa proteins or protein complexes, it has gradually improved to the point where even 130 kDa membrane proteins can be solved at ~4 Å resolution *de novo*. frPanx1 may be a choice candidate to pursue with cryo-EM. The protein complex is large enough, has a high degree of internal symmetry, and purification procedures have already been established. Future work may benefit from pursuing this this direction, thereby circumventing the need to continue screening crystallization conditions.

REFERENCES

1. Hollenstein K, Dawson R, and Locher K. 2007. Structure and mechanism of ABC transporter proteins. *Current Opinion in Structural Biology*. 17:412-418.

2. Adelstein R. 1980. Regulation and kinetics of the actin-myosin-ATP interaction. *Ann. Rev. Biochem.* 49:921-956.

3. Cohen P. 2000. The regulation of protein function by multisite phosphorylation – a 25 year update. *Trends in Biochemical Sciences.* 25:596-601.

4. Burnstock G. 2006. Historical review: ATP as a neurotransmitter. *Trends in Pharmacological Sciences.* 27:166-176.

5. Khakh B and Burnstock G. 2009. The double life of ATP. *Sciencific American.* 301:84-92.

6. Savi P, Labouret N, Guette F, Lupker J, and Herbert J. 2001. P2Y12, a new platelet ADP receptor, target of Clopidogrel. *Biochemical and Biophysical Research Communications.* 283:379-383.

7. Storey R. 2006. Biology and pharmacology of the platelet P2Y12 receptor. *Current Pharmaceutical Design.* 12:1255-1259.

8. Hollopeter G, Jantzen H-M, Vincent D, Li G, England L, Ramakrishnan V, Yang R-B, Nurden P, Nurden A, Julius D, and Conley P. 2001. Identification of the platelet ADP receptor targeted by antithrombotic drugs. *Nature.* 409:202-207.

9. Niitsu Y, Jakubowski J, Sugidachi A, and Asai F. 2005. Pharmacology of CS-747 (prasugrel, LY640315), a novel, potent antiplatet agent with in vivo P2Y12 receptor antagonist activity. *Semin Thromb Hemost*. 31:184-194.

10. Storey R. 2011. Pharmacology and clinical trials of reversibly-binding P2Y12 inhibitors. *Thromb Haemost.* 105:575-581.

11. Robson S, Sevigny J, and Zimmermann H. 2007. The E-NTPDase family of ectonucleotidases: structure and function relationships and pathophysiological significance. *Purinergic Signalling*. 2:409

12. Zimmerman H. 2008. Ectonucleotidases in the nervous system. *Novartis Foundation Symposia.* 276, 1.

13. Bodin P and Burnstock G. 2001. Purinergic signaling: ATP release. *Neurochemical Research*. 26:959-969.

14. Dowdall M, Boyne A, and Whittaker V. 1974. Adenosine triphosphate: a constituent of cholinergic synaptic vesicles. *Biochemical Journal.* 140:1-12.

15. Yuri P, Lalo U, Verkhratsky A, and North A. 2006. Vesicular release of ATP at central synapses. *Pflugers Archiv.* 452:589-597.

16. Chekeni F, Elliott M, Sandilos J, Walk S, Kinchen J, Lazarowski E, Armstrong A, Penuela S, Laird D, Salvesen G, Isakson B, Bayliss D, Ravichandran K. 2010. Pannexin 1 channels mediate 'find-me' signal release and membrane permeability during apoptosis. *Nature*. 467:863-867.

17. Elliott M, Chekeni F, Trampont P, Lazarowski E, Kadl A, Walk S, Park D, Woodson R, Ostankovich M, Sharma P, Lysiak J, Harden T, Leitinger N, Ravichandran K. 2009. Nucleotides released by apoptotic cells act as a find-me signal to promote phagocytic clearance. *Nature.* 461:282-286.

18. Cotrina M, Lin J, Alves-Rodrigues A, Liu S, Li J, Azmi-Ghadimi H, Kang J, Naus C, and Nedergaard M. 1998. Connexins regulate calcium signaling by controlling ATP release. *PNAS.* 95:15735-15740.

19. Stout C, Constantin J, Naus C, and Charles A. 2002. Intercellular calcium signaling in astrocytes via ATP release through connexins hemichannels. *J. Biol. Chem.* 277:10482-10488.

20. Taruno A, Matsumoto I, Ma Z, Marambaud P, Foskett K. 2013. How do taste cells lacking synapses mediate neurotransmission? CALHM1, a voltage-gated ATP channel. *BioEssays.* 35(12).

21. Islam R, Uramoto H, Okada T, Saboriv R. 2012. Maxi-anion channel and pannexin 1 hemichannel constitute separate pathways for swelling-induced ATP release in murine L929 fibrosarcoma cells. *American Journal of Physiology*. 303(9).

22. Panchin Y, Kelmanson I, Matz M, Lukyanov K, Usman N, Lukyanov S. 2001. A ubiquitous family of putative gap junction molecules. *Current Biology*. 10:473-474.

23. Ray A, Zoidl G, Wahle P, Dermietzel R. 2006. Pannexin expression in the cerebellum. *The Cerebellum.* 5:189-192.

24. Wang X-H, Streeter M, Liu Y-P, Zhao H-B. 2008. Identification and characterization of pannexin expression in the mammalian cochlea. *Journal of Comparative Neurology.* 512:336-346.

25. Bruzzone R, Hormuzdi S, Barbe M, Herb A, Monyer H. 2003. Pannexins, a family of gap junction proteins expressed in brain. *PNAS*. 100:13644-13649.

26. Locovei S, Bao L, Dahl G. 2006. Pannexin 1 erythrocytes: function without a gap. *PNAS*. 103:7655-7659.

27. Le Vasseur M, Lelowski J, Bechberger J, Sin W-C, Naus C. 2014. Pannexin 2 protein expression is not restricted to the CNS. *Front. Cell. Neurosci.* 8:392.

28. Bond S, Lau A, Penuela S, Sampaio A, Underhill T, Laird D, Naus C. 2011. Pannexin 3 is a novel target for Runx2, expressed by osteoblasts and mature growth plate chondrocytes. *Journal of Bone and Mineral Research.* 26:12.

29. Iwamoto T, Ishiukawa M, Ono M, Nakamura T, Kukumoto S, Yamada Y. 2012. Biological roles of gap junction proteins in cartilage and bone development. *Journal of Oral Biosciences.* 55:29-33.

30. Sosinsky G, Boassa D, Dermietzel R, Duffy H, Laird D, MacVicar B, Naus C, Penuela S, Scemes E, Spray D, Thompson R, Zhao H-B, Dahl G. 2011. Pannexin channels are not gap junction hemichannels. *Channels.* 5:193-197.

31. Penuela S, Bhalla R, Gong X-Q, Cowan K, Celetti S, Cowan B, Bai D, Shao Q, Laird D. 2007. Pannexin 1 and pannexin 3 are glycoproteins that exhibit many distinct characteristics from the connexins family of gap junction proteins. *Journal of Cell Science.* 120:3772-3783.

32. Penuela S, Bhalla R, Nag K, Laird D. 2009. Glycosylation regulations pannexin intermixing and cellular localization. *Molecular Biology of the Cell.* 20:4267-4470.

33. Ransford G, Gregien N, Qiu F, Dahl G, Conner G, Salathe M. 2008. Pannexin 1 contributes to ATP release in airway epithelia. *AJRCMB.* 41:525-534.

34. Wiszniewski L, Sanz J, Scerri I, Gasparotto E, Dudez T, Lacroix JS, Suter S, Gallati S, Chanson M. 2007. Functional expression of connexin30 and connexin 31 in the polarized human airway epithelium. *Differentiation.* 75:382-392.

35. Bargiotas P, Krenz A, Monyer H, Schwaninger M. 2012. Functional outcome of pannexin-deficient mice after cerebral ischemia. *Channels.* 6:453-456.

36. Weaver J, Arandjelovic S, Brown G, Mendu S, Schappe M, Buckley M, Chiu Y-H, Shu S, Kim J, Chung J, Krupa J, Jevtovic-Todorovic V, Desai B, Ravichandran K, Bayliss D. 2017. Hematopoietic pannexin 1 function is critical for neuropathic pain. *Scientific Reports.* 42550.

37. Bao L, Locovei S, Dahl G. 2004. Pannexin membrane channels are mechanosensitive conduits for ATP. *FEBS Lett.* 572:65-68.

38. Wang J, Ambrosi C, Qiu F, Jackson D, Sosinsky G, Dahl G. 2014. The membrane protein pannexin1 forms two open-channel conformations depending on the mode of activation. *Sci. Signal.* 7(335).

39. Ma W, Compan V, Zheng W, Martin E, North RA, Verkhratsky A, Surprenant A. 2012. Pannexin 1 forms an anion-selective channel. *Pflugers Arch.* 463:585-592.

40. Romanov R, Bystrova M, Rogachevskaya O, Sadovnilov V, Shestopalov V, Kolesnikov S. 2012. The ATP permeability of pannexin 1 channels in a heterologous system and in mammalian taste cells is dispensable. *J. Cell. Sci.* 125:5514-5523.

41. Dahl G and Locovei S. 2006. Pannexin: to gap or not to gap, is that a question? *IUBMB Life*. 58:409-419.

42. Lohman A, Leskov I, Butcher J, Johnstone S, Stokes T, Begandt D, DeLalio L, Best A, Penuela S, Teitinger N, Ravichandran K, Stokes K, Isakson B. 2015. Pannexin 1 channels regulate leukocyte emigration through the venous endothelium during acute inflammation. *Nat. Comm.* 7965.

43. Chiu Y-H, Jin X, Medina C, Leonhardt S, Kiessling V, Bennett B, Shu S, Tamm L, Yeager M, Ravichandran K, Bayliss D. 2017. A quantized mechanism for activation of pannexin channels. *Nat. Comm.* 14324.

44. Pelegrin P and Surprenant A. 2006. Pannexin-1 mediates large pore formation and interleukin-1β relrease by the ATP-gated P2X7 receptor. *EMBO.* 25:5071-5082.

45. Ma W, Hui H, Pelegrin P, Surprenant A. 2009. Pharmacological characterization of pannexin-1 currents expressed in mammalian cells. *Journal of Pharmacology and Experimental Therapeutics.* 328:409-418.

46. Pelegrin P and Surprenant A. 2007. Pannexin-1 couples fo maitotoxin and nigericin-induced interleukin-1β release through a dye uptake-independent pathway. *J. Biol. Chem. 282:2386-2394.*

47. Xu X, Boumechache M, Robinson L, Marschall V, Gorecki D, Masin M, Murrell-Lagnado R. 2012. Splice variants of the P2X7 receptor reveal differential agonist dependence and functional coupling with pannexin-1. *J. Cell. Sci.* 125:3776-3789.

48. Karasawa A, Michalski K, Mikhelzon P, Kawate T. 2017. The P2X7 receptor forms a dye-permeable pore independent of its intracellular domain but dependent on membrane lipid composition. *eLife.* 6:e31186.

49. Sandilos J, Chiu Y-H, Chekeni F, Armstrong A, Walk S, Ravichandran K, Bayliss D. 2012. Pannexin 1, an ATP release channel, is activated by caspase cleavage of its pore-associated C-terminal autoinhibitory region. *J. Biol. Chem.* 287:11303-11311.

50. Lohman A, Weaver J, Billaud M, Sandilos J, Griffiths R, Straub A, Penuela S, Leitinger N, Laird D, Bayliss D, Isakson B. 2012. S-nitrosylation inhibits pannexin 1 channel function. *J. Biol. Chem.* 287:36902-36912.

51. Levitan I. 1994. Modulation of ion channels by protein phosphorylation and dephosphorylation. *Annu. Rev. Physiol.* 56:193-212.

52. Thompson R, Jackson M, Olah M, Rungta R, Hines D, Beazely M, MacDonald J, MacVicar B. 2008. Activation of pannexin-1 hemichannels augments aberrant bursting in the hippocampus. *Science*. 322:1555-1559.

53. Weilinger N, Lohman A, Rakai B, Ma E, Bialecki J, Maslieieva V, Rilea T, Bandet M, Ikuta N, Scott L, Colicos M, Teskey G, Winship I, Thompson R. 2016. Metabotrobic NMDA receptor signaling couples Src family kinases to pannexin-1 during excitotoxicity. *Nature Neuroscience.* 19:432-442.

54. Weilinger N, Tang P, Thompson R. 2012. Anoxia-induced NMRA receptor activation opens pannexin channels via Src family kinases. *J. Neurosci.* 32:12579-12588.

55. Billaud M, Lohman A, Straub A, Looft-Wilson R, Johnstone S, Araj C, Best A, Chekeni F, Ravichandran K, Penuela S, Laird D, Isakson B. 2011. Pannexin1 regulations α1-adrenergic receptor-mediated vasoconstriction. *Circulation Research*. 122(9).

56. Billaud M, Chiu Y-H, Lohman A, Parpaite T, Butcher J, Mutchler A, DeLalio L, Artamonov M, Sandilos J, Best A, Somlyo A, Thompson R, Le T, Ravichandran K, Bayliss D, Isakson B. 2015. A molecular signature in the pannexin1 intracellular loop confers channel activation by the α1 adrenoreceptor in smooth muscle cells. *Sci. Signal.* 8(364).

57. Yang N, George A, Horn R. 1996. Molecular basis of charge movement in voltage-gated sodium channels. *Neuron.* 16:113-122.

58. Chiu Y-H, Schappe M, Desai B, Bayliss D. 2018. Revisiting multimodal activation and channel properties of pannexin 1. *J. Gen. Physiol.* 150:19-39.

59. Dahl G and Kean R. 2012. Pannexins: from discovery to bedside in 11±4 years?. *Brain Res.* 1487:150-159.

60. Penuela S, Hardland L, Simek J, Laird D. 2014. Pannexin channels and their links to human disease. *Biochem. J.* 461:371-381.

61. Prochnow N, Abdulazim A, Kurtenbach S, Wildforster V, Dvoriantchikova G, Hanske J, Petrasch-Parwez E, Shestopalov V, Dermietzel R, Manahan-Vaughan D, Zoidl G.

2012. Pannexin1 stabilizes synaptic plasticity and is needed for learning. *PLoS One.* 7:e51767.

62. Bernardinelli Y, Salmon C, Jones E, Farmer T, Stellwagen D, Murai K. 2011. Astrocytes display complex and localized calcium responses to single-neuron stimulation in the hippocampus. *Journal of Neuroscience.* 31:8905-8919.

63. Sandilos JK and Bayliss DA. 2012. Physiological mechanisms for the modulation of pannexin 1 channel activity. *J Physiol.* 590:6257-6266.

64. Sridharan M, Adderley S, Bowles E, Egan T, Stephenson A, Ellsworth M, Sprague R. 2010. Pannexin 1 is the conduit for low oxygen tension-induced ATP release from human erythrocytes. *American Physiology Society.* 299:1146-1152.

65. Boassa D, Ambrosi C, Qiu F, Dahl G, Gaietta G, Sosinsky G. 2007. Pannexin1 channels contain a glycosylation site that targets the hexamer to the plasma membrane. *J Biol Chem.* 282:31733-31743.

66. Dourado M, Wong E, Hackos D. 2014. Pannexin-1 is blocked by its C-terminus through a delocalized non-specific interaction surface. *PLoS One*. 9:e99596.

67. Engelhardt K, Schmidt M, Tenbusch M, Dermietzel R. 2015. Effects on channel properties and induction of cell death induced by C-terminal truncations of pannexin1 depend on domain length. *J Membr Biol.* 248:285-294.

68. Jackson D, Wang J, Keane R, Scemes E, Dahl G. 2014. ATP and potassium ions: a deadly combination for astrocytes. *Sci Rep.* 4:4576.

69. MacKinnon R, Reinhart P, White M. 1988. Charybdotoxin block of K+ channels suggests that different types of K+ channels share common structural features. *Neuron*. 1:997-1001,

70. Swartz K and MacKinnon R. 1997a. Hanatoxin modifies the gating of a voltage-dependent K+ channel through multiple binding sites. *Neuron*. 18:665-673.

71. Swartz K and MacKinnon R. 1997b. Mapping the receptor site for hanatoxin, a gating modifier of voltage-dependent K+ channels. *Neuron*. 18:675-6822.

72. Bohlen C, Priel A, Zhou S, King D, Siemens J, Julius D. 2010. A bivalent tarantula toxin activates the capsaicin receptor, TRPV1, by targeting the outer pore domain. *Cell.* 141:834-845.

73. Wang J and Dahl G. 2010 SCAM analysis of Panx1 suggests a peculiar pore structure. *J Gen Physiol.* 136:515-527.

74. Bunse S, Schmidt M, Hoffmann S, Engelhardt K, Zoidl G, Dermietzel R. 2011. Single cysteines in the extracellular and transmembrane regions modulate pannexin 1 channel function. *J Membr Biol.* 244:21-33.

75. Qiu F and Dahl G. 2009. A permeant regulating its permeation pore: inhibition of pannexin 1 channels by ATP. *Am J Physiol Cell Physiol.* 296:C250-C255.

76. Qiu F, Wang J, Dahl G. 2012. Alanine substitution scanning of pannexin1 reveals amino acid residues mediating ATP sensitivity. *Purinergic Signal.* 8:81-90.

77. Wang J, Jackson D, Dahl G. 2013. The food dye FD&C Blue No. 1 is a selective inhibitor of the ATP release channel Panx1. *J Gen Physiol.* 141:649-656.

78. Dahl G and Keane R. 2012. Pannexin: from discovery to bedside in 11 ± 4 years?. *Brain Research.* 1487:150-159.

79. Dahl G. 2015. ATP release through pannexon channels. *Phil Trans R Soc B.* 370:20140191.

80. MacVicar B and Thompson R. 2010. Non-junction functions of pannexin-1 channels. *Trends in Neuroscience.* 33:93-202.

81. Furlow P, Zhang S, Soong T, Halberg N, Goodarzi H, Mangrum C, Wu Y, Elemento O, Tavazoie S. 2017. Mechanosensitive pannexin-1 channels mediate microvascular metastatic cell survival. *Nat Cell Bio*. 17:943-952.

82. Velasquez S, Eugenin E. 2014. Role of pannexin-1 hemichannels and purinergic receptors in the pathogenesis of human diseases. *Front Physiol.* 5(96).

83. Thompson R. 2014. Pannexin channels and ischaemia. *The Journal of Physiology*. 593:3463-3470.

84. Jiang J and Penuela S. 2016. Connexin and pannexin channels in cancer. *BMC Cell Biology.* 17(Suppl 1):12.

85. Silverman W, Vaccari J, Locovei S, Qiu F, Carlsson S, Scemes E, Keane R, Dahl G. 2009. The pannexin 1 channel activates the inflammasome in neurons and astrocytes. *J Biol Chem.* 284:18143-18151.

86. Gulbransen B, Bashashati M, Hirota S, Gui X, Roberts J, MacDonald J, Muruve D, McKay D, Beck P, Mawe G, Thompson R, Sharkey K. 2012. Activation of neuronal P2X7 receptor-Pannexin-1 mediates death of enteric neurons during colitis. *Nat Med.* 18:600-604.

87. Isakson B and Thompson R. 2014. Pannexin-1 as a potentiator of ligand-gated receptor signaling. *Channels.* 8:118-123.

88. Kyle J, Minogue P, Thomas B, Domowicz D, Berthoud V, Hanck D, Beyer E. 2008. An intact connexin N-terminus is required for function but not gap junction formation. *J Cell Sci.* 121:2744-2750.

89. Kyle J, Berthoud V, Kurutz J, Minogue P, Greenspan M, Hanck D, Beyer E. 2009. The N terminus of connexins 37 contains an α-helix that is required for channel function. *J Biol Chem.* 284:20418-20427.

90. Kronengold J, Srinivas M, Verselis V. 2012. The N-terminal half of the connexins protein contains the core elements of the pore and voltage gates. *J Membr Biol*. 245:453-463.

91. Harris A and Contreras J. 2014. Motifs in the permeation pathway of connexins channels mediate voltage and Ca2+ sensing. *Front Physiol*. 5(113).

92. Maeda S, Nakagawa S, Suga M, Yamashita E, Oshima A, Fujiyoshi Y, Tsukihara T. 2009. Structure of the connexins 26 gap junction channel at 3.5 Å resolution. 458:597-602.

93. Verselis V, Ginter C, Bargiello T. 1994. Opposite voltage gating polarities of two closely related connexins. 368:348-351.

94. Purnick P, Oh S, Abrams C, Verselis V, Bargiello T. 2000. Reversal of the gating polarity of gap junctions by negative charge substitutions in the N-terminus of connexin 32. *Biophysical Journal*. 79:2403-2415.

95. Oh S, Rivkin S, Tang Q, Verselis V, Bargiello T. 2004. Determinants of gating polarity of a connexin 32 hemichannel. *Biophysical Journal*. 87:912-928.

96. Boutina J. 1997. Myristoylation. *Cellular Signaling.* 9:15-35.

97. Penna A, Demuro A, Yeromin A, Zhang S, Safrina O, Parker I, Cahalan M. 2008. The CRAC channel consists of a tetramer formed by Stim-induced dimerization of Orai dimers. *Nature*. 456:116-120.

98. Hou X, Pedi L, Diver M, Long S. 2012. Crystal structure of the calcium release-activated calcium channel Orai. *Science*. 1228757.

99. Bharill S, Fu Z, Palty R, Isacoff E. 2014. Stoichiometry and specific assembly of Best ion channels. *PNAS*. 111:6491-6496.

100. Kane Dickson V, Pedi L, Long S. 2014. Structure and insights into the function of a Ca2+-activated Cl- channel. *Nature*. 516:213-218.

101. Scemes E, Suadicani S, Dahl G, Spray D. 2007. Connexin and pannexin mediated cell-cell communication. *Neuron Glia Biol*. 3:199-208.

102. Oshima A, Tani K, Fujiyoshi Y. 2016. Atomic structure of the innexin-6 gap junction channel determined by cryo-EM. *Nat Comm.* 13681.

103. Ambrosi C, Gassmann O, Pranskevich J, Boassa D, Smock A, Wang J, Dahl G, Steinem C, Sosinsky G. 2010. Pannexin1 and pannexin2 channels show quaternary similarities similar to connexins and different oligomerization numbers from each other. *J Biol Chem.* 285:24420-24431.

104. Jiang L-H, Rassendren F, Surprenant A, North A. 2000. Identification of amino acid residues contributing to the ATP-binding site of a purinergic P2X receptor. *J Biol Chem.* 275:34190-34196.

105. Kawate T, Carlisle Michel J, Birdsong W, Gouaux E. 2009. Crystal structure of the ATP-gated P2X4 ion channel in the closed state. *Nature.* 460:592-598.

106. Hattori M and Gouaux E. 2012. Molecular mechanism of ATP binding and ion channel activation in P2X receptors. *Nature*. 485:207-212.

107. Karasawa A and Kawate T. 2016. Structural basis for subtype-specific inhibition of the P2X7 receptor. *eLife*. 5:e22153.

108. Kawate T and Gouaux E. 2006. Fluorescence-detection size-exclusion chromatography for precrystallization screening of integral membrane proteins. *Structure.* 14(4):673-681.

109. Cambrosio A and Keating P. 1988. “Going monoclonal”: art, science, and magic in the day-to-day use of hybridoma technology. *Social Problems.* 35(3):244-260.

110. Karasawa A and Kawate T. 2017. Expression and purification of a mammalian P2X7 receptor from Sf9 insect cells. *Bio. Protoc.* 7(17):e2544.